Geoid Determination Based on a Combination of Terrestrial and Airborne Gravity Data in South Korea

by

Hyo Jin Yang

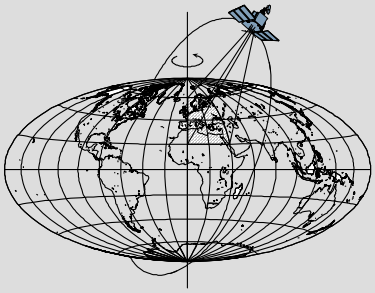

Report No. 507

Geodetic Science

The Ohio State University
Columbus, Ohio 43210

December 2013

Geoid Determination Based on a Combination of Terrestrial and Airborne Gravity Data in South Korea

by

Hyo Jin Yang

Report No. 507

Geodetic Science

The Ohio State University

Columbus, Ohio 43210

December 2013

PREFACE

This report was prepared for and submitted to the Graduate School of the Ohio State University as a dissertation in partial fulfillment of the requirements for the PhD degree. The work was supported in part by a grant from the University of Seoul, Seoul, Korea, under the auspices of the Ministry of Land, Transport and Maritime Affairs, Korea.

ABSTRACT

The regional gravimetric geoid model for South Korea is developed by using heterogeneous data such as gravimetric measurements, a global geopotential model, and a high resolution digital topographic model. A highly accurate gravimetric geoid model, which is a basis to support the construction of the efficient and less costly height system with GPS, requires many gravimetric observations and these are acquired by several kinds of sensors or on platforms. Especially airborne gravimetry has been widely employed to measure the earth's gravity field in last three decades, as well as the traditional measurements on the earth's physical surface. Therefore, it is necessary to understand the characters of each gravimetric measurement, such as the measurement surface and involved topography, and also to integrate these to a unified gravimetric data base which refers to the same gravitational field. This dissertation illustrates the methods for combining two types of available gravity data for South Korea, one is terrestrial data obtained on the earth's surface and another is airborne data measured at altitude, and shows an accessible accuracy of the geoid model based on these data.

It is found that there exists some bias between terrestrial and airborne gravimetric data probably due to their different properties, and the bias is significantly reduced by the terrain effects determined by the Bouguer reduction. Therefore, the gravimetric data should be merged to a unified data base in terms of the Bouguer gravity anomaly. The reductions are the important roles not only to combine gravimetric data, but also to satisfy the boundary conditions of the Stokes's integral. The Stokes's integral is applied to the unified gravimetric data set in order to model the geoid undulation for South Korea. Also the systematic effects on the fundamental equation of physical geodesy are numerically demonstrated on the gravity anomaly and geoid undulation. These are shown to be negligible. In addition, the limitations of the Stokes's integral caused by truncation of the integration area and discontinuity of data are reduced by the empirical application of the Stokes's kernel modification and the Remove-Compute-Restore technique.

The demonstration of accuracy of the developed geoid model, which is compared to GPS/leveling, shows the model based on the gravity anomaly with respect to the terrain effects have better accuracy than the model based on the free-air gravity anomaly. The achievement on the precision of geoid undulation, computed on a 2 arcmin grid, is 5.6 cm in standard deviation. This model is based on the airborne-only gravity data considering not only the terrain effects but also the downward continuation. The bias in the gravimetric geoid of about 15.5 cm, determined from the comparison with the GPS/leveling data, agrees with previously determined values.

TABLE OF CONTENTS

CHAPTER 1 INTRODUCTION

1.1 Background

The Geoid as a fundamental surface of physical geodesy is defined as an equipotential surface that is the closest to mean sea level; it is usually used as a mathematical model to represent the physical feature of the earth (Heiskanen and Moritz, 1967). The geoid is emphasized in physical geodesy because it is referred to in geodetic measurements and it serves as a reference surface for the vertical system (Torge, 2001). The orthometric height (H), a geometric distance between the geoid and the earth's surface that follows along the curved plumb line, has traditionally been used as the vertical system in many countries. It has usually been measured by leveling, which has required an additional orthometric correction in order to transform the leveled height into the orthometric height and has taken much time and cost. More directly, the orthometric height can be determined by subtracting the geoid undulation (N) from the ellipsoidal height (h).

$$H = h - N \quad (1)$$

The geoid undulation is a height from a reference ellipsoid to the geoid; its direction is normal to the ellipsoid, and the ellipsoidal height as the sum of the orthometric height and the geoid undulation is defined by a distance from the ellipsoid to the earth's surface. It is a very simple and cost-efficient method if the ellipsoidal height and the geoid undulation are known. Ellipsoidal height is very accurately accessible through the Global Positioning System (GPS), but the geoid undulation still has limitations in terms of the precision and accuracy. Height system modernization in many countries is based on determining the orthometric height by GPS and a geoid model, instead of leveling, therefore there is a strong need for modeling an accurate geoid undulation for global or regional areas.

The development of a geoid model requires gravimetric measurements on or above the earth's surface, where key parameters are spatial extent, station separation and accuracy (Torge, 1989). The measurement of gravity is categorized according to absolute and relative, static and kinematic, or in terms of coverage. Absolute gravimeters observe two fundamental quantities, distance and time; on the other hand, relative gravimeters measure one of the fundamental quantities. The relative gravimeter has made it possible to measure more gravity stations efficiently. The absolute gravity value is determined from a relative gravimeter by calculating the difference between times or locations and tying in with the absolute gravity station. The static gravimeter is fixed on the earth's

surface, and it is more stable, but measurement points tend to be more irregularly distributed. On the other hand, kinematic gravimetry means that the gravimeter is attached on moving platforms, such as airborne or shipborne, and it is faster, more efficient, and points are more regularly distributed. Terrestrial, airborne, and satellite gravimetry will be introduced shortly as the typical measurements of gravity in accord with geodetic purposes such as geoid model determination.

As a static and relative approach, terrestrial gravimetry has been a very common and traditional method for regional and local gravity surveys since the development of static spring gravimeters. These measure the relative gravity point by point on the earth's surface, requiring only the accessibility of the station. The accuracy of terrestrial gravimetric data depends on errors in gravity measurement and uncertainties of the gravity reductions, which handle topographic masses above the geoid and a change of reference surface for measurements (Torge, 1989); thus the accurate three-dimensional position of the point as well as the gravity value is necessary. Generally nations have designed gravity control networks along roads or vertical control networks, and surveyed gravity and position then tied the measurements to absolute gravity stations. The airborne method, which is kinematic and relative, has been recently adopted to obtain gravity field information for regional areas. It is very suitable for large, inaccessible areas, such as mountains and coastlines. It provides relative gravity quantities at certain intervals of time along survey profiles. The accuracy of airborne data depends on errors in the position of aircraft and calibration parameters. The absolute gravity of airborne measurement is determined by connecting to ground control points.

Satellite systems have the advantage of acquiring more global and uniformly distributed data for the earth's static gravity field and/or its temporal variation. In particular, CHAllenging Minisatellite Payload (CHAMP), Gravity Recovery and Climate Experiment (GRACE), Gravity field and steady-state Ocean Circulation Explorer (GOCE) have been designed for measuring the earth's gravity field during the last couple of decades. The CHAMP mission had adopted Satellite-to-Satellite Tracking (SST) using the GPS in high-low mode, and measured perturbing accelerations caused by the earth's gravitation (Reigber et al., 2002). The GRACE mission, using SST of two identical satellites in low-low mode, had observed ranges and range rates between satellites and perturbing accelerations (Tapley et al., 2004). The most recent mission, GOCE, was mainly designed to measure the stationary gravity field of the earth and construct a very accurate geoid model; it measured the gravitational acceleration differences, called the gravity gradients using a gradiometer (Pail et al., 2010). Each satellite mission has a different type of sensor, measurement, resolution, and accuracy, but all have contributed to the generation of global or regional geoid models in the form of spherical harmonic coefficients.

Based on gravimetric measurements, a large number of geoid models for global or regional areas have been published. Two different types of solutions exist for the geodetic boundary value problem with gravimetric measurements as a boundary condition. One is the spherical harmonic expansion, which is useful for global representation, and the other is Stokes's integral, which has benefits for regional areas. During the last few decades,

Global Geopotential Models (GGMs) have been developed by several organizations, such as the Ohio State University (OSU), International Centre for Global Earth Models (ICGEM), and National Geospatial-Intelligence Agency (NGA); they have been used to represent the long wavelengths (low frequencies) of the gravity field for the entire earth. For example, the Earth Gravitational Model 1996 (EGM96) was developed to degree and order 360, and was used widely as a reference field to determine regional geoid models or to study the spectrum of the earth's gravitational field (Rapp and Pavlis, 1990, and Lemoine et al., 1998). Recently, the NGA published Earth Gravitational Model 2008 (EGM08) with maximum degree and order 2160, which included a GRACE-derived spherical harmonic coefficient model, ocean-wide altimetry-derived gravity anomalies, and additional terrestrial data. Compared with GPS/Leveling the estimated global accuracy of the model is 13.0 cm in geoid height (Pavlis et al., 2012). A consortium of institutes in Europe composed GOCO, a combination of GOCE data with complementary gravity field information. Since 2010, they have published the satellite-only gravity field model series, GOCO01S, GOCO02S and GOCO03S, based on the satellite missions such as GOCE and GRACE. GOCO01S is the model to degree and order 200, GOCO02S and GOCO03S are the updated versions with degree and order 250. The difference of latter two models is the durations of used GOCE mission data, which are 8 months for GOCO02S and 18 months for GOCO03S. The accuracy of GOCO02S compared to GPS/leveling is estimated at 6.8 cm in Germany, 11.5 cm in Japan, and 15.4 cm in Canada (Pail et al., 2010; Gioiginger et al., 2011). Also, the accuracy of GOCO03S estimated only in Germany is 5.5 cm (Mayer-Guerr et al., 2012). In addition, the European Space Agency (ESA) project GOCE High-level Processing Facility (HPF) computed gravity models using GOCE Satellite Gravity Gradiometry (SGG) data alone or combined with SST data such as GRACE in three different approaches. One of the models, called GO_CONS_GCF_2_DIR, was based on GOCE, GRACE, and LAser GEOdynamics Satellites (LAGEOS) (Pail et al., 2011). The details will be shown in Chapter 3. Regional geoid models have been developed in some countries; in particular, the United States, Canada, Australia, and the European Union have made continuous efforts to determine and improve the geoid model representing each country or region. The National Geodetic Survey (NGS) in the United States recently published the gravimetric geoid models, called UGSS2009 and UGSS2012, which were based on terrestrial gravity data, the Danish National Space Center 08 (DNSC08) altimetry-derived anomalies, and a Digital Elevation Model (DEM) from the Shuttle Radar Topography Mission (SRTM). The model took the accurate long-wavelength contents from GRACE through adopting EGM08, and finally had 5 cm accuracy with 1′ by 1′ resolution (Wang et al., 2011). National Resource Canada developed the Canadian gravimetric Geoid Model 2010 (CGG2010), and it used terrestrial and marine gravity measurements, DNSC08 altimetry-derived anomaly, and the Canadian Digital Elevation Data (CDED). They combined GOCO01S with EGM08 in order to acquire better long wavelength information of their territory. CGG2010 has 2′ by 2′ resolution and its accuracy was estimated from 2 to 10 cm in standard deviation (Huang et al., 2012). Geoscience Australia also published their latest gravimetric quasi-geoid model for Australia, called AUSGeoid09. The gravimetric component of the model used terrestrial gravity measurements, DNSC08 altimetry-derived anomalies, and the GEODATA-DEM9S Australian DEM. The model took the very high degree and order EGM08 model, so the

contribution of the actual measurements beyond EGM08 was quite small (Featherstone et al., 2010). The European Gravity and Geoid Project (EGGP), under IAG Commission 2, developed European Gravimetric Geoid (EGG) models and published them in 1997 and 2007. They gathered terrestrial and marine gravity data from the countries in Europe, and focused on merging all data sources with due the consideration of the reference datum. The latest EGG07 model was based on the terrestrial and marine gravity data, and the SRTM and Global 30 Arc-Second Elevation Data Set (called GTOPO30) (Denker et al., 2009). It included the European Improved Gravity model of the Earth by New technique GRACE- and LAGEOS-based combination gravity field model, EIGEN-GL04C, in order to represent the long wavelength contents of the gravity field of continental Europe. More details will be given in Chapter 5.

1.2 Statement of problem

Theoretical developments for a geoid model have been studied by many geodesists during the last century, but they have also exhibited practical or numerical problems when applied to real data. Ideally, Stokes's integral assumes integration over the entire earth with continuous anomalous gravity, called gravity anomaly, on the geoid with the additional condition that there is no mass above it (Hofmann-Wellenhof and Moritz, 2006). However, in practice the integral is reduced to a limited area and gravity anomalies exist discontinuously on or above the earth's surface. The gaps between theoretical and practical aspects incur several kinds of errors, which geodesists have tried to reduce. Those classical issues are related to modifying the computation and reduction methodologies optimally for the area of interest, which depend on the type or density of observations, topographical characteristics, and size of the area of interest. The latest research topics focus on handling heterogeneous data in order to combine all available observations optimally and produce more accurate geoid models. Moving platforms such as airborne, shipborne, and satellites are employed to measure the gravity field; moreover, global high resolution GGMs and topographic models are now available. Thus new research is demanded in order to understand the characteristics of different measurement types, develop reductions from the measurement surfaces, analyze spectral contents, and finally unify all possible data. In addition, it is known that additional gravimetric measurements are needed for precise geoid computation beyond even the very high degree and order GGMs. For example, recently published EGM08 has 5 arcmin spatial resolution and globally 13.0 cm uncertainty as described in the previous section. Such models are not sufficient for the requirements of higher spatial resolution and greater accuracy such as 1 cm or 5 cm, which means that additional gravity measurements are needed.

In this dissertation, all practical computations are done for South Korea, which is a limited area with 5 deg by 5 deg in latitude and longitude. The territory of South Korea includes mountains over 1,500 m in elevation and a thousand islands, meaning a

complicated topography, and its west half is relatively smoother than the east half. South Korea's government has continually made an effort to acquire gravity measurements for the territory during the last two decades. Due to the topography, more terrestrial gravity measurements are regularly located on the west half than the other, where measurements usually follow vertical control networks or roads. In 2008 and 2009, an airborne gravity survey was conducted for the territory including all coastal areas. The airborne gravity measurements are very regularly distributed over the entire territory, but they are measured at about 3,000 m altitude.

Terrestrial and airborne measurements do not seem to be consistent; thus it is very critical to determine the cause of the inconsistency. Both data sets are considered with respect to reduction from the measurement surfaces in order to satisfy the boundary conditions for Stokes's integral as well as generate a unified dataset. In order to develop the most accurate geoid model, we need to choose the optimal long-wavelength field model from an existing GGM, as well as modify Stokes's integral in order to reduce the truncation error incurred by limitation to data in the relatively small area of South Korea. This dissertation will investigate the development of a regional gravimetric geoid model for South Korea based on gravity data on the terrestrial surface as well as data newly measured by an airborne gravimeter, and analyze the contributions of the latter, particularly with respect to the recent GGMs which were developed without the airborne gravity data of South Korea.

1.3 Objectives and chapter description

The purpose of this dissertation is to determine a regional gravimetric geoid model using heterogeneous data. The detailed objectives are listed here. The first objective is to develop a geoid model for South Korea, and demonstrate the accuracy of the regional geoid model using additional measurements when it is compared to the recently published very high degree geopotential model. EGM08 has 5 arcmin (about 9 km) spatial resolution and as high as 6.0 cm uncertainty for the geoid undulations by GPS/leveling in South Korea. It is a quite good accuracy compared to 13.0 cm uncertainty for globally distributed geoid undulations, which are determined by GPS/leveling and confined to only land area (Pavlis et al., 2012). However, higher spatial resolution and better accuracy, such as 1 cm or 5 cm, for the regional geoid model are needed for many reasons. Therefore, this analysis will be compared to a geoid model over South Korea, which is developed by using additional gravimetric measurements, and show a possible improvement on the accuracy.

The second objective concerns the reduction issues, which are related to the reference surface and the masses above the geoid. Two conditions are required in order to use Stokes's integral as a computation method for geoid height. As a boundary condition, all measurements are located on the geoid and no mass should be above this surface. In reality, however, the measurements are located on or above the earth's surface and

masses exist above the geoid, requiring consideration of gravity reductions like terrain corrections and downward continuations in order to satisfy both boundary conditions.

The third objective is the development of an optimal methodology for combining heterogeneous data, which include satellite, airborne, terrestrial gravimetric data, and a high resolution digital terrain model. Because these data have different features, like spatial resolutions, accuracies, measurement surfaces, and related reduction issues, methodologies are needed to combine them optimally in order to achieve the goal accuracy for the geoid model and to analyze the contribution of additional measurements (e.g., airborne gravimetry). In particular, it is very critical to verify the consistency between terrestrial and airborne and merge these two dataset together in order to ensure that they represent the same gravitational field.

The fourth objective is to modify Stokes's kernel function and determine the integration area for geoid computation in order to minimize the truncation error associated with the limited integration area and the discontinuity of the data (Featherstone, 2013). In addition, the maximum degree of GGMs, describing the long wavelength information of the gravity field for a regional area, should be determined to combine them with the gravity data in the region. Various studies have proven that the accuracy of geoid undulations based on locally distributed data depends practically on the kernel function, the size of integral area, and the maximum degree and accuracy of reference GGMs (Wang et al., 2011; Huang et al., 2012; Featherstone et al., 2010). Therefore, the optimal choice among them should be determined for South Korea.

The fifth objective is to verify or reduce approximation errors and side effects incurred during the development of geoid model. Stokes's integral is based on anomalous gravity values as boundary condition and the boundary is the geoid surface. It includes many approximations such as linearization, simplifications of directional derivatives, and approximating the boundary as a sphere. Their effects on the regional area are expected to be small and negligible, but still should be considered.

Chapter 2 introduces the details of the basic theories for the geoid model computation and the methodologies for the measurement reduction. Chapter 3 describes the gravimetric measurements, the global geopotential model and high resolution topographic model, which are used in this dissertation, and includes possible and reliable combination methods of gravimetric measurements considering the topographic reduction and the analytic continuation. In Chapter 4, the kernel modification method and the Remove-Compute-Restore (RCR) technique, which are concerned with overcoming the limitations of Stokes's integral, are introduced and verified with simulated and actual data. Chapter 5 reviews regional geoid models developed in several nations, and compares them with the developed geoid model for South Korea, which is also verified by comparing it with EGM08 as well as GPS/leveling geoid undulations. Chapter 6 summarizes the results of this study and proposes future work.

CHAPTER 2 THEORETICAL BACKGROUND OF GEOID DETERMINATION

This chapter focuses on introducing the theories belonging to the determination of the geoid undulation. Section 2.1 describes the geodetic boundary value problem, how we solve it in order to determine the gravity potential and ultimately estimate the geoid undulation. Section 2.2 summarizes the well-known computation formula, which is called Stokes's integral, for the geoid undulation based on the gravity measurement. Section 2.3 considers the various effects of approximations incurred during the development of the theoretical relationship between gravity data and the geoid undulation. Section 2.4 describes the reduction methods applied to the actual measurements so that they satisfy the boundary condition for Stokes's integral, also explains harmonic continuation methodologies and how they are applied in the reductions. Finally Section 2.5 introduces the Remove-Compute-Restore (RCR) technique that is required in order to include the low frequency gravity field of the earth, and it summarizes the geoid modeling considering all reductions and corrections with proper equations.

2.1 Geodetic Boundary Value Problem and Bruns' equation

The geoid undulation is the height from a reference ellipsoid to the geoid, and its determination starts from defining both surfaces. The geoid is a continuous equipotential surface of the gravity potential such that it closely approximates mean sea level, and it is perpendicular to the direction of gravity. The potential on the geoid is denoted

$$W = W_0 \tag{2}$$

where the gravity potential is the resultant of gravitational and centrifugal potentials, and W_0 indicates a constant. The gravitational potential (V) is due to the mass attraction of the earth, and the centrifugal potential (Φ) is caused by the rotation of the earth.

The reference ellipsoid is chosen to represent the earth with the normal gravity potential, U. Defining normal gravity potential makes it easy to handle the gravity potential mathematically because the residual between the actual and normal gravity field, called disturbing potential, T, is a quite small. At an arbitrary point, P, the disturbing potential is

$$T_P = W_P - U_P \quad (3)$$

The disturbing potential outside of the earth satisfies Laplace's equation, which means the Laplace operator (Δ) applied to T is zero, because the centrifugal potentials are cancelled and it is assumed to be a mass-free area.

$$\Delta T = \nabla^2 T = 0 \quad (4)$$

The Geodetic Boundary Value Problem (GBVP) refers to the problem of determining the earth's physical surface and exterior gravity field from geodetic measurements such as gravity and potential difference (Moritz, 1980; Torge, 2001). Depending on the given boundary condition, the classical GVBP is one of three kinds; the first is Dirichlet's problem if the given boundary values are the potential. The second is Neumann's problem if the normal derivative of the potential is given. If the boundary value is a linear combination of potential and its normal derivative, the GBVP is called Robin's problem. The classical solution of GBVP is given in the form of spherical harmonic expansions or integral formulas, if the boundary is a sphere (Heiskanen and Moritz, 1967)

The disturbing potential relates to the geoid undulation based on a linearization, as follows. The normal gravity potential, U_P, in Equ (3) is extended from the normal gravity potential at the corresponding point, Q, on the reference ellipsoid by Taylor series expansion. And then, Equ (3) becomes

$$W_P = T_P + \left[U_Q + \frac{\partial U_Q}{\partial h}\Big|_{P=Q} h + \frac{1}{2}\frac{\partial^2 U_Q}{\partial h^2}\Big|_{P=Q} h^2 + \cdots \right] \quad (5)$$

where h is a distance from P and Q, and indicates the geoid undulation, N. If only the first derivative of the normal gravity potential is considered, it is replaced by the magnitude of normal gravity on the ellipsoid, $-\gamma_Q$, which is directly perpendicular to the ellipsoid.

$$N = \frac{T_P}{\gamma_Q} - \frac{(W_P - U_Q)}{\gamma_Q} \quad (6)$$

W_P equals W_0 on the geoid surface. Often an assumption is made that the normal gravity potential on the reference ellipsoid, U_Q, is equivalent to W_P. Then Equ (6) is simplified

$$N = \frac{T_P}{\gamma_Q} \quad (7)$$

Equ (6) is the generalized or extended Bruns's equation; Equ (7) is called Bruns's equation. They show the relation between the disturbing potential and the geoid undulation.

2.2 Determination of geoid undulation

The gravity anomaly is defined and used as a boundary condition in order to model the disturbing potential and geoid undulation. In Section 2.2 and 2.3, it is assumed that the gravity anomaly refers to the geoid surface and there is no mass above the surface. The assumptions are related to reduction problems which will be dealt with in Section 2.4.

2.2.1 Gravity anomaly

The gravity anomaly (Δg) is a difference between magnitudes of gravity, g, at P on the geoid, and normal gravity, γ, at Q on the reference ellipsoid. The magnitude of normal gravity, γ, is computed by Somigliana's formula (Heiskanen and Moritz, 1967).

$$\gamma = \frac{a\gamma_a cos^2\varphi + b\gamma_b sin^2\varphi}{\sqrt{a^2 cos^2\varphi + b^2 sin^2\varphi}} \quad (8)$$

where a, b are semi- major and minor axes of the ellipsoid, and γ_a, γ_b are normal gravity at the equator and the pole of the ellipsoid, respectively. The gravity anomaly has traditionally been adopted as the boundary value to model the disturbing potential, and ultimately the geoid undulation, which is Stokes's integral. We have,

$$\Delta g = g_P - \gamma_Q = -\frac{\partial W_P}{\partial n} + \frac{\partial U_Q}{\partial h} \quad (9)$$

where the directions of derivatives are along the normal to ellipsoid (h) and to the geoid (n). The gravity anomaly is simplified by approximations and assumptions; first, the direction of the normal to the geoid is approximated by the normal to the ellipsoid:

$$\Delta g = -\frac{\partial W_P}{\partial h} + \frac{\partial U_Q}{\partial h} \quad (10)$$

A Taylor series expansion of normal gravity, γ, is:

$$\gamma_P = \gamma_Q + \frac{\partial \gamma_Q}{\partial h}\Big|_{P=Q} h + \frac{1}{2}\frac{\partial^2 \gamma_Q}{\partial h^2}\Big|_{P=Q} h^2 + \cdots \quad (11)$$

The Taylor series expansion is inserted into Equ (9), and where the first approximation is used.

$$\frac{\partial W_P}{\partial n} \cong \frac{\partial W_P}{\partial h} \left(also, \gamma_P \cong \frac{\partial U_P}{\partial h}\right) \quad (12)$$

Then,

$$\Delta g = g_P - \left(\gamma_P - \left.\frac{\partial \gamma_Q}{\partial h}\right|_{P=Q} h - \frac{1}{2}\left.\frac{\partial^2 \gamma_Q}{\partial h^2}\right|_{P=Q} h^2 - \cdots \right)$$
$$= -\frac{\partial W_P}{\partial h} + \frac{\partial U_P}{\partial h} + \left.\frac{\partial \gamma_Q}{\partial h}\right|_{P=Q} h + \frac{1}{2}\left.\frac{\partial^2 \gamma_Q}{\partial h^2}\right|_{P=Q} h^2 + \cdots$$

(13)

Second, only the normal gravity and its first derivative are considered. Third, the gravity potential at P is assumed to be equivalent to the normal gravity potential at Q when Bruns's equation is applied, (of course W_P is constant):

$$\Delta g = -\frac{\partial T_P}{\partial h} + \left.\frac{1}{\gamma_Q}\frac{\partial \gamma}{\partial h}\right|_{P=Q} T_P \qquad (14)$$

This, called the fundamental equation of physical geodesy, is the boundary condition of Robin's problem because it is in the form of a linear combination of potential and its normal derivative. Furthermore, if the derivative along the normal to the ellipsoid is approximated as the radial derivative and normal gravity is approximated as shown,

$$\frac{\partial}{\partial h} \approx \frac{\partial}{\partial r}, \gamma \approx \frac{GM}{r^2}, then\ \frac{\partial \gamma}{\partial h} \approx -2\frac{\gamma}{r} \qquad (15)$$

Then the fundamental equation of the physical geodesy is simplified as

$$\Delta g = -\frac{\partial T}{\partial r} - \frac{2}{r}T \qquad (16)$$

The effects, caused by all these approximations and assumptions on the gravity anomaly will be given in Section 2.3.

2.2.2 Stokes's integral

The disturbing potential at an arbitrary point satisfying the Laplace's equation is given by Pizzetti's formula using the gravity anomaly as a boundary condition on the sphere (Heiskanen and Moritz, 1967):

$$T_P = \frac{R}{4\pi}\iint_\sigma \Delta g(\theta', \lambda') S(\psi) d\sigma \qquad (17)$$

Pizzetti's formula assumes, first, the total mass difference between the geoid (earth) and ellipsoid is zero which makes the zero-degree harmonic equal to zero. Second, it assumes the coordinate origin is at the center-of-mass, then the first-degree harmonics are also zero. There is a significant approximation here, as well, namely the spherical approximation that 1) assumes the integration surface, the geoid is a sphere, and 2) that the spherical form of the fundamental equation of phsycial geodesy is used. $S(\psi)$ is called Stokes's function,

$$S(\psi_{PQ}) = \sum_{n=2}^{\infty} \frac{2n+1}{n-1} P_n(cos\psi_{PQ}) \quad (18)$$

where P is the computation point, Q is the integration point over unit sphere, σ, and P_n is Legendre's polynomial. The ψ_{PQ} is the central angle between P and Q computed by

$$cos\psi_{PQ} = cos\theta_P cos\theta_Q + sin\theta_P sin\theta_Q cos(\lambda_Q - \lambda_P) \quad (19)$$

Stokes's function is also expressed in

$$S(\psi_{PQ}) = \frac{1}{sin\psi_{PQ}} - 6sin\frac{\psi_{PQ}}{2} + 1 - cos\psi_{PQ}\left(5 + 3\,ln\left(sin\frac{\psi_{PQ}}{2} + sin^2\frac{\psi_{PQ}}{2}\right)\right) \quad (20)$$

Pizzetti's formula is combined with Bruns's equation, and then the geoid undulation is determined by

$$N_P = \frac{R}{4\pi\gamma_Q}\iint_{\sigma} \Delta g(\theta', \lambda') S(\psi) d\sigma \quad (21)$$

This is Stokes's integral which shows that the geoid undulation is computed by an integral over the entire sphere with continuous gravity anomaly on it. It is noted that the disturbing potential should satisfy Laplace's equation above the geoid and that the gravity anomaly is given on the geoid. In other words, there is no mass above the surface on which the gravity anomaly is located.

By the assumptions, which are that zero and first degree harmonics are zero, the geoid undulation computed by Stokes's integral refers to the ellipsoid that fits best to the global geoid and is called the best fitting ellipsoid, not a priori defined ellipsoid. Also, Stokes's integral assumes that the gravity potential on the geoid is equivalent to the normal gravity on the ellipsoid. Therefore, for an arbitrary and defined ellipsoid, the extended Bruns's equation should be combined with Pizzetti's formula. The geoid undulation with respect to this ellipsoid then includes a constant, called N_0. Usually N_0 is determined by the spherical harmonic model for the disturbing potential and satellite altimetry (Bursa et al., 1999). In general (Heiskanen and Moritz, 1967)

$$N_0 = \frac{1}{\gamma}\frac{G\delta M}{R} - \frac{1}{\gamma}\delta W \quad (22)$$

where G is the gravitational constant, δM is difference of mass between the geoid and the ellipsoid, δW is difference between gravity potential on the geoid and normal gravity potential on the ellipsoid. By defining the reference ellipsoid such as $\delta M = 0$, then N_0 only includes the second term in Equ (22). Moreover, if $\delta W = 0$, then N_0 would be zero.

2.3 Systematic effects

The approximations made in the previous section affect the gravity anomaly, and consequently the geoid undulation estimated by Stokes's integral. The errors or corrections are expected to be small and negligible for a regional or local area, but they are systematic and still worthy of consideration. The directional derivative, linear, and spherical approximations and the atmospheric and ellipsoidal corrections are depicted in this section.

2.3.1 Atmospheric correction

The atmospheric effect has to be removed from the gravity anomaly defined by Equ (9). The normal gravity is defined by semi-major axis of the ellipsoid (a), geocentric gravitational constant of the earth (GM), dynamical form factor of the earth (J_2), and angular velocity of the earth (ω). Among them, GM includes the atmosphere, so that the atmosphere correction, δg_A, should be added to the measured gravity (Rapp and Pavlis, 1990), which accounts for the attraction of atmospheric masses above the measurement point as if they are below, as assumed for the normal gravity (spherically layered atmosphere).

$$\delta g_A[mgal] = 0.8658 - 9.727 \times 10^{-5} H[m] + 3.482 \times 10^{-9} H^2[m^2] \qquad (23)$$

2.3.2 Directional Derivative error

As first approximation in Section 2.2, the derivative of the gravity potential with respect to the plumb line is approximated by the derivative with respect to the perpendicular to the ellipsoid. Equs (10) and (9) show the approximation, and the directional derivative error is estimated by the difference.

$$\varepsilon_{\Delta g}^{(dir.dev)} = \frac{\partial W_P}{\partial h} - \frac{\partial W_P}{\partial n} \qquad (24)$$

In this section, ε is an error on the indicated subscript and incurred by the superscript. The derivative with respect to the plumb line is related to the derivative with respect to the normal to the ellipsoid according to

$$\frac{\partial}{\partial n} = cos\Theta \frac{\partial}{\partial h} + \xi \frac{\partial}{\partial s_\theta} + \eta \frac{\partial}{\partial s_\lambda} \qquad (25)$$

where Θ is the total deflection of the vertical with north and east components, ξ and, η respectively, and, s_θ and s_λ are distances in the north and east directions (Jekeli, 1981). Combing Equs (25) to (24), the directional derivative error is

$$\varepsilon_{\Delta g}^{(dir.der.)} = (1 - cos\Theta)\frac{\partial W_P}{\partial h} - \xi\frac{\partial W_P}{\partial s_\theta} - \eta\frac{\partial W_P}{\partial s_\lambda} \quad (26)$$

where $-\frac{\partial \mathrm{W}_P}{\partial \mathrm{h}} \cong g_P \cong \gamma_P$. If the gravity potential is replaced by the sum of disturbing and normal gravity potentials, the derivative of the normal gravity potential with respect to distance in longitude is zero because it depends only on the latitude. Then

$$\varepsilon_{\Delta g}^{(dir.der.)} \approx \frac{1}{2}(\xi^2 + \eta^2)\gamma - \xi\left(\frac{\partial U}{\partial s_\theta} + \frac{\partial T}{\partial s_\theta}\right) - \eta\frac{\partial T}{\partial s_\lambda} \quad (27)$$

Here, it is assumed that the total deflection of the vertical is quite small. The derivatives of T are replaced by the components of the deflection of the vertical multiplied by the normal gravity, and then

$$\begin{aligned}\varepsilon_{\Delta g}^{(dir.der.)} &= \frac{1}{2}(\xi^2 + \eta^2)\gamma - \left(\xi\frac{\partial U}{\partial s_\theta} + \xi^2\gamma\right) - \eta^2\gamma \\ &= -\frac{1}{2}(\xi^2 + \eta^2)\gamma - \xi\frac{\partial U}{\partial s_\theta}\end{aligned} \quad (28)$$

The second term in Equ (28), the derivative of the normal gravity potential with respect to the north distance is

$$\frac{\partial U}{\partial s_\theta} = \frac{\partial}{r\partial\theta}U(r,\theta) = \frac{GM}{r^2}\sum_{n=1}^{\infty}\left(\frac{a}{r}\right)^{2n}\sqrt{\frac{n(2n+1)}{4n+1}}J_{2n}\bar{P}_{2n,1}(cos\theta) \quad (29)$$

where GM is the gravitational constant of the earth, a is the semi-major axis of the ellipsoid, and $\mathrm{J}_{2\mathrm{n}}$ are spherical harmonic coefficients of the normal gravitational potential.

2.3.3 Linear approximation error

When the normal gravity potential at P was substituted with a Taylor series expansion with respect to the point, Q, only the linear terms for the potential and the normal gravity were considered in the derivations of Bruns's equation and the fundamental equation of the physical geodesy. The ignored higher order derivatives generate the linear approximation errors on the geoid undulation and the gravity anomaly, but only the second order derivative is considered in computing this error because third and higher order derivatives are very small. From Equs (6) and (5), the linear approximation error on the geoid undulation is

$$\varepsilon_N^{(lin.approx.)} = \frac{1}{2\gamma_Q}\frac{\partial\gamma}{\partial h}\Big|_Q N^2 \quad (30)$$

The linear approximation error on the geoid undulation is simply estimated by using the spherical approximation, Equ (15). It is less than 0.5 mm if the geoid undulation reaches

to 50 m. For the derivation of the fundamental equation of the physical geodesy, the linear approximation error in the gravity anomaly is the difference between Equs (14) and (13).

$$\varepsilon_{\Delta g}^{(lin.approx.)} = -\frac{1}{2}\left(\frac{\partial^2\gamma}{\partial h^2}\Big|_Q - \frac{1}{\gamma_Q}\left(\frac{\partial\gamma}{\partial h}\Big|_Q\right)^2\right)\left(\frac{T_P}{\gamma_Q}\right)^2 \quad (31)$$

2.3.4 Spherical approximation error

The fundamental equation of the physical geodesy in spherical approximation assumes that the derivative along the ellipsoid normal is the same as the derivative along the radial direction. The error is denoted as

$$\varepsilon_{\Delta g}^{(sphere.approx.)} = \Delta g^{(sphere.approx.)} - \Delta g \quad (32)$$

This is the difference between Equs (16) and (14). The first term on the right side in Equ (14) can be written using

$$\frac{\partial}{\partial h} = \frac{\partial}{\partial r} - e^2 sin\theta cos\theta \frac{\partial}{r\partial\theta} \quad (33)$$

where e is the first eccentricity of the ellipsoid. The second term in Equ (14) is simply replaced by

$$\frac{1}{\gamma}\frac{\partial\gamma}{\partial h} = -\frac{2}{r}\left(1 - 3J_2\left(\frac{a}{r}\right)^2 P_2(cos\theta) + \frac{3\omega^2 r^3}{2GM} sin^2\theta\right) \quad (34)$$

J_2 is the dynamical form factor of the earth and ω is the angular velocity of the earth. Then, Equ (14) with Equs (33) and (34) becomes

$$\Delta g = -\frac{\partial T}{\partial r} + e^2 sin\theta cos\theta \frac{\partial T}{r\partial\theta} - \frac{2}{r}T + \frac{6}{r}J_2\left(\frac{a}{r}\right)^2 P_2(cos\theta)T - \frac{3\omega^2 r^2}{GM} sin^2\theta T \quad (35)$$

Finally, Equ (32) is determined with Equs (16) and (35).

$$\varepsilon_{\Delta g}^{(spher.appox.)} = -e^2 sin\theta cos\theta \frac{\partial T}{r\partial\theta} - \left(6J_2\frac{a^2}{r^3}P_2(cos\theta) - \frac{3\omega^2 r^2}{GM} sin^2\theta\right)T \quad (36)$$

2.3.5 Ellipsoidal correction

The boundary, assumed as the sphere, more accurately should be an ellipsoid. This spherical approximation is corrected by the so-called ellipsoidal correction, which is added to the geoid undulation determined by Stokes's integral derived under the spherical approximation. Fei and Sideris (2000) gave a nice review of previous researches done by Molodensky et al. (1962), Moritz (1980), Martinec and Grafarend (1997), and derived an alternative ellipsoidal correction for the disturbing potential and then the geoid undulation through Bruns's equation:

$$N_P = N_P^{(0)} + e^2 N_P^{(1)} \tag{37}$$

where the first term on the right side, $N_P^{(0)}$, is computed by the Stokes's integral under the spherical approximation, and the second term called the ellipsoidal correction is determined by

$$N_P^{(1)} = N_P^{(11)} + \frac{1}{4\pi}\iint_\sigma N^{(0)}(Q) K\left(\psi_{PQ}, \theta_P, \theta_Q\right) d\sigma \tag{38}$$

$N_P^{(1)}$ is the resultant of $N_P^{(11)}$ and an integral of $N_P^{(0)}$ with kernel $K\left(\psi_{PQ}, \theta_P, \theta_Q\right)$. $N_P^{(11)}$ consists of $N_P^{(0)}$ and low-degree geopotential coefficients of the disturbing potential:

$$N_P^{(11)} = \left(\frac{1}{2} sin^2\theta_P - \frac{1}{3}\right) N_P^{(0)}$$

$$-\frac{GR}{\gamma_0}\left(\frac{\sqrt{5}}{15} C_{2,0} + cos\theta_P \frac{3\sqrt{7}}{35} C_{3,0} + sin\theta_P \frac{\sqrt{42}}{35}\left(C_{3,1} cos\lambda_P + C_{3,-1} sin\lambda_P\right)\right) \tag{39}$$

where γ_0 is an average value of gravity, $C_{n,m}$ are the unit-less harmonic coefficients of the disturbing potential. Also the kernel, a simplified version of $K\left(\psi_{PQ}, \theta_P, \theta_Q\right)$ (under the assumption $K\left(\psi_{PQ}, \theta_P, \theta_Q\right) \ll 1$), is given by

$$K\left(\psi_{PQ}, \theta_P, \theta_Q\right) \approx \frac{3cos^2\theta_P - sin^2\theta_P cos^2\alpha_{PQ} - \frac{3}{2} sin2\theta_P cos\alpha_{PQ}}{\psi_{PQ}} \tag{40}$$

The detailed derivations are given in Fei and Sideris (2000). The ellipsoidal correction ($e^2 N_P^{(1)}$) is expected to be very small because the flattening of the ellipsoid is only about 0.003, but it is significant. However, higher-order effects can be neglected (Heiskanen and Moritz, 1967; Fei and Sideris, 2000).

2.4 Reductions

The boundary for Stokes's integral must satisfy the conditions that it is free of mass in the exterior and that the gravity anomalies are located on it (Heiskanen and Moritz, 1967). In reality, masses exist between the geoid and the earth's physical surface, and also gravity is measured on or above the earth's surface. The gravity reduction handles the masses above the geoid and transfers gravity values to the geoid.

2.4.1 Topographic effects

Topographic masses exist between the geoid and the measurement surface. These masses must be completely removed and relocated on or under the geoid. The topographic masses above the geoid generate a gravitational potential according to Newton's density integral with a constant density (ρ), and the negative vertical derivative of the potential is the corresponding gravitational attraction. In this chapter, two well-known methods are introduced to handle the topographic masses above the geoid: Bouguer reduction and Helmert's second condensation. While the purpose of the Bouguer reduction is to completely remove the topographic masses above the geoid (Heiskanen and Moritz, 1967), Helmert's second condensation method condenses them into the geoid in the form of an infinitely thin layer (Heck, 2003). Both reductions guarantee that Laplace's equation is satisfied outside the geoid. Instead of the full topography above the geoid, also a long-wavelength elevation surface is considered with respect to which the residual topography enters in the reductions. This process has the advantage of preventing the subtraction of duplicate topographic effects when the Global Geopotential Model (GGM) is applied to the geoid computation in the Remove-Compute-Restore procedure (Forsberg, 1994).

The effect caused by the regional topography contributes to the short wavelength information of the gravity field, so removing or modeling of the topographic effect smooth the gravity measurements (Jekeli and Serpas, 2003; Huang and Veronneau, 2005). The local topographic reductions also tend to remove the correlation between the free-air anomalies and height. In this section, the equations of each reduction method are summarized. The Bouguer reduction and Helmert's second condensation follow the study of Jekeli and Serpas (2003), and the RTM method follows the study of Forsberg (1994). Consider the following geometry; P is the evaluation point and P_0 is the projection of P onto the earth's surface. Also Q is the integration point and Q_0 is defined as the radial projection of Q onto the level surface of P_0. They all are described in a spherical coordinate system, and the distance, l, between two points , (r, θ, λ) and (r', θ', λ') is

$$l^2 = r^2 + r'^2 - 2rr'cos\psi \qquad (41)$$

r is a sum of the radius of the geoid, R, and the height, h, above the geoid (Figure 1).

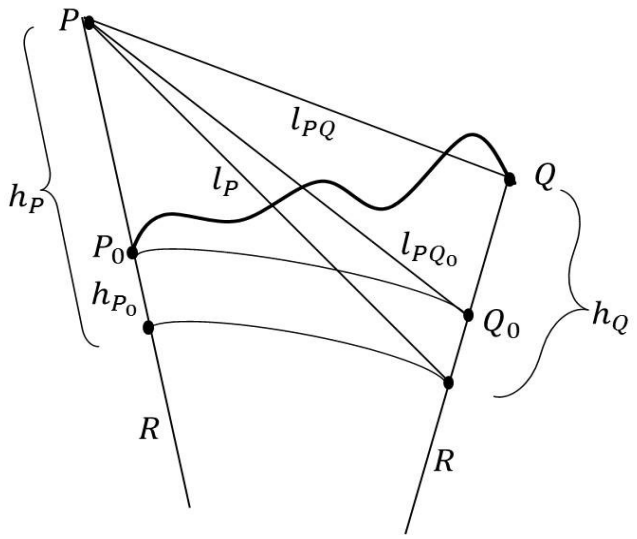

Figure 1. The geometry for reduction methods

2.4.1.1 Bouguer reduction

The refined Bouguer reduction eliminates the gravitational effect of all masses (with assumed constant density) above the geoid surface from the observed gravity. The gravitational potential at P due to the masses is

$$\left(\delta V_{topo}\right)_P = G\rho \iiint_v \frac{dv}{l_{PQ'}} = G\rho R^2 \iint_\sigma \int_R^{R+h_Q} \frac{dr}{l_{PQ'}} d\sigma \qquad (42)$$

where G is Newton's gravitational constant and v is the volume of the topography. Here, an additional variable Q' is defined as an integration point within the mass distribution with vertical limits Q and Q_0. We may separate the masses into a Bouguer shell (δM_{shell}), which has a constant thickness (h_{P_0}), and a residual topography with respect to it.

$$\left(\delta V_{topo}\right)_P = \frac{G\delta M_{shell}}{r_P} + G\rho R^2 \iint_\sigma \int_{R+h_{P_0}}^{R+h_Q} \frac{dr}{l_{PQ'}} d\sigma \qquad (43)$$

where $\delta M_{shell} = 4\pi\rho h_{P_0} R^2 \left(1 + \frac{h_{P_0}}{R} + \frac{h_{P_0}^2}{3R^2}\right)$. The gravitational component of the topographic effect is defined by the negative vertical derivative of the potential.

$$\left(\delta g_{togo}\right)_P = -\frac{\partial\left(\delta V_{topo}\right)_P}{\partial r_P}$$

$$= \frac{G\delta M_{shell}}{r_P^2} + \frac{G\rho R^2}{r_P}\iint_{\sigma}\int_{R+h_{P_0}}^{R+h_Q}\frac{\partial}{\partial r_P}\left(\frac{r_{Q'}}{l_{PQ'}}\right)dr_{Q'}d\sigma$$

(44)

Then, the terrain effect at P is exactly computed by

$$\left(\delta g_{togo}\right)_P = \frac{G\delta M_{shell}}{r_P^2} + G\rho\frac{R^2}{r_P}\iint_{\sigma}\left(\frac{R+h_Q}{l_{PQ}} - \frac{R+h_{P_0}}{l_{PQ_0}}\right)d\sigma \quad (45)$$

where l_{PQ} and l_{PQ_0} are

$$l_{PQ} = \sqrt{r_P^2 + (R+h)^2 - 2r_P(R+h)cos\psi} \quad (46)$$

$$l_{PQ_0} = \sqrt{r_P^2 + (R+h_P)^2 - 2r_P(R+h_P)cos\psi} \quad (47)$$

Define another distance, l_P, between P and the radial projection of Q onto the sphere of radius, R:

$$l_P = \sqrt{r_P^2 + R^2 - 2r_P R cos\psi} \quad (48)$$

If l_{PQ} and l_{PQ_0} in Equs (46), (47) are replaced by the exact relations with l_P ,

$$l_{PQ} = \sqrt{\frac{R+h}{R}l_P^2 - \frac{h}{R}r_P^2 + h_P(R+h)} \quad (49)$$

$$l_{PQ_0} = \sqrt{\frac{R+h_P}{R}l_P^2 - \frac{h_P}{R}r_P^2 + h_P(R+h_P)} \quad (50)$$

Under several approximations (see the Appendix A), Equ (45) simplifies to

$$\left(\delta g_{togo}\right)_P = 4\pi G\rho h_{P_0} + G\rho\frac{R^2}{2}\iint_{\sigma}\frac{1}{l_P}\left(\frac{h_Q - h_{P_0}}{R} + \frac{1}{l_P^2}\left(h_P\left(h_Q - h_{P_0}\right) - \left(h_Q^2 - h_{P_0}^2\right)\right)\right)d\sigma$$

(51)

The Bouguer reduction, alone, generates a large change of gravitational potential, and ultimately geoid surface, thus creating an unacceptably large indirect effect.

2.4.1.2 Helmert's second condensation

Helmert's second condensation assumes that the topographic masses above the geoid after removal are condensed onto the geoid as an infinitely thin layer; thus this reduction only considers the residual between the removed (δg_{topo}) and the restored (δg_{layer}) effects.

$$(\delta\Delta g)_P = \left(\delta g_{layer}\right)_P - \left(\delta g_{topo}\right)_P \qquad (52)$$

The potential caused by the surface layer, which has surface density $k(\theta,\lambda) = \rho h(\theta,\lambda)$, is derived similar to Equ (42).

$$\left(\delta V_{layer}\right)_P = G\rho R^2 \iint_\sigma \frac{h_Q}{l_P} d\sigma \qquad (53)$$

The potential can also be separated into the effect of a spherical layer of uniform surface density, ρh_P, and the residual effect with respect to it.

$$\left(\delta V_{layer}\right)_P = \frac{G\delta M_{sheet}}{r_P} + G\rho R^2 \iint_\sigma \frac{h_Q - h_{P_0}}{l_P} d\sigma \qquad (54)$$

where $\delta M_{sheet} = 4\pi R^2 \rho h_{P_0}$. The gravitational component of the topographic effect is the negative vertical derivative, so it is exactly estimated by

$$\left(\delta g_{layer}\right)_P = -\frac{\partial\left(\delta V_{layer}\right)_P}{\partial r_P} = \frac{G\delta M_{sheet}}{r_P^2} - G\rho\frac{R^2}{2r_P}\iint_\sigma \left(h_Q - h_P\right)\left(\frac{R^2 - r_P^2}{l_P^3} - \frac{1}{l_P}\right) d\xi \qquad (55)$$

Then the effect of a reduction by the Helmert's second condensation, Equ (52), is exactly computed by Equs (45) and (55).

$$\delta\Delta g(x_P) = -\frac{4\pi GRh_P^2\left(1 + \frac{h_P}{3R}\right)}{r_P^2} - G\rho\frac{R^2}{r_P}\iint_\sigma \left(\frac{h_Q - h_P}{2}\left(\frac{R^2 - r_P^2}{l_P^3} - \frac{1}{l_P}\right) + \left(\frac{R + h_Q}{l_{PQ}} - \frac{R + h_P}{l_{PQ_0}}\right)\right) d\xi \qquad (56)$$

Similar to the Bouguer reduction given in Equ (51), the effect of a reduction by the Helmert's second condensation is approximately determined by (see Appendix A)

$$\delta\Delta g(x_P) \approx G\rho\frac{R^2}{2}\iint_\sigma \frac{h_Q^2 - h_P^2}{l_P^3} d\xi \qquad (57)$$

Since Helmert's second condensation restores topographic effects removed by the Bouguer reduction, its indirect effect on geoid undulation is comparatively small.

2.4.1.3 Residual Terrain Model

The Residual Terrain Model (RTM) only accounts for the residual topographic effect with respect to a smooth mean elevation surface. The formula for RTM is similar to Equ (45), but with respect to the mean surface (h_{ref})

$$(\delta g_{RTM})_P = G\rho \frac{R^2}{r^P} \iint_\sigma \left(\frac{R+h_Q}{l_{PQ}} - \frac{R+h_{Q_{ref}}}{l_{PQ_{ref}}} \right) d\sigma \qquad (58)$$

where $h_{Q_{ref}}$ is a reference hight at integral point, Q, l_{PQ} is given in Equ (46) and $l_{PQ_{ref}}$ is defined by

$$l_{PQ_{ref}} = \sqrt{r_P^2 + \left(R + h_{Q_{ref}}\right)^2 - 2r_P \left(R + h_{Q_{ref}}\right) cos\psi} \qquad (59)$$

The RTM has an advantage when we need to estimate or filter only the shorter wavelengths of the topographic effect with respect to the reference mean elevation surface. For example, if the geoid modeling includes a reference geopotential model through the Remove-Compute-Restore (RCR) principle and the reference geopotential model includes the long-wavelength topographic effect. We can then use the RTM in order to include the terrain effects without a duplicate accounting of the longer wavelengths of the topography. The terrain effect with respect to the RTM decreases in magnitude as the resolution or detail of the reference surface increases (Forsberg, 1984). This means that errors in modeling the terrain effect are also reduced. The mean or reference elevation surface (h_{ref}) usually refers to the spatial resolution of maximum degree (n_{max}) of the reference geopotential model (Forsberg, 1994).

2.4.2 Indirect effect

Changing the masses above the geoid generates effects on the gravitational potential and its derivatives, called the direct effect, and on the geoid as well, which is called the indirect effect. In other words, the indirect effect is the difference between the geoid, which should be determined, and the co-geoid that is computed from the gravity anomaly with applied topographic reduction. Moreover, Stokes's integral should be applied to the gravity anomaly on the co-geoid not on the geoid because of the indirect effect, so that the gravity anomaly on the geoid should be again reduced to the co-geoid. This is called the secondary indirect effect on the gravity anomaly.

The geoid undulation relates to the co-geoid undulation by

$$N_{geoid} = N_{co-geoid} + \delta N \qquad (60)$$

where $N_{co-geoid}$ is a distance from the ellipsoid to the co-geoid surface, and δN is the indirect effect, given with Bruns's equation by

$$\delta N = \frac{\varepsilon_T^{(ind.eff.)}}{\gamma} \qquad (61)$$

$\varepsilon_T^{(ind.eff.)}$ is the change of potential caused by changing the masses, so it depends on the reduction method. Generally, gravity reductions must be done so as to minimize the indirect effect when they are used to model the geoid undulation. Bouguer's reduction creates a large indirect effect because the effect of the total mass above the geoid is completely removed from the actual measurement. On the other hand, Helmert's second condensation has less indirect effect because it redistributes the masses onto the geoid as an infinite layer. Thus, Helmert's gravity anomaly is generally used to develop a geoid model rather than the Bouguer gravity anomaly (Heck, 2003; Jekeli and Serpas, 2003). For Helmert's second condensation, the indirect effect is (Wichiencharoen, 1982)

$$\delta N = -\frac{\pi G \rho h_P^2}{\gamma} - \frac{G\rho R^2}{6\gamma} \iint_\sigma \frac{h_Q^3 - h_P^3}{l^3} d\sigma \qquad (62)$$

The secondary indirect effect is a difference of gravity anomalies on geoid and co-geoid surfaces, and it is based on a simple first order analytic continuation in free air

$$\varepsilon_{\Delta g}^{(sec.ind.eff.)} = \Delta g_{geoid} - \Delta g_{co-geoid} \approx \frac{\partial \gamma}{\partial h} \delta N \approx -\frac{2}{R} \gamma \delta N \qquad (63)$$

2.4.3 Analytic continuation

The solution of Laplace's equation is a harmonic function, and every harmonic function is analytic. It means that the function is continuous and has continuous derivatives of any order in the area where the function satisfies Laplace's equation. The disturbing potential exterior to the surface enclosing all masses is harmonic, also $r\Delta g$ in spherical approximation is harmonic because it also satisfies Laplace's equation. Any harmonic function can be expanded into a Taylor series or extended by another analytical method such as Poisson's integral. The harmonic or analytic continuation is useful for reducing or relocating the gravity anomaly where it satisfies Laplace's equation, and combining measurements taken on difference surfaces, such as satellite orbit, airborne altitude, and on the topography. In this section, we introduce: Free-air reduction, Poisson's integral and Taylor series expansion methods.

2.4.3.1 Free-air Reduction

The gravity anomaly defined by Equ (9) indicates the gravity is on the geoid and the normal gravity refers on the reference ellipsoid. The classical free-air reduction simply reduces the gravity at the earth's surface to the geoid by analytic continuation. It is premised on the assumption that the space above the geoid is mass-free. The free-air gravity anomaly is

$$\Delta g_{geoid}^{Free-air} = \left(g_P - \frac{\partial g}{\partial H}H - \cdots\right) - \gamma_Q \qquad (64)$$

where P is on the measurement surface, Q is the corresponding point on the reference ellipsoid, and H is an orthometric height. If only the first derivative is considered, and it is approximated by an average value of the first derivative of normal gravity with respect to the normal to the ellipsoid, then that free-air reduction is

$$F = -\frac{\partial g}{\partial H}H \cong -\frac{\partial \gamma}{\partial h}H = 0.3086H\left[\frac{mgal}{m}\right] \qquad (65)$$

2.4.3.2 Possion's integral

The Poisson's integral can be applied to any harmonic function, T, in order to determine the function exterior to a spherical boundary. It is given by

$$T(r,\theta,\lambda) = \frac{R(r^2-R^2)}{4\pi}\iint_\sigma \frac{T(R,\theta',\lambda')}{l^3}d\sigma \qquad (66)$$

where the boundary sphere has radius R and l is defined in Equ (48). It shows that the harmonic function on the sphere with radius r can be determined from the harmonic

function on the sphere with radius, R. As mentioned, $r\Delta g$ is harmonic so that it is expressed with Poisson's integral as

$$r\Delta g(r,\theta,\lambda) = R\Delta g(R,\theta,\lambda)\frac{R(r^2-R^2)}{4\pi}\iint_{\sigma}\frac{1}{l^3}d\sigma$$

$$+\frac{R(r^2-R^2)}{4\pi}\iint_{\sigma}\frac{R\Delta g(R,\theta',\lambda')-R\Delta g(R,\theta,\lambda)}{l^3}d\sigma \qquad (67)$$

where we have

$$\frac{R(r^2-R^2)}{4\pi}\iint_{\sigma}\frac{1}{l^3}d\sigma = \frac{R}{r} \qquad (68)$$

(The derivation of Equ (68) is given in Appendix B). Then the gravity anomaly on an arbitrary point above the geoid is explicitly determined from Δg on the geoid (approximated by a sphere with radius R).

$$\Delta g(r,\theta,\lambda) = \frac{R^2}{r^2}\Delta g(R,\theta,\lambda) + \frac{R^2(r^2-R^2)}{4\pi r}\iint_{\sigma}\frac{\Delta g(R,\theta',\lambda')-\Delta g(R,\theta,\lambda)}{l^3}d\sigma \qquad (69)$$

This is called the upward continuation by Poisson's integral. On the other hand, the downward continuation, which evaluates the harmonic function on the geoid or earth's physical surface from values in the exterior space, requires an iterative or inverse approach (Vanicek et. al., 1996). With the initial assumption, $\Delta\, g^{(0)}(R,\theta,\lambda) = \Delta g(r,\theta,\lambda)$, the gravity anomaly on the sphere, R, is computed from the gravity anomaly exterior to the sphere, iteratively:

$$\Delta g^{(n)}(R,\theta,\lambda) = \frac{r^2}{R^2}\Delta g(r,\theta,\lambda) - \frac{r(r^2-R^2)}{4\pi}\iint_{\sigma}\frac{\Delta g^{(n-1)}(R,\theta',\lambda')-\Delta g^{(n-1)}(R,\theta,\lambda)}{l^3} \qquad (70)$$

It is the downward continuation of the gravity anomaly by Poisson's integral.

2.4.3.3 Talyor series

Downward continuation by a Talyor series introduces another spherical surface, R_1, which has $R_1 > r > R$. The gravity anomaly on the sphere with radius, R_1, moves to the point, (r, θ, λ).

$$\Delta g(r,\theta,\lambda) = \Delta g(R_1,\theta,\lambda) + \left.\frac{\partial(\Delta g)}{\partial r}\right|_{r=R_1}(r-R_1) + \frac{1}{2}\left.\frac{\partial^2(\Delta g)}{\partial r^2}\right|_{r=R_1}(r-R_1)^2 - \cdots \quad (71)$$

The vertical derivative of gravity anomaly is (Heiskanen and Moritz, 1967)

$$\left.\frac{\partial(\Delta g)}{\partial r}\right|_{r=R_1} = -\frac{2}{R_1}\Delta g(R_1,\theta,\lambda) + \frac{R_1^2}{2\pi}\iint_{\sigma}\frac{\Delta g(R_1,\theta',\lambda') - \Delta g(R_1,\theta,\lambda)}{l_1^3}d\sigma \quad (72)$$

This method would be appropriate for airborne gravimetric data, which has nearly constant altitude.

In addition, we can use the Least Square Collocation (LSC) or a spectral method in order to analytically continue the gravity anomaly from an exterior surface to the geoid or the earth' surface, and vice versa. The LSC method requires auto-covariances and cross-covariances under the assumption that the measurements satisfy all premises of the LSC. The covariance matrices are typically computed by using an analytical model that empirically fits the physical statistics of the measurements. The spectral method of analytic continuation is typically based on the planar approximation using the Fast Fourier Transformation (FFT) (Forsberg, 2002).

2.5 Remove-Compute-Restore principle and chapter summary

The geoid undulation computation using Stokes's method shows that the integration is done for the entire unit sphere, σ; however, practically it is limited to an area where the gravity measurements exist. The gravity anomalies given in the limited area cannot resolve the long wavelengths or the trends of the gravity field. Therefore they are complemented by a low-degree spherical harmonic expansion of the field (Global Geopotential Model, GGM) according to the Remove-Compute-Restore (RCR) principle (Hofmann-wellenhof and Moritz, 2006). The gravity anomaly generated from the model is subtracted from the measured gravity anomaly, and the residual is used to compute a residual geoid undulation by the Stokes's integral over a cap, σ_c, centered on the evaluation point. The geoid undulation calculated from the GGM is then restored to the residual geoid undulation. Equ (21) is modified by the RCR technique according to

$$N(\theta,\lambda) = \frac{R}{4\pi\gamma_Q}\iint_{\sigma}\left(\Delta g(\theta',\lambda') - \Delta g_M(\theta',\lambda')\right)S(\psi)d\sigma + N_M(\theta,\lambda) \qquad (73)$$

With long-wavelengths of the geoid provided by N_M, it is now better justified to limit the integration area to a neighborhood, σ_c. Here, the subscript, M, means the quantities come from the reference model.

The residual gravity anomalies in Equ (73) include errors such as commission and omission errors. Especially, when the RCR technique is applied, it is necessary to determine how much error from the reference model is included in the final geoid computation. The commission and omission errors on the geoid undulation can be formulated according to the following:

$$\varepsilon_N = \frac{R}{4\pi\gamma}\iint_{\sigma_c}\varepsilon_{\Delta g}(\theta',\lambda')S(\psi)d\sigma_c - \frac{R}{4\pi\gamma}\iint_{\sigma_c}\varepsilon_{\Delta g_M}(\theta',\lambda')S(\psi)d\sigma - \frac{R}{4\pi\gamma}\iint_{\sigma-\sigma_c}\left(\Delta g_M(\theta',\lambda') - \Delta g(\theta',\lambda')\right)S(\psi)d\sigma \qquad (74)$$

The first term is the commission error due to the error in the measured gravity anomaly, the second is the commission error due to the error in the reference model, and the third explains the omission or truncation error. The omission error is defined as neglecting harmonic coefficients higher than the highest degree in the model. The errors from the reference model (second and third terms in Equ (74)) can be expressed by (Jekeli, 1980)

$$\varepsilon_{N_M} = \frac{R}{2\gamma}\sum_{n=2}^{n_{max}} Q_n \varepsilon_{\Delta g_M} - \frac{R}{2\gamma}\sum_{n=n_{max}+1}^{\infty} Q_n \Delta g_n \quad (75)$$

where Q_n are the Fourier (Legendre) coefficients of the error kernel, $\Delta K(\psi) = \begin{cases} 0, & 0 < \psi \leq \psi_0 \\ S(\psi), & \psi_0 < \psi \leq \pi \end{cases}$,

$$Q_n = \int_{-1}^{\psi_0} S(\psi) P_n(cos\psi)\, sin\psi d\psi \quad (76)$$

If Stokes's integral was evaluated over the entire sphere, σ, the error in the GGM would cancel in the RCR process. However, the integral is always practically limited to σ_c and the error from the GGM increases generally with the maximum degree of the reference model (Equ (75)). If there is no gravity data, only the second and third integrals over the entire sphere exist in Equ (74) and they come from the reference model itself. (Featherstone, 2013).

It is basically required to determine the maximum degree (n_{max}) of the GGMs for the RCR technique, and the chosen n_{max} is related to the spatial resolution, $\Delta\theta$, according to

$$\Delta\theta = 180°/n_{max} \quad (77)$$

n_{max} decides the contribution of the reference model and determines how much the gravimetric measurements beyond the resolution defined by n_{max} contribute to the geoid undulation computation. The recently launched satellite missions gave very accurate low degree harmonics, and those would make the RCR technique more reliable.

In summary, this chapter explains the theories and formulas for the gravimetric geoid undulation computation, based on Bruns's equation and Stokes's integral, and the related assumptions and approximations. Also, the reduction methods applied to the gravity measurements were introduced to satisfy the conditions for the boundary values of Stokes's integral. The boundary value, Δg^e, including several corrections due to approximations and reductions is

$$\Delta g^e(P_0) = \Delta g(P) + \delta g_{TE}(P) + \delta g_A - \varepsilon_{\Delta g}^{(lin.approx.)}(P) - \varepsilon_{\Delta g}^{(dir.der.)}(P) - \varepsilon_{\Delta g}^{(sec.ind.eff.)}(P) \quad (78)$$

The atmosphere correction, linear and directional derivative errors refer to Equs (23), (31) and (28), the second indirect effect comes from Equ (63). δg_{TE} indicates the applied topographic reductions and harmonic continuation. The geoid computation is done by the combination of Stokes's integral (Equ (21)), the ellipsoidal correction (Equ (37)), RCR procedure (Equ (73)), and indirect effect caused by changing of topographic masses.

$$N_P = \frac{R}{4\pi\gamma}\iint_{\sigma_c}\left(\Delta g^e(Q) - \Delta g_M^s(Q)\right)S\left(\psi_{PQ}\right)d\sigma$$

$$+N_M(P) + \delta N(P) + e^2 N_P^{(1)} \qquad (79)$$

If Δg_M^s also includes the terrain effects, it can be written by

$$\Delta g_M^s(Q) = \Delta g_M^s(Q) + \delta g_{TE_M}(Q) \qquad (80)$$

Based on Equs (78) and (80) with only consideration of the terrain effects, the residual gravity anomaly in Equ (79) will be

$$\begin{aligned}\Delta g^e(Q) - \Delta g_M^s(Q) &= \Delta g^e(Q) + \delta g_{TE}(Q) - \left(\Delta g_M^s(Q) + \delta g_{TE_M}(Q)\right)\\ &= \Delta g^e(Q) - \Delta g_M^s(Q) + \left(\delta g_{TE}(Q) - \delta g_{TE_M}(Q)\right)\end{aligned} \qquad (81)$$

The bracket in Equ (81) explains the residual terrain effects caused by the difference between total and reference topography. In other words, it is the Residual Terrain Model (RTM), which means that only residual shorter wavelengths of the topographic field with respect to the reference surface are considered and applied in the geoid computation. The reference surface is determined by the spatial resolution of the reference geopotential model.

Another issue on the practical evaluation of Stokes's integral is the singularity of Stokes's function. If we set up a near zone (σ_I) around the computation point, which has small angular radius ψ, then Stokes's kernel in Equ (20) is

$$S(\psi) \approx \frac{1}{S(\psi)} = \frac{2R}{l} \qquad (82)$$

where l is the straight-line distance from the integral to computation point. From Equs (73) and (82), the computation of geoid undulation in the near zone is

$$N_I = \frac{R^2}{2\pi\gamma}\iint_{\sigma_I}\frac{\left(\Delta g^e(Q) - \Delta g_M^s(Q)\right)}{l}d\sigma \qquad (83)$$

The singularity can be solved by using planar coordinate approximation, x' and y', and defining the polar coordinate system, s and α, passing through the computation point. Changing the variables of integration with respect to the new coordinate system are

$$R^2 d\sigma = dx'dy' = sdsd\alpha \qquad (84)$$

Then, the geoid computation in the near zone given by Equ (83) is

$$N_I = \frac{1}{2\pi\gamma}\int_{\alpha=0}^{2\pi}\int_{s=0}^{s_0}\frac{\left(\Delta g^e(s,\alpha)-\Delta g_M^S(s,\alpha)\right)}{s}sdsd\alpha$$

$$\cong \frac{\Delta g^e - \Delta g_M^S}{\gamma}s_0$$

(85)

Finally, the geoid undulation is determined by combining Equs (22), (79), and (83).

$$N = N_0 + N_I + \frac{R}{4\pi\gamma}\iint_{\sigma_c-\sigma_I}\left(\Delta g^e(Q)-\Delta g_M^S(Q)\right)S\left(\psi_{PQ}\right)d\sigma + N_M(P)$$

$$+\delta N(P) + e^2 N_P^{(1)}$$

(86)

CHAPTER 3 CONSTRUCTION OF UNIFIED GRAVITY ANOMALY DATASET

All gravity measurements should have consistency and satisfy the conditions of the boundary value problem. The gravimetric measurements have different character according to sensors, platforms, or measurement surfaces, and they should be analytically combined in order to generate a unified gravimetric dataset. Moreover, in developing a geoid model one requires additional information such as a Global Geopotential Model (GGM) for long wavelength components and topographic models for high frequency content of the earth's gravity field. This chapter describes all available data which are used to get numerical results for South Korea, and suggests a method to combine the datasets.

3.1 Datasets for South Korea

The South Korea peninsula is an area 5 deg by 5 deg in latitude and longitude. The north boundary of South Korea faces North Korea, and the other sides are surrounded by ocean. Topographically, the western half of the mainland is relatively lower and smoother than the other half, especially considering the high mountains in the northeast and south central areas. The neighboring sea is studded with thousands of islands, large and small. Two types of gravimetric observations are used to develop the geoid model for South Korea: terrestrial and airborne gravimetric measurements. Both data are expected to complement each other. The properties of each measurement, with the strengths and weaknesses of each, are introduced in the following sub-sections. In addition, GPS/leveling data exist for the area of interest and will later be used as an independent set to verify the accuracy of the GGM and the developed geoid model.

First of all, it is necessary to introduce the reference coordinate system and the ellipsoid. South Korea adopted the World Geodetic System 1984 (WGS84) for its horizontal coordinates and the Korea Geodetic Datum 2002 (KGD 2002) for vertical control. WGS84 is a right-handed, earth-fixed orthogonal coordinate system which defines the origin and three axes in order to uniquely determine the coordinates of any point on or above the earth. The origin is the earth's center of mass, the Z-axis is directly associated with the IERS Reference Pole (IRP), the X-axis is associated with the mean Greenwich

meridian, and the Y-axis is determined by the right-handed convention. The geometric center of the WGS84 ellipsoid coincides with the origin of the WGS84 coordinate system, and the rotational axis of the ellipsoid of revolution is the Z-axis. KGD 2002 is based on the mean sea surface that the National Geographic Information Institute (NGII) determined by tide gauge measurements at Incheon Bay during 1913 - 1916 and had set it as zero. In 1964, the origin of heights was set up by Inha Technical College by a precise leveling survey from the mean sea surface, and it is located on the north-east side of the South Korea peninsula.

It is also necessary to choose a reference ellipsoid for the normal gravity filed. Geodetic Reference System 1980 (GRS80) is used to compute the normal gravity. It had been chosen at the XVII General Assembly of the International Union of Geodesy and Geophysics (IUGG) for geodetic and geophysical applications. GRS80 is defined by four parameters, which are the semi-major axis of the ellipsoid (a), the gravitational constant of the earth (GM), the dynamical form factor of the earth (J_2), and the angular velocity of the earth (ω). Table 1 describes the defining parameters for WGS84, KGD2002, and GRS80 (and some derived parameters for the latter). The following sub-sections explain the terrestrial and airborne gravimetric, and GPS/Leveling measurements and include the results of an analysis of the consistency of both gravimetric measurements.

Table 1. Parameters for reference datum and reference ellipsoid

Geodetic Coordinate system	WGS84	
	Semimajor axis of the ellipsoid	6378137m
	Flattening of the ellipsoid	$1/298.257223563$
Vertical datum	KGD2002	
	Location	253, Yonghyun-dong Num-Ku Incheon, Korea
	Coordinates	$37°27'20''\text{N}, 129°40'20''\text{E}$
	Orthometric height for origin point	26.6871m
Reference ellipsoid for the normal field	GRS80	
	Semimajor axis of the ellipsoid	$6378137m$
	Geocentric gravitational constant of the earth	$3986005 \cdot 10^8 m^3 s^{-2}$
	Dynamic form factor of the earth	$108263 \cdot 10^{-8}$
	Angular velocity of the earth	$7292115 \cdot 10^{-11} rads^{-1}$
	Semiminor axis of the ellipsoid	$6356752.3141m$
	Normal gravity at the equator	$9.7803267715 ms^{-2}$
	Normal gravity at the pole	$9.8321863685 ms^{-2}$

3.1.1 Terrestrial gravity measurement

Terrestrial gravimetry consists of point measurements of the earth's gravity field on its physical surface. Terrestrial gravity on a complex physical surface contains all spectral information of gravity. The acquisition of terrestrial gravity measurements takes much time, effort and requires accessibility to an area. The terrestrial gravimetric data for South Korea had been acquired by several organizations for their own purposes during the last a couple of decades. The Korea Institute of Geoscience and Mineral Resources (KIGAM), Pusan National University (PNU), and the National Geographic Information Institute (NGII) had collected terrestrial gravimetric measurements more recently. The terrestrial gravimetric data measured by the KIGAM are concentrated in the western half of South Korea, and the data by the PNU are distributed in the north- and south-central areas. Also, the terrestrial data constructed by the NGII are at some of the vertical and horizontal bench marks, and the Unified Control Points (UCP). The Bureau Gravimetrique International (BGI) and the University of Leeds also have gathered gravity measurements, but they were measured several decades ago and included ill-defined information about reference coordinate systems and reduction procedures. Therefore, the terrestrial gravity data from the BGI and the University of Leeds were not included in the terrestrial dataset considered here.

The total number of terrestrial gravimetry measurements is 18677, and the dataset includes horizontal coordinates (latitude, longitude), heights (orthometric heights), the height anomaly, gravity, and free-air gravity anomaly. The normal gravity for the gravity anomaly is determined by using GRS80. The height anomaly is generated from the EGM08 geopotential model with degree and order 2160 (Pavlis et. al., 2012). The computation method of the height anomaly will be described in Section 3.2. The range of the terrestrial free-air gravity anomaly values is from -18.840 mgal to 174.369 mgal, 22.438 mgal in the mean and 21.909 mgal in standard deviation. The spatial resolution for terrestrial data is about 35 km in the northeast quadrant and about 3 km in the southwest quadrant, where the northeast quadrant is less dense than the other because there is limited access due to the high mountains. Table 2 shows the statistics of the terrestrial gravity dataset, and Figure 2 shows the distribution and values of the terrestrial free-air gravity anomaly.

Table 2. Statistics of each property of terrestrial data

	Mean	St.Dev.	Maximum	Minimum
Orthometric Height (m)	171.254	215.138	1668.600	-3.600
Height anomaly (m)	26.636	2.149	30.200	17.497
Free-air gravity anomaly (mgal)	22.438	21.909	174.369	-18.840

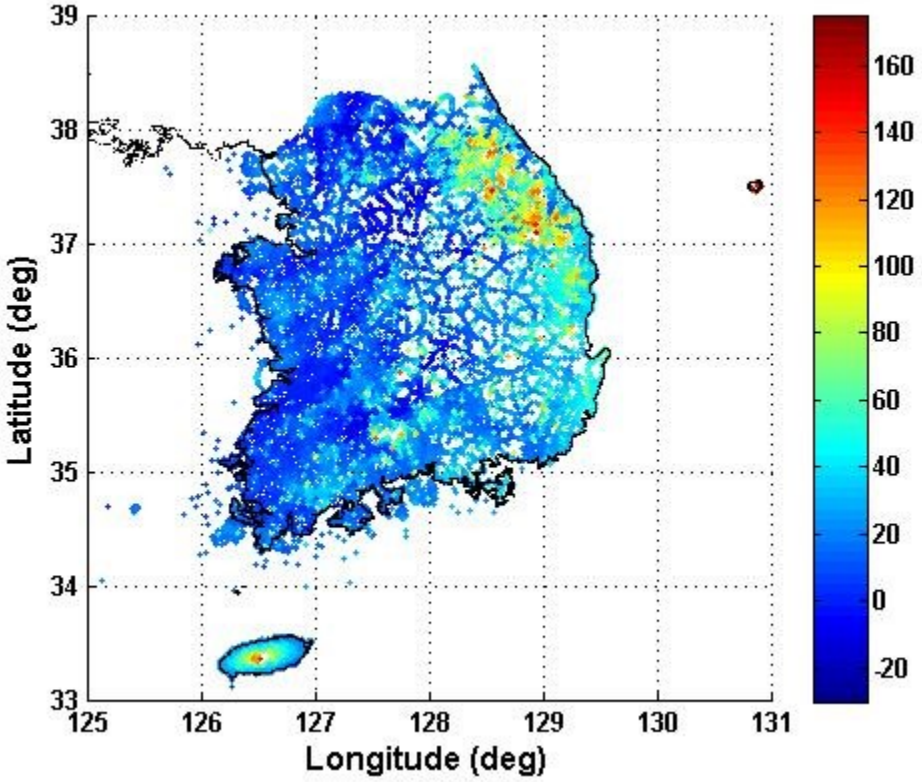

Figure 2. Free-air gravity anomalies of terrestrial data for South Korea. [unit : mgal]

3.1.2 Airborne gravity measurement

Airborne gravity at flight level yields a band-limited spectrum of gravity. The airborne method has better consistency of measurement accuracy and no limitation on accessibility of survey area (e.g., mountains, coastlines) (Forsberg et al., 2000). Generally with airborne gravimetry comes a measurement of an ellipsoidal height using GPS, so it is possible to compute the gravity disturbance, but this is transformed to the gravity anomaly in this dissertation. The airborne gravity anomaly is determined by the total gravity minus the normal gravity, which is extended from the normal gravity on the reference ellipsoid by the free-air reduction. It uses the altitude which is obtained by subtracting the height anomaly from the altitude of measurement above the ellipsoid, and which is assumed to be equal to altitude of the measurement above the geoid. Total gravity values are the measurements tied to the ground reference station and the national gravity network

The airborne gravity anomaly will be used to generate a unified gravimetric dataset with terrestrial data. South Korea sponsored the airborne gravity survey from December 2008 to January 2009 (Olesen, 2009), aimed at constructing a precise geoid model. There were 35 tracks in the north-south direction, 11 tracks in the east-west direction and 5 additional tracks in the Kangwon-area (total: 51 tracks). The airborne altitude was nearly constant at almost 3000 m. The raw data were preprocessed by time synchronization with GPS and a k-factor, which determines the scale factor relating gravimeter spring beam velocity and the spring tension (Forsberg et al., 2000). There were also corrections for the Eötvös effect, cross-coupling, tilt/bias effect, GPS error, and lever arm effect (Olesen, 2009).

The total number of processed airborne gravimetric measurements was 27436. The airborne set includes horizontal coordinates (latitude, longitude), height (ellipsoidal height), the height anomaly, the gravity, and the free-air gravity anomaly with respect to GRS80. The free-air gravity anomaly also includes the atmospheric correction. The height anomaly at the locations of the airborne data is generated from the EGM08 geopotential model with degree and order 2160 (Pavlis et. al., 2012). The cross-track spatial resolution or the interval between tracks was 10 km in the east-west direction and 50 km in the north-south direction. Airborne measurements were filtered by the 150 second Butterworth filter which reduced the resolution to about 5.2 km (Olesen, 2009), but the final airborne gravimetric data were generated at 1 km spatial interval in each track. The range of values of airborne free-air gravity anomalies is from -26.680 mgal to 118.120 mgal, 26.698 mgal in the mean and 17.797 mgal in standard deviation.

Table **3** shows the statistics of the airborne gravity dataset, and Figure 3 shows the distribution and values of the airborne free-air gravity anomaly.

Table 3. Statistics of each property for airborne data

	Mean	St.Dev.	Maximum	Minimum
Ellipsoidal altitude (m)			3321.569	2772.566
Height anomaly (m)	26.194	2.323	30.004	20.358
Free-air gravity anomaly (mgal)	26.698	17.797	118.120	-26.680

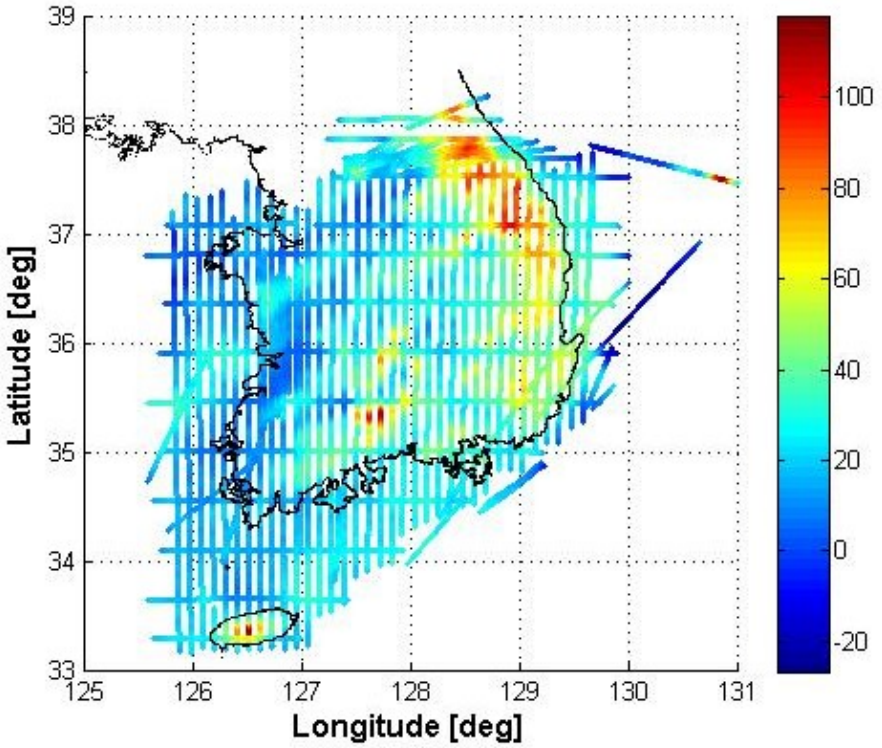

Figure 3. Free-air gravity anomalies of airborne data for South Korea. [unit : mgal]

3.1.3 Consistency between gravimetric measurements

Terrestrial and airborne gravity measurements have differences in spatial resolution, accuracy (including random and systematic error), acquiring surface, and topographic effect. The gravimetric data are compared to each other in order verify whether they are consistent or not, and to quantify existing differences.

The terrestrial data are measured on the earth's surface at elevations less than 1800 m, while the airborne set was acquired at airborne altitude, approximately 3000 m above the geoid. However, Tables 2 and 3 showed that the terrestrial free-air gravity anomalies have the mean of 22.4 mgal, and the standard deviation of 21.9 mgal, whereas corresponding values for the airborne data are 26.7 mgal and 17.8 mgal. According to Newton's law of gravitation, the gravitational attraction increases as the measurement point is closer to the mass. The simple statistics of both measurements show that the terrestrial data seem to have less energy than the airborne data.

Datasets are separately regularized to grids with equiangular spacing of 30 arcsec in order to compare them in a more systematic way. That is, the measurements in a grid cell are averaged and referred to the coordinates of the center of cell. The cell without a measurement is just blank. The regularized terrestrial data occupy 14239 cells, the airborne data are in 21175 cells, and the number of commonly occupied cells is 1368. Figure 4 shows the distributions of the regularized datasets. The common points in both regularized datasets refer to the same coordinates, and the differences in the data, terrestrial minus airborne, have the following statistics. The mean difference is -9.0 mgal and the standard deviation is 11.6 mgal (

Table **4**). As with the previous indication, the terrestrial gravimetric measurements have generally smaller values than the airborne measurements. This inconsistency problem, manifested in the significant bias between the data types, should be analyzed and solved in order to unify all gravity measurements. A possible cause of the inconsistency is that the terrestrial data especially in mountainous areas are primarily along roads in valleys where the gravitational effect of the topographic masses above is in the opposite direction than for the airborne data. Therefore, handling the topographic gravitational effects is probably the key to combining the gravimetric datasets (Section 3.3).

Table 4. The difference between the terrestrial and the airborne free-air gravity for common cells after regularization with 30 arcsec interval [unit : mgal]

Mean	St.Dev.	RMS	Maximum	Minimum
-8.970	11.565	14.636	42.115	-58.600

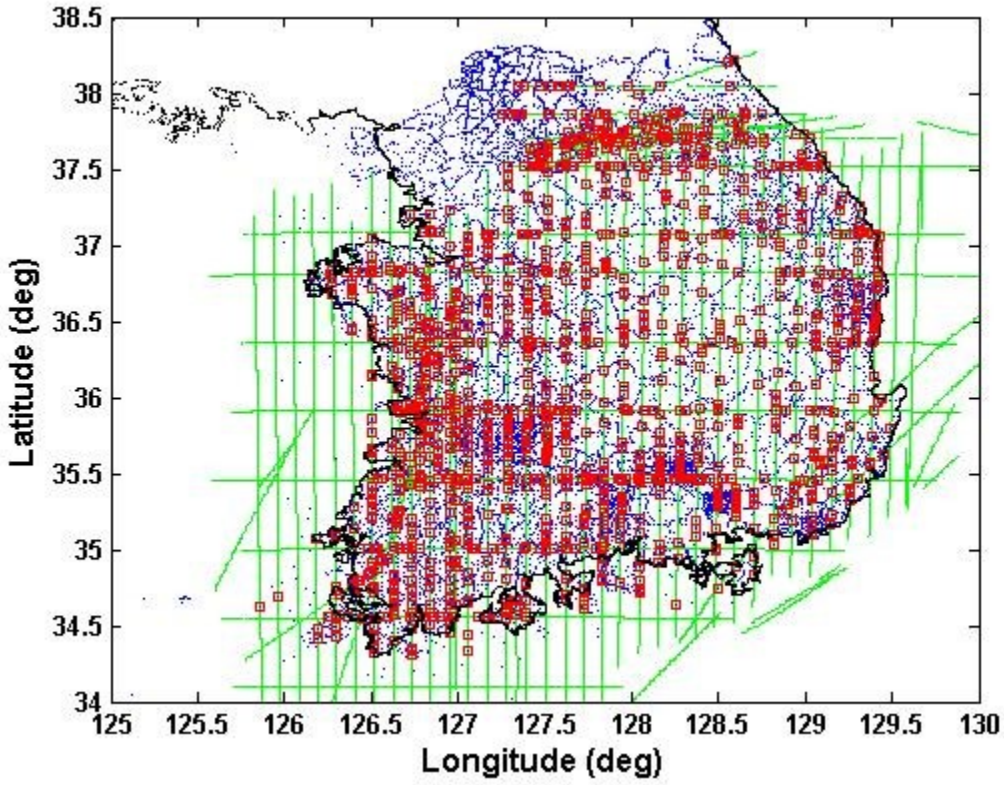

Figure 4. Distributions of the regularized data at 30 arcsec resolution : The blue-dot is regularized terrestrial, the green-dot is regularized airborne, and the red-square is common point

3.1.4 GPS/leveling data

GPS/leveling is a method to determine the geoid undulation by subtracting the orthometric height from the ellipsoidal height at a point (Equ (1)). The ellipsoidal height, h, is measured by GPS and the orthometric height, H, is available from leveling (and gravimetry). As an independent measurement, the GPS/leveling undulation is suitable for verification of developed geoid models based on the gravimetric measurements. NGII had constructed the Unified Control Point (UCP) network which covers South Korea with 10 km regular interval, and they supplied GPS/leveling undulations at the network.

The total number of GPS/leveling stations for South Korea is 1032. GPS/leveling data include horizontal coordinates (latitude, longitude) and the computed geoid undulation. The range of values of the geoid undulation by GPS/leveling is from 21.292 m to 29.977 m (Table 5), and the distribution is given in Figure 5.

Table 5. The statistics for GPS/leveling data in South Korea [unit : meter]

Mean	St.Dev.	Maximum	Minimum
26.471	2.163	29.977	22.292

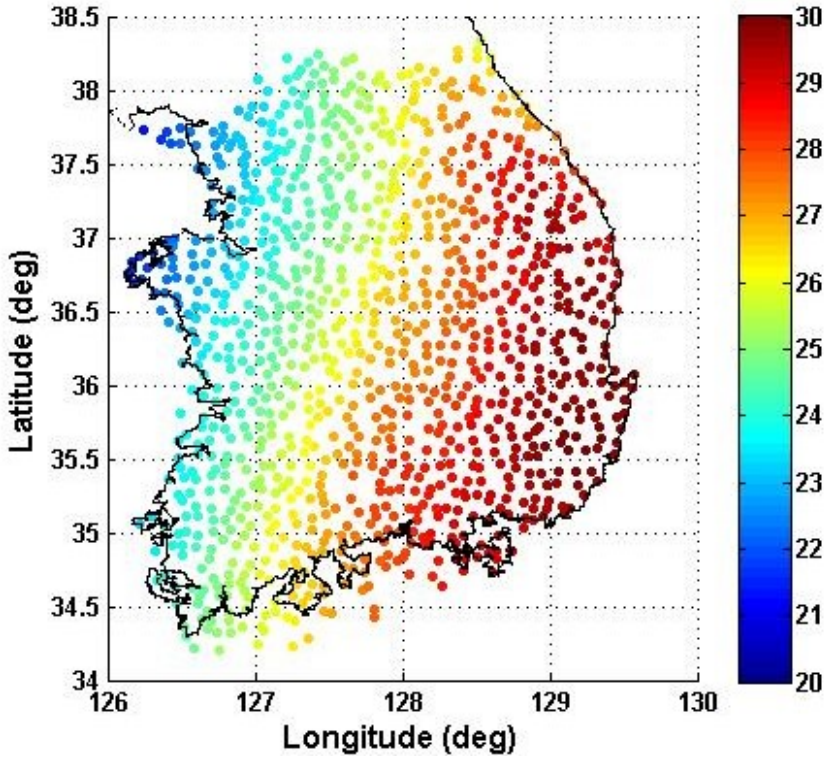

Figure 5. Geoid undulation determined by GPS/Leveling [unit : meter]

3.2 Global Geopotential Models (GGMs)

Global Geopotential Models provide long wavelength information of the earth's gravity field and contribute to the regional geoid model through the Remove-Compute-Restore (RCR) technique. The recent developments of GGMs have been based on satellite-only solutions or solutions that combine satellite and terrestrial measurements; and, they have been produced in the form of spherical harmonic expansions (Torge, 2001). As one of the combination models, Earth Geopotential Model 1996 (EGM96) is an expansion of spherical harmonics up to degree and order 360 (Lemoine et al., 1998). Recent satellite missions such as CHAllenging Minisatellite Payload (CHAMP), Gravity Recovery and Climate Experiment (GRACE), and Gravity field and steady-state Ocean Circulation Explorer (GOCE), aimed specifically to measure the global gravitational field of the earth, have contributed to improve the long wavelength accuracies of GGMs (Reigber et al., 2002; Tapley et al., 2004; Pail et al., 2010; Mayer-Guerr et al., 2012). The newly published Earth Geopotential Model 2008 (EGM08) up to degree 2190 has included the harmonics from the GRACE mission for its lower degrees (Pavlis et al., 2012). In addition, recently published satellite-only GGMs such as GOCO03S (Mayer-Guerr et al., 2012) and GO_CONS_GCF_2_DIR (Pail et al., 2011) are based on the GOCE mission launched by ESA in 2009. In this chapter, GGMs are introduced and analyzed with respect to actual measurements for South Korea. This section introduces the models, estimates the errors inherent in the models, and also verifies the possible contribution of the additional gravity measurements for geoid computation in South Korea.

3.2.1 Earth Gravitational Models 1996 and 2008

Earth Gravitational Model 1996 (EGM96), which had been developed collaboratively by NASA Goddard Space Flight Center (GSFC), the National Imagery and Mapping Agency (NIMA), and the Ohio State University (OSU), is a spherical harmonic model of the earth's gravitational field up to degree and order 360, and its spherical resolution is 30 arcmin (about 55 km) at the equator. As an updated version of EGM96, Earth Gravitational Model 2008 (EGM08) was developed and published by the National Geospatial-Intelligence Agency (NGA) (Pavlis et al., 2008; Pavlis et al., 2012). It is also a fully normalized spherical harmonic model of the earth's gravitational field up to degree and order 2160 and with degrees up to 2190. The spatial resolution of EGM08 is 5 arcmin (about 9 km) at the equator. Compared to EGM96, EGM08 has the advantage of employing the satellite-only gravity model from GRACE, ITG-GRACE03S, up to degree and order 180 (Mayer-Guerr, 2007).

Area-mean free-air gravity anomalies on a global 5 arcmin grid were generated for the development of EGM08 by merging terrestrial gravity data, altimetry-derived gravity anomalies computed at the Danish National Space Center (DNSC) and the Scripps Institution of Oceanography/National Oceanic and Atmospheric Administration

(SIO/NOAA), airborne gravity, and filled-in gravity anomalies using forward modeling based on a Residual Terrain Model (RTM). ITG-GRACE03S is then combined with the gravitational information based on the area-mean free-air gravity anomalies by least square combination.

The omission error in the geoid undulation due to the finite resolution of EGM08 is less than 1 cm globally determined by a power law model for its power spectral density (Jekeli, 2009). The commission error caused by the errors on the observations is estimated as 18.3 cm in geoid undulation (Pavlis et al., 2008; Pavlis et al., 2012). The accuracy compared to independent GPS/Leveling datasets, which include 12387 points and are globally distributed over 52 countries and territories, was estimated as ±13.0 cm after removing a bias, and ±10.3 cm after a removing a linear trend. The details are given in Pavlis et al. (2012).

NGA provides the fully-normalized, unit-less, spherical harmonic coefficients of the earth's gravitational potential, $\bar{C}_{nm}, \bar{S}_{nm}$, and the associated error standard deviations, $sigma\bar{C}_{nm}$, $sigma\bar{S}_{nm}$ (http://earth-info.nga.mil/GandG/wgs84/gravitymod/egm2008). The spherical harmonic expansion of the earth's gravitational potential is

$$V(r,\theta,\lambda) = \frac{GM}{r}\left[1 + \sum_{n=2}^{N_{max}} \left(\frac{a}{r}\right)^n \sum_{m=0}^{n} (\bar{C}_{nm} cosm\lambda + \bar{S}_{nm} sinm\lambda)\bar{P}_{nm}(cos\theta)\right] \tag{87}$$

where the scaling parameters are $GM = 3986004.415 \times 10^8 m^3 s^{-2}$, $a = 6378136.3m$. Both zero-tide and tide-free coefficients are provided with the consideration of the tide effect. The zero-tide model includes the permanent gravitational effect of Earth tides, and the tide-free coefficients have all tide effects removed. The models will be analyzed using GPS/leveling undulations and combined with gravity measurements in Stokes's integral, both of which include the permanent Earth-tide effect. Therefore, we use the zero-tide coefficient model.

Eliminating the defined normal gravitational potential generates the disturbing potential, and the gravity quantities such as gravity anomaly, height anomaly, and geoid undulation are based on the following equations. The spherically approximated gravity anomaly is determined by Equ (16)**,** and the height anomaly is determined by

$$\zeta = \frac{T}{\gamma} \tag{88}$$

and, the geoid undulation is approximated by

$$N = \zeta + \frac{\Delta g_B}{\bar{\gamma}} H \tag{89}$$

where $\Delta g_B = \Delta g - 0.1119H$ and $\bar{\gamma}$ is mean normal gravity along the plumbline (usually approximated by a constant γ_0).

The offset in geoid undulation caused by the difference between the best-fitting and the WGS84 ellipsoid, $\Delta N_{ellipsoid}$, is determined by (Rapp, 1993)

$$\Delta N_{ellipsoid} = -\sqrt{1 - e^2 sin^2\phi}\Delta a + a\frac{1-f}{\sqrt{1 - e^2 sin^2\phi}} sin^2\phi \Delta f \approx -\Delta a(1 - f sin^2\phi_0) + a sin^2\phi_0 \Delta f \quad (90)$$

where Δa is the difference in semi-major axis, Δf is the difference in flattening, and ϕ_0 is the mean geodetic latitude for South Korea . The parameters for the best-fitting ellipsoid come from (Bursa et al. 1999). From (Jekeli et al. 2012), we have

$$\Delta N_{ellipsoid} = -0.41 \pm 0.013\, m \quad (91)$$

3.2.2 Global Geopotential Models based on GOCE

Recently, the European Space Agency (ESA) launched the Gravity field and steady-state Ocean Circulation Explorer (GOCE) in order to map the earth's gravity field. It carried a full-tensor gradiometer consisting of 6 three-degree-of-freedom accelerometer pairs oriented in three orthogonal directions over a very short baseline. All nine components of the differential acceleration tensor were measured independently, though not all with equal precision. The gravitational gradients are derived from them and angular accelerations and velocities derived from symmetry properties and star tracker data (Rummel et al., 2011).

ESA has generated various levels of data products and provides them to the scientific and engineering research communities for geodetic and geological studies. The level-2 products are fully normalized spherical harmonic coefficients for the gravitational potential. The GOCE High-level Processing Facility (HPF) computes gravity models using GOCE Satellite Gravity Gradiometry (SGG) data alone or combined with Satellite-to-Satellite Tracking (SST) data such as GRACE in three different ways; the direct, time-wise, and space-wise approaches (Pail et al., 2011). These three approaches give very similar results when compared to other satellite-only or combined models. The direct approach, giving the GO_CONS_GCF_2_DIR model, uses the EIGEN-5C combined gravity model, as prior information so it is superior to the time- and space-wise approaches at the degrees and orders higher than 150. The GO_CONS_GCF_2_DIR model is based on two months of GOCE, GRACE, and LAser GEOdynamics Satellites (LAGEOS) data, and is expanded up to degree and order 240. The accuracy of this model is globally estimated as 10 cm in geoid undulation, 3 mgal in gravity anomaly for degrees up to 200 (Pail et al., 2011).

A consortium of institutes in Europe composed GOCO, a combination of GOCE data and complementary gravity field data. In 2010, they published the satellite-only gravity field model GOCO01S based on GOCE and GRACE. It is a spherical harmonic model up to

degree and order 224, and its accuracy (only up to degree and order 200) compared to GPS/leveling is estimated at 14.3 cm in Germany, 13.0 cm in Japan, and 17.0 cm in Canada (Pail et al., 2010). GOCO02S was based on 8 months data of GOCE mission and developed for the degree and order up to 250, and its accuracy (only up to degree and order 200) compared to GPS/leveling is estimated at 6.8 cm in Germany, 11.5 cm in Japan, and 15.4 cm in Canada (Gioiginger et al., 2011). Most Recently, GOCO03S used the extended data up to 18 months of the GOCE mission and was developed for degree and order up to 250. The accuracy of GOCO03S in Germany is estimated as 5.5 cm compared to GPS/leveling (Mayer-Guerr et al., 2012).

3.2.3 Analysis of Global Geopotential Models for South Korea

The accuracies in the reviewed GGMs are evaluated by comparisons with independent datasets, such as the geoid undulation and the gravity anomaly, described in Section 3.1 for South Korea. These gravity quantities for each model are computed in the same way as EGM08 (Refer to Equs (16), (88) and (89)). This analysis then determines which model to adopt as reference for South Korea, and also shows their accuracy. Moreover, the analysis will be used to show the contribution of additional measurements beyond the maximum degree of the GGMs in the development of the geoid model for South Korea.

First, the geoid undulations based on the GGMs are compared to GPS/leveling data at their locations shown in Figure 5. As shown in Equs (88) and (89), the geoid undulation is corrected from the height anomaly which is first determined by GGMs. The correction requires an orthometric height, but GPS/leveling for South Korea does not include it separately. So we use the SRTM elevations as substitution for the orthometric height, and compute the geoid undulation from the GGMs. The difference between the geoid undulations is

$$\Delta N = N_{GGMs} - N_{GPS/leveling} \qquad (92)$$

ΔN usually indicates the precision of the geoid undulation generated from GGMs, under the assumption that the geoid undulation by GPS/leveling is significantly more precise than by GGMs. However, $N_{GPS/leveling}$ also includes errors incurred by the leveling and GPS. The standard deviations of the GPS/leveling for South Korea, which indicate the precision, are estimated as 1 cm for orthometric height by leveling and 2 cm for ellipsoidal height by GPS (Jekeli et al., 2012)

From Table 6 we see that GPS/leveling has slightly better consistency (about 5.6 cm in standard deviation) with EGM08 than the most recent GOCE model (GOCO03S) when both models use only degree and order up to 250. EGM08 with degree and order 2160 compares even better to GPS/leveling, where the differences have a mean of 17.3 cm and a standard deviation of 6.0 cm. Figure 6 shows the differences between GPS/leveling and EGM08 degree and order up to 2160 in the map. The large difference in the mean, given in second column of Table 6, comes from N_0 which is caused by the assumptions described in Section 2.2.2. In Equ (92), N_{GGMs} is a geoid undulation with respect to the

best-fitting ellipsoid and the global geoid surface, however $N_{GPS/leveling}$ refers to the WGS84 for the ellipsoidal height and KGD2002 for the orthometric heights. As given in Section 3.2.2 the difference ($\Delta N_{ellipsoid}$) between the WGS84 and the best-fitting ellipsoid was $-41 \pm 1.3\ cm$. The offset of vertical datum (ΔN_{datum}), difference between the global to the KGD2002 geoid surface, was estimated as $26.5 \pm 1.3\ cm$ by Jekeli et al. (2012). The sum of differences seems to generate the large mean difference between GGMs and GPS/leveling. If we re-write Equ (92) with respect to the reference surfaces,

$$\begin{aligned} \Delta N &= N_{best}^{global} - N_{WGS84}^{KGD2002} \\ &= \left(h_{best} - H_{global}\right) - \left(h_{WGS84} - H_{KGD2002}\right) \\ &= -\left(H_{global} - H_{KGD2002}\right) - \left(h_{WGS84} - h_{best}\right) \\ &= -\left(\Delta N_{datum} + \Delta N_{ellipsoid}\right) \end{aligned} \qquad (93)$$

Therefore, ΔN in Equ (93) is estimated as 14.5 cm.

Table 6. Statistics for ΔN [unit : cm]

Model (Nmax)	Mean	St.Dev.	Maximum	Minimum
GOCE(250)	15.6	25.3	87.7	-45.9
EGM08(250)	17.4	19.7	70.4	-41.8
EGM08(2160)	17.3	6.0	39.3	-7.3

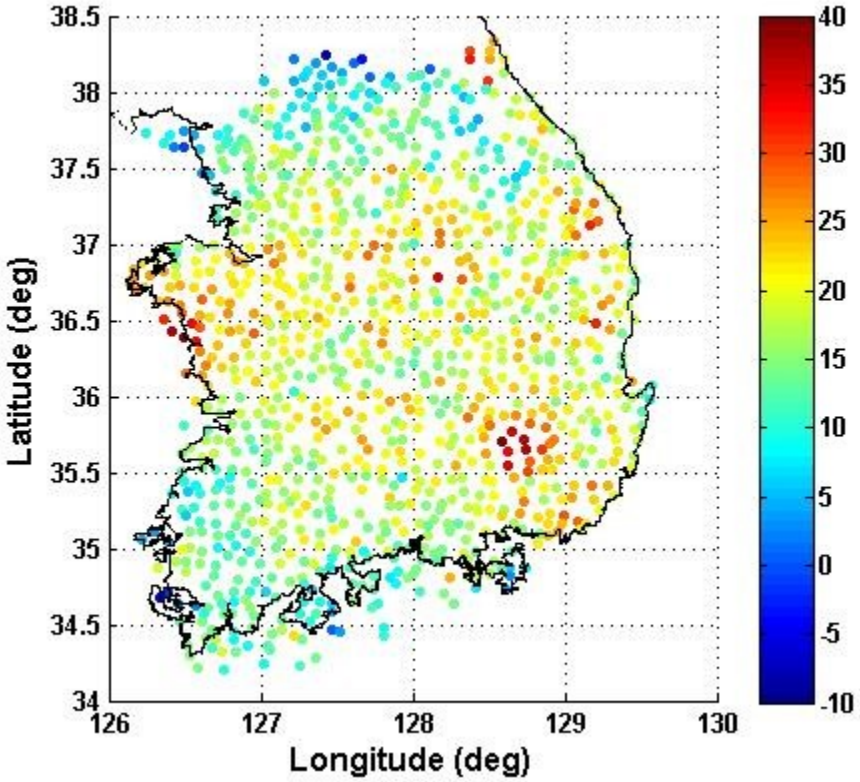

Figure 6. The comparison of geoid undulations measured by GPS/leveling and generated from EGM08 ($n_{max} = 2160$) [unit : cm]

Second, the gravity anomalies generated from the GGMs are compared to the terrestrial and airborne gravimetric data described in Section 3.1. As an input for computing the GGM gravity anomaly we use the geodetic latitude, longitude, and ellipsoidal height and they are changed to spherical coordinates in computing the spherical harmonic series. The ellipsoidal height for terrestrial gravity is approximated by the sum of the orthometric height and the height anomaly. Tables 7 and 8 show the statistics of the comparison at the actual measurement points. EGM08 and GOCE models yield similar results (up to degree and order 250), but EGM08 has the slightly better results in standard deviations when compared to the terrestrial and airborne data. The lower degree harmonics reflect the 'trends' of the gravity field, so if the lower degree harmonics of the global geopotential model are removed from the measurements, the residual only includes the shorter-wavelength gravity field and is smaller than the original data. If we compare Tables 7 and 8, the residual terrestrial gravity anomalies have values 6 mgal to 9 mgal in the mean and 14 mgal to 20 mgal in standard deviation, while the airborne data have smaller residuals. Therefore, we conclude that the airborne data have better agreement with the GGMs than the terrestrial data.

Table 7. Statistics of comparison between terrestrial measurements and GGM free-air gravity anomalies (unit : mgal)

Model (Nmax)	Mean	St.Dev.	Maximum	Minimum
GOCE(250)	-6.391	19.428	144.383	-57.159
EGM08(250)	-8.159	18.354	140.777	-58.571
EGM08(2160)	-8.666	13.575	122.815	-86.808

Table 8. Statistics of comparison between airborne measurements and GGM free-air gravity anomalies (unit : mgal)

Model (Nmax)	Mean	St.Dev.	Maximum	Minimum
GOCE(250)	1.226	12.217	101.634	-38.515
EGM08(250)	0.886	11.692	100.254	-33.793
EGM08(2160)	0.681	3.715	34.716	-17.431

Based on the comparison results of the GGMs with independently measured data, EGM08 has slightly better precision than the GOCE model so it is chosen as a reference model for the RCR technique. The residual gravity anomalies are computed on a regular grid with 30 arcsec interval as described in Section 3.1.3.

$$\Delta g_{res} = \Delta g - \Delta g_{EGM08} \qquad (94)$$

Tables 9 and 10 show the statistics of the residual free-air gravity anomaly of terrestrial and airborne datasets, respectively. As the maximum degree used for EGM08 increases, the airborne data have less difference with EGM08 but there is no improvement in the comparison to the terrestrial data. It means, again, that the EGM08 model is not consistent with terrestrial data as well as with the airborne measurements. Therefore, it seems that the use of higher degree and order for the reference GGMs does not improve the consistency between terrestrial and airborne. Even though higher maximum degrees do not contribute to the data combination (based on the comparisons shown in Table 11), the various maximum degrees of the reference model for RCR technique will be tested in Chapter 4 in order to decrease the truncation error of the geoid model due to the practical application of the Stokes's integral.

Table 9. Residual free-air gravity anomalies of terrestrial measurements at regularized locations (unit : mgal)

Nmax	Mean	St.Dev	Maximum	Minimum
36	-0.577	22.265	153.830	-38.429
72	-2.680	25.294	156.165	-48.036
90	-3.990	19.837	145.397	-44.753
120	-6.220	19.903	140.374	-54.053
180	-6.763	19.413	144.761	-57.502
240	-8.700	18.378	135.722	-56.215
360	-9.283	16.818	134.526	-67.640
720	-9.716	16.096	118.128	-73.236
2160	-8.813	13.981	122.785	-85.540

Table 10. Residual free-air gravity anomalies of airborne measurements at regularized locations (unit : mgal)

Nmax	Mean	St.Dev	Maximum	Minimum
36	5.834	18.549	92.854	-46.283
72	5.441	20.835	92.029	-41.091
90	3.212	15.140	86.367	-48.595
120	1.753	14.459	88.459	-42.075
180	1.587	13.428	83.927	-37.501
240	1.114	11.991	79.619	-36.541
360	1.072	9.261	70.444	-35.013
720	0.854	6.562	51.770	-28.824
2160	0.826	3.643	23.878	-15.034

Table 11. The difference between the residual terrestrial and the airborne free-air gravity for common cells (1368) after regularization [unit : mgal]

Nmax	Mean	St.Dev	Maximum	Minimum
36	-9.108	11.564	41.984	-58.671
72	-9.173	11.560	41.813	-58.548
90	-9.213	11.605	41.958	-59.047
120	-9.233	11.664	42.409	-59.682
180	-9.297	11.693	42.467	-59.557
240	-9.445	11.708	41.897	-59.656
360	-9.446	11.748	42.251	-60.922
720	-9.429	11.986	41.847	-63.912
2160	-9.123	11.949	40.339	-62.932

Table 12 is summary of comparison results of various maximum degree of EGM08 with GPS/leveling. The standard deviations are dramatically changed up to degree 360, but they are only improved by about 6.7 cm from degree 360 to 2160. The results would be used to verify the contributions of additional gravimetric dataset beyond the maximum degree of reference model.

Table 12. Statistics for ΔN [unit : cm] : This results are based on the Zero-Tide coefficients of EGM08.

Nmax	Mean	St.dev	Maximum	Minimum
72	-24.9	113.9	192.3	-288.4
90	-7.2	42.8	68.1	-150.3
180	14.0	32.5	93.1	-84.5
240	16.9	23.1	83.9	-51.1
360	17.7	12.7	59.2	-25.6
720	18.0	8.3	50.0	-13.2
2160	17.3	6.0	39.3	-7.3

3.3 Topographic effect for South Korea

Topographic reductions for the gravity anomalies may contribute to finding a key to unify the terrestrial and airborne gravity measurements as well as satisfying the conditions of the boundary value problem, solved by Stokes's integral. The numerical computation of the topographic effects described in section 2.4 requires a height data set, typically available as a Digital Elevation Model (DEM) or Digital Terrain Model (DTM). Nations or international organizations have produced topographic models or maps as essential geo-information, which have a variety of resolution, accuracy, and reference datum. The topographic effects depend primarily on resolution, but also on accuracy of topographic models, as well as the reduction methods. This section summarizes a topographic model and gives the numerical results of the topographic effects on the terrestrial and airborne data.

3.3.1 Shuttle Radar Topography Mission (SRTM)

The National Aeronautics and Space Administration (NASA), the National Geospatial-Intelligence Agency (NGA), and the German and Italian Space Agencies cooperated in the project, Shuttle Radar Topography Mission (SRTM), to map the earth's land topography using radar altimetry from the Shuttle spacecraft. The result was the most detailed global DEM of the earth. SRTM used two synthetic aperture radars with a very small base to height ratio, and the phase-difference measurements were derived from the radars to determine topography. The DEM from SRTM covered the land areas from 60º north to 56 º south in latitude, and heights are referred to the WGS84 geoid. The DEM comes in several different types of resolution sampled from 1 arcsec by 1 arcsec data. The model with 3 arcsec resolution is available to the public and the accuracy was estimated as better than 16 m globally (Farr et al., 2007).

Figure 7 shows the SRTM topography model based on the 3 arcsec grid for South Korea. The elevation of topography for South Korea is less than 1800 m, and its mean is about 230 m. As described in a previous section, the eastern half of the territory is more rough and higher than the western half and high mountains exist in the north-east and south-central areas. The accuracy of SRTM for South Korea is verified by comparing to the averaged and interpolated orthometric heights associated with the terrestrial gravity data set, and it has a mean of -5.7 m and a standard deviation of 17.8 m.

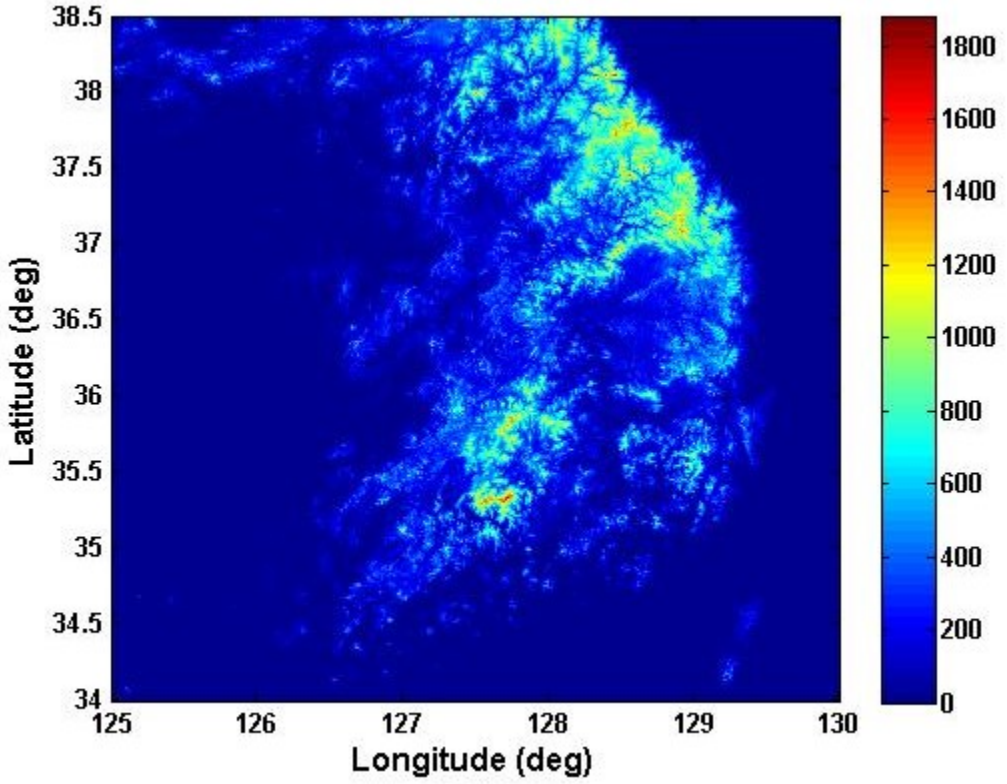

Figure 7. Topography of South Korea (SRTM ; 3 arcsec by 3 arcsec)

3.3.2 Topographic effects on gravimetric measurements

The Bouguer reduction, Equs (45) and (51), and the Helmert's second condensation, Equs (56) and (57), are applied to the terrestrial and airborne data sets. Computing terrain effects, especially at the terrestrial measurement locations, has a numerical singularity problem if the computation and integral points are very close to each other but not at exactly same location. It seems that more investigation is needed in order to verify the required distance between the computation and integral points when the singularity causes numerical problems. In this dissertation, we use the data regularization described in Section 3.1.3 to compute topographic effects with no apparent singularity problems. After the regularization, the computation points refer to the coordinates of center of the grid cells, and the computation of terrain correction (integral in Equ (45)) is ignored for the integral cell that is the same as the computation cell.

The topographic effects based on 30 arcsec averaged SRTM are determined for the 30 arcsec regularized datasets. These are shown in Figure 8 and their statistics are given in Table 13 which also includes the differences between the exact and approximation equations described in Section 2.4.1 and Appendix A We used only the exact equations

since the tests with the approximate formulas indicated the possibility of obtaining unsatisfactory results, especially for the airborne data. While the topographic effects by the Bouguer reduction are very slightly larger in the mean and less in the standard deviation for the terrestrial than the airborne data, the Helmert's second condensation effects for the terrestrial data are much larger than for the airborne data. It may be caused by the relationship between topographic masses and measuring surfaces. That is, the topographic masses above the geoid are completely below the airborne altitude, so the removed topographic effects at altitude are large but the removed/restored effects are small. In the case of terrestrial points, the topographic masses above the Bouguer shell act in the upward direction, so the removed topographic effects are smaller. In addition, the terrestrial data are affected more by removing and restoring masses because these are closer to the masses than the airborne data. The terrain effects summarized in this section will be more analyzed further in Section 3.3.3 in order to explain the gap between terrestrial to airborne data and how these affect the consistency.

Table 13. Topographic Effects, computed by the Bouguer reduction ($\boldsymbol{\delta g_{topo}}$) and including the Helmert's second condensation ($\boldsymbol{\delta \Delta g}$), on the terrestrial and airborne gravity measurements using the 30 arcsec SRTM data [unit : mgal]

		Equation	Mean	St.Dev	Maximum	Minimum
Terrestrial	δg_{topo}	Exact	38.180	47.724	331.233	-3.771
		Approximate	38.344	48.205	339.310	-3.887
		Difference	-0.164	0.646	0.406	-9.023
	$\Delta\delta g$	Exact	2.017	6.393	35.962	-44.352
		Approximate	1.859	6.801	33.379	-52.257
		Difference	0.158	0.633	8.896	-0.407
Airborne	δg_{topo}	Exact	37.797	48.412	307.567	0.183
		Approximate	37.843	48.738	327.963	0.183
		Difference	-0.046	1.148	7.790	-20.396
	$\Delta\delta g$	Exact	-0.032	0.782	2.093	-16.767
		Approximate	-0.043	1.664	6.509	-36.828
		Difference	0.011	1.132	20.061	-7.912

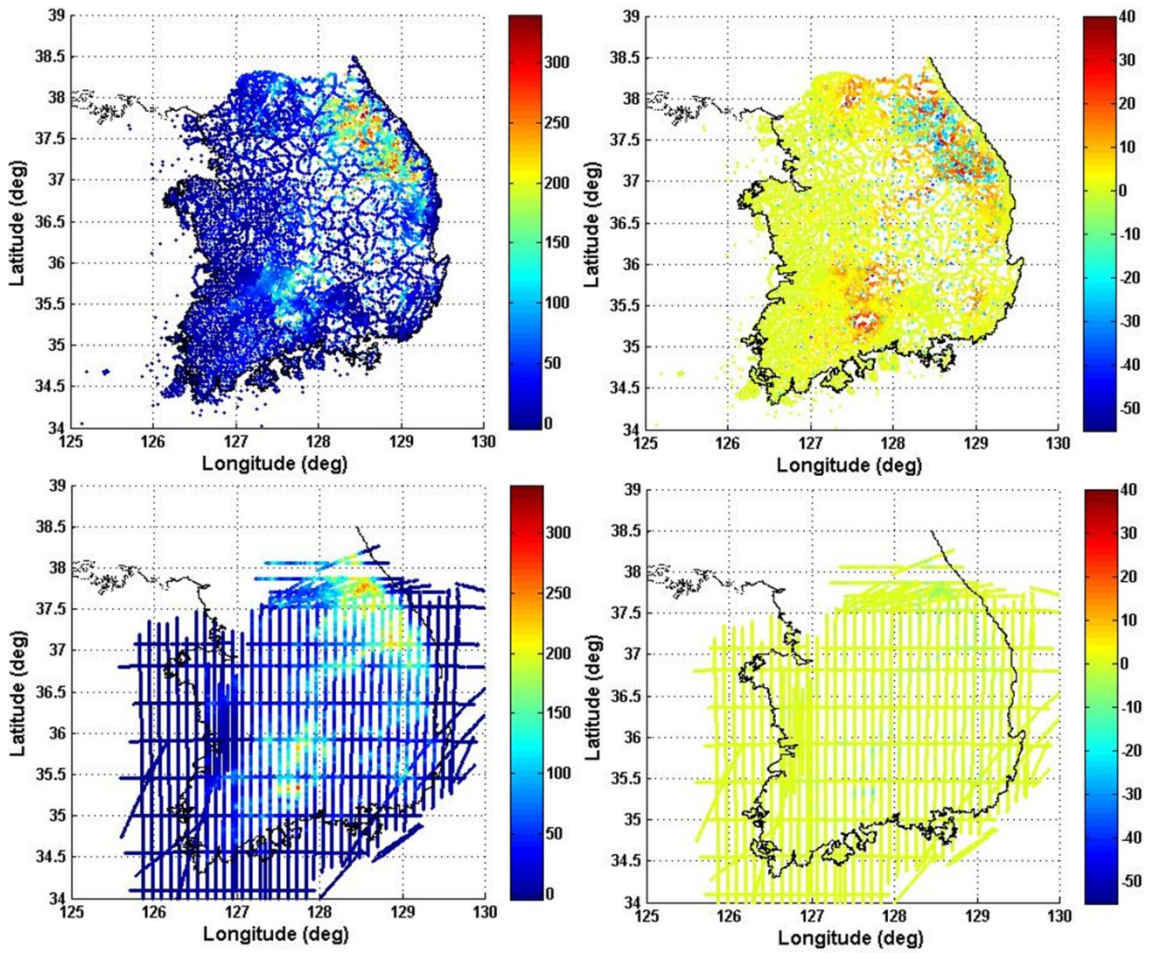

Figure 8. Terrain effects are computed at 30 arcsec regularized locations using averaged 30 arcsec SRTM data. The exact formulas only are used. (a) upper-left : the refined Bouguer reduction effects ($\boldsymbol{\delta g_{topo}}$) for terrestrial data, (b) upper-right : the terrain effects ($\boldsymbol{\delta \Delta g}$) by the Helmert's second condensation at terrestrial data, (c) bottom-left : the refined Bouguer reduction effects ($\boldsymbol{\delta g_{topo}}$) for airborne data, (d) bottom-right : the terrain effects ($\boldsymbol{\delta \Delta g}$) by the Helmert's second condensation at airborne data

3.3.3 Consistency analysis

The refined Bouguer anomaly is determined by subtracting the terrain effect, δg_{topo}, from the free-air terrestrial and airborne gravity anomalies, and the Helmert anomaly is computed by subsequently adding the effect of the condensation layer to the Bouguer anomaly. No downward continuation is applied to the airborne data. We have

$$\Delta g_B = \Delta g - \delta g_{topo} \qquad (95)$$

where δg_{topo} is given by Equ (45), and

$$\Delta g_H = \Delta g + \delta \Delta g \qquad (96)$$

where $\delta \Delta g$ is given by Equ (56). The integration area was the same 4.5 degree by 5 degree area in latitude and longitude direction for all computations. The terrain effects (given in Table 13) are subtracted or added to the regularized free-air gravity anomalies, then Table 14 indicates the statistics of the gravity anomalies for the terrestrial and airborne data. As expected by the statistics of the estimated terrain effects, the Bouguer gravity anomalies have large variations, but the Helmert anomalies are similar to the free-air anomaly especially in case of airborne data.

The terrestrial and airborne gravity anomalies are compared to determine the effects of terrain reductions on the consistency between the two. The data distribution is given in Figure 4. Table 15 gives the comparison results of the free-air, Bouguer, and Helmert gravity anomalies at the commonly occupied cells in 30 arcsec resolution. While the difference between terrestrial and airborne free-air gravity anomaly has a mean value of -9.0 mgal and a standard deviation of 11.6 mgal, the Bouguer gravity anomaly differs only -0.5 mgal in the mean and 7.0 mgal in the standard deviation. The Helmert gravity anomaly has slightly better consistency in standard deviation than the free-air gravity anomaly. Therefore, it is clear that the terrain effect is a key parameter when combining the two different types of measurements; and we conclude that we have the best consistency between terrestrial and airborne gravity anomalies when applying the Bouguer reduction.

Table 14. Statistics of gravity anomalies with topographic effects using 30 arcsec averaged SRTM at the regularized data with 30 arcsec interval [unit : mgal]

		Mean	St.Dev	Maximum	Minimum
Terrestrial	Free-air gravity anomaly	20.934	21.721	174.369	-18.790
	Bouguer gravity anomaly	-17.246	33.940	85.923	-196.968
	Helmert gravity anomaly	22.951	20.200	159.813	-14.115
Airborne	Free-air gravity anomaly	27.326	17.851	115.420	-26.680
	Bouguer gravity anomaly	-10.471	36.280	47.841	-192.547
	Helmert gravity anomaly	27.294	17.500	104.710	-26.647

The free-air, Bouguer, and Helmert gravity anomalies at the regularized 30 arcsec grids given in Table 14 are averaged to lower resolutions such as 5, 3, 2, and 1 arcmin. Again, it is emphasized that the terrain effects determined by the Bouguer reduction and the Helmert's second condensation are based on 30 arcsec SRTM data. As in Table 15, the terrestrial and airborne data are compared in terms of the free-air, Bouguer, and Helmert gravity anomalies. In Table 16, the parenthetical values in the second column indicate the number of commonly occupied cells between averaged terrestrial and airborne data at each resolution. The comparisons of the Free-air and Helmert gravity anomalies are almost the same even if the data resolution is changed. On the other hand, the Bouguer gravity anomalies have different consistency depending on the data resolutions; especially the higher resolution data have the smaller differences in the mean. The reason why the lower resolution have worse consistency is probably because the terrestrial data do not represent the cell with larger grid size. As a conclusion, we should combine the terrestrial and airborne Bouguer gravity anomalies at 30 arcsec resolution.

Table 15. Statistics of differences between terrestrial and airborne gravity anomalies at commonly occupied cells (1368). [unit : mgal]

	Mean	St.Dev	RMS	Maximum	Minimum
Free-air gravity anomaly	-8.970	11.565	14.636	42.115	-58.600
Bouguer gravity anomaly	-0.408	6.987	6.999	31.038	-42.150
Helmert gravity anomaly	-7.217	8.097	10.846	27.794	-44.050

Table 16. Statistics of differences between terrestrial and airborne gravity anomalies at commonly occupied cells on lower data resolution [unit : mgal]

	Data resolution	Mean	St.Dev	RMS	Maximum	Minimum
Free-air gravity anomaly	5 arcmin (1216)	-7.903	10.125	12.844	59.000	-60.600
	3 arcmin (2085)	-7.218	12.104	14.093	59.852	-55.995
	2 arcmin (2509)	-7.718	13.156	15.253	62.837	-60.457
	1 arcmin (2411)	-7.953	12.609	14.907	62.737	-59.350
Bouguer gravity anomaly	5 arcmin (1216)	4.203	12.156	12.862	80.073	-68.086
	3 arcmin (2085)	2.743	13.844	14.113	66.578	-86.752
	2 arcmin (2509)	2.365	14.002	14.200	69.053	-71.341
	1 arcmin (2411)	0.918	11.500	11.536	49.130	-65.279
Helmert gravity anomaly	5 arcmin (1216)	-6.462	7.249	9.711	53.438	-38.105
	3 arcmin (2085)	-6.039	7.929	9.967	53.457	-38.629
	2 arcmin (2509)	-6.383	8.422	10.568	53.631	-40.506
	1 arcmin (2411)	-6.561	8.332	10.605	37.879	-45.087

3.4 Downward continuation applied to airborne measurement

3.4.1 Validation of algorithms

This section analyses the algorithms for analytic downward continuation described in Section 2.4. It is based on using the EGM08 model, instead of the actual measurements, because the gravity anomalies thus generated at different altitudes are mutually consistent and the tests can focus on the effect of downward continuation. Basically, two regular grids of gravity anomalies for 4.5 deg by 5 deg in latitude and longitude are generated with 5 arcmin and 30 arcsec intervals, and at altitude 3000 m and on the earth's surface, using the EGM08 (zero-tide) model to nmax 2160. The earth's surface for the 5 arcmin data is represented by the interpolated heights of the actual terrestrial data, and for the 30 arcsec data we used the 30 arcsec SRTM elevation model. The gravity anomaly at altitude 3000 is downward continued to the earth's surface because the downward continuation must be done in harmonic field. The generated free-air gravity anomalies at altitude 3000m are downward continued to the geoid surface first, then these are again upward continued to the earth's surface, according to the methods introduced in Section 2.6. The downward (and upward) continued gravity anomalies, from at the altitude 3000 to the earth's surface, are compared to the free-air gravity anomalies generated from EGM08 at the earth's surface.

The statistics in Table 17 for 5 arcmin resolution and Table 18 for 30 arcsec resolutiuon are only for the land area. The second rows in both tables show the differences in gravity anomalies generated by EGM08 at the different surfaces without downward continuation. The third and fourth rows in each table show the statistics of the differences after downward continuation. For the Taylor series method, we considered only up to first derivatives of gravity anomaly in Equ (71). These reveal that the differences of the two datasets decrease significantly when the downward continuation is applied. The analytic methods have similar statistics. Figure 9 shows the effect of downward continuation at two profiles at 127.725 deg in longitude and at 37.150 deg in latitude, and for the 30 arcsec simulated data. The gravity anomaly at airborne altitude (blue-line) is smoother than the gravity anomaly at the earth's surface (green-line), and the downward continued gravity anomaly (red-line) is closer to the green-line. The 5 arcmin and 30 arcsec datasets have very similar results which are not surprising because EGM08 essencially has no power beyond the 5 arcmin resolution. We conclude that the algorithms are working for the simulated data by EGM08.

Table 17. The effects of downward continuation on gravity anomalies generated by EGM08. The statistics are only for the land area with 5 arcmin grids.

	Mean	St.Dev	RMS	Maximum	Minimum
No downward continuation	0.645	5.047	5.088	24.717	-16.236
Poisson's integral	0.173	1.260	1.272	6.100	-4.716
Talyor Series	0.198	1.810	1.821	8.121	-5.746

Table 18. The effects of downward continuation on gravity anomalies generated by EGM08. The statistics are only for the land area with 30 arcsec grids.

	Mean	St.Dev	RMS	Maximum	Minimum
No downward continuation	0.214	4.369	4.375	24.251	-17.329
Poisson's integral	0.153	1.075	1.086	9.362	-6.112
Talyor Series	0.007	0.890	0.890	7.925	-5.431

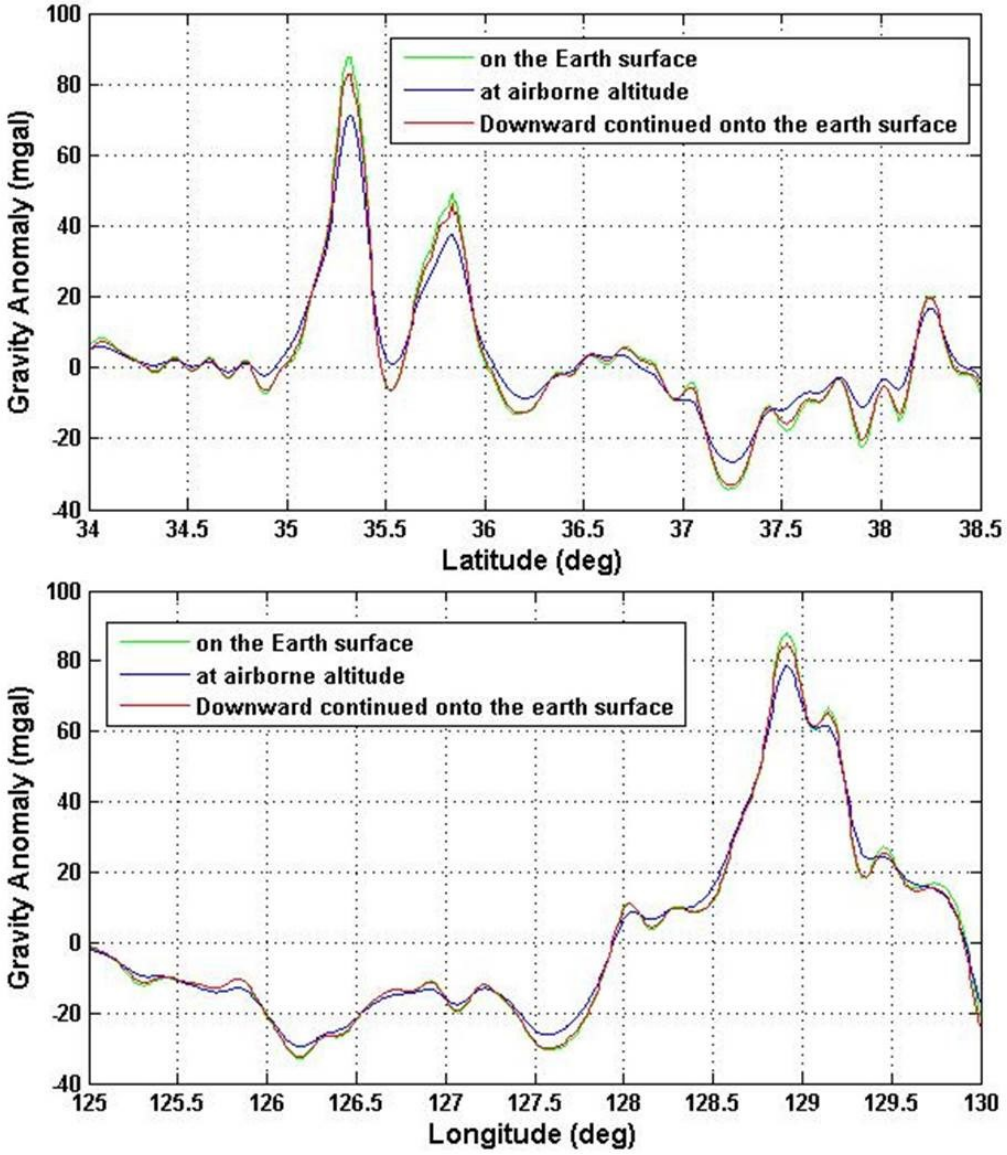

Figure 9. Both profiles are extracted from the simulation data with 30 arcsec interval. Blue-line means the gravity anomaly at the airborne altitude approximated to 3000 m, green-line is the gravity anomaly at the earth's surface, and red-line is downward continued gravity anomaly from the airborne altitude to the earth's surface. (Top) Profile at 127.725 deg in longitude. (Bottom) Profile at 37.150 deg in latitude.

3.4.2 Numerical computation results of each methods

The analytic continuation is required to combine the gravity data measured on different surfaces; especially the downward continuation is necessary for the geoid computation using airborne gravity data or combined with terrestrial. Many studies have introduced the numerical computations of downward continuation and demonstrated the effects on the gravity anomaly or geoid undulation (Vanicek et al., 1996; Novak and Heck, 2002; Novak et al., 2003; Forsberg and Olesen, 2007; Hwang et al., 2007). In this section, the analytic downward continuation is applied to the actual airborne gravity anomalies. It is expected that the downward continued airborne gravity anomalies diverge even more from the terrestrial anomalies because, the airborne anomalies are already larger than the terrestrial anomalies as shown in Section 3.1, and the downward continued anomaly onto the earth's surface will be larger in magnitude than at airborne altitude.

The downward continuation requires fully occupied grids by the gravity anomalies for South Korea, and the grids can be filled by interpolating airborne data or using EGM08. In order to avoid the interpolation error, the empty cells of airborne data are filled with the gravity anomalies generated from EGM08 at airborne altitude. It is assumed that the airborne data and EGM08 have good agreement as shown in Section 3.2, and thus they are assumed to be complementary for this purpose. The fully occupied data grid at airborne altitude is downward continued to the averaged 30 arcsec SRTM surface. Then, we extract the cells occupied by airborne measurements from the entire downward continued data, and these are compared to the terrestrial gravity anomalies at commonly occupied cells. The downward continuation is applied to the free-air, Bouguer, and Helmert gravity anomalies. The terrain effects, used to generate the Bouguer and Helmert airborne gravity anomalies, are also applied to gravity anomalies generated from EGM08 for the empty cells.

Table 19 summarizes the comparison results between terrestrial and airborne gravity anomalies before and after downward continuation by Poisson's integral. We recognize the downward continuation of airborne data decreases the consistency with respect to the terrestrial data for every type of gravity anomaly. Especially the effect of downward continuation on the Bouguer gravity anomaly is very large. Therefore, the downward continuation is not used to combine the terrestrial and airborne, but it is worth to demonstrate its effect on modeling the geoid undulation.

Table 19. The comparison results between terrestrial and airborne gravity anomalies at commonly occupied cells of 30 arcsec resolution data (the number of cell : 1368).

		Mean	St.Dev	RMS	Maximum	Minimum
Free-air gravity anomaly	No downward continuation	-8.970	11.565	14.636	42.115	-58.600
	Poisson's integral	-8.806	12.564	15.343	40.923	-61.829
Bouguer gravity anomaly	No downward continuation	-0.408	6.987	6.999	31.038	-42.150
	Poisson's integral	-10.098	17.023	19.793	56.287	-88.433
Helmert gravity anomaly	No downward continuation	-7.217	8.097	10.846	27.793	-44.050
	Poisson's integral	-7.281	9.370	11.866	26.992	-45.840

We still have many questions on the downward continuation, so there need to be further investigations on the analytic continuation even though we do not include the downward continuation to data combination in this dissertation. As future work, we may apply the downward or upward continuation to the gravity anomaly and terrain effects separately, as well as by other method such as the Least Square Collocation or the higher order Taylor series, in order to reduce the difficulty on the downward continuation of the Bouguer gravity anomaly and combine the airborne data to terrestrial data with better consistency.

3.5 Summary

This section summarizes the entire Chapter 3 and suggests a methodology to unify different types of gravimetric measurements based on the analysis results given in previous sections. Section 3.1 introduced the terrestrial, airborne, and GPS/leveling measurements for South Korea. The consistency test showed that the free-air terrestrial gravity anomaly is less than airborne data contrary to our expectation based on the Newton's law of gravitation. Section 3.2 described the recently published Global Geopotential Models (GGMs) such as EGM08 and GOCO03S. Compared to the actual measurements, EGM08 has slightly better consistency than GOCO03S if we use only the degree and order 250. In addition, the higher maximum degree for the GGMs leads to better agreement with airborne data while it is hard to see the contribution of higher maximum degree on the consistency with terrestrial data. GGMs will be used to prove the contribution of additional measurements on the geoid modeling as well as the Remove-Compute-Restore principle. Section 3.3 included the terrain effects according to the Bouguer reduction and Helmert's second condensation, which are required to satisfy the boundary conditions for the Stokes's integral. Moreover, the refined Bouguer reduction increases the consistency between the terrestrial and airborne data. The differences between the Bouguer gravity anomalies are reduced to almost zero in the mean and 7 mgal in standard deviation. Therefore, we conclude the terrain effect is a critical issue to explain the inconsistency problem and to merge the two gravimetric data to the unified set. As another reduction issue, the downward continuation was applied to simulated and actual data in Section 3.4. The simulation data, generated from EGM08, showed that the downward continuation helped to reduce the differences of gravity anomalies generated at two different surfaces. However, it did not have an advantage on the consistency with the terrestrial data when applied to the actual airborne gravity data.

Therefore, the gravimetric terrestrial and airborne measurements are merged to a unified dataset in terms of the Bouguer gravity anomaly. We just averaged terrestrial and airborne for the commonly occupied cells, but later outlier detection or combination weights will be considered. The Bouguer gravity anomalies in the unified data vary from -197 mgal to 86 mgal as shown in Table 20 and Figure 10. The total number of 30 arcsec cells for the land area is 171012, and 27192 cells are occupied by the unified data. They cover 16% of the land area. The unified data will be averaged to lower resolutions, and the averaged data at the lower resolution cover a larger percentage of the land area. We will also demonstrate the effects of data resolution on the geoid undulation.

Table 20. The unified gravimetric data for South Korea includes the refined Bouguer gravity anomalies at 30 arcsec regularized point. [unit : mgal]

mean	St.Dev.	Maximum	Miminum
-13.087	35.639	85.923	-196.968

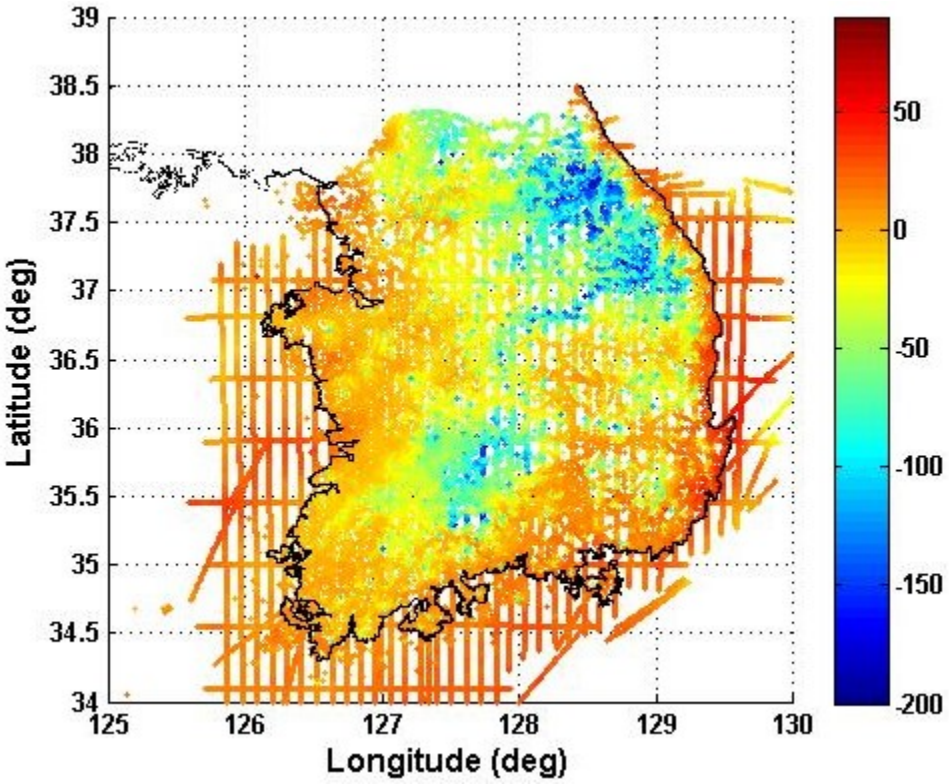

Figure 10. The distribution of unified data [unit : mgal]

The combined Bouguer gravity anomaly data will be used to compute a geoid model with the consideration of restoring the effects of Bouguer reduction. As described in Section 2.4, the Bouguer reduction generates a large effect on the gravity anomaly and ultimately a huge indirect effect on the geoid undulation, so the Bouguer gravity anomaly is not suitable for computing the geoid undulation. In order to keep the consistency between the terrestrial and airborne data and reduce the variation of the gravity values and indirect effects, the condensed layer as given in Equ (55) is restored to the unified Bouguer gravity anomaly data. Figure 11 shows the flow to generate the unified data and prepare a dataset for modeling geoid undulation. The combined Bouguer gravity anomalies are merged to the Bouguer gravity anomalies generated from EGM08 and 30 arcsec SRTM data in order to fill the cells without measurements. We have the entire grids occupied by the Bouguer gravity anomaly for South Korea, and then add the terrain effects caused by the condensed layer. As a resultant, we have the Helmert gravity anomaly for South Korea. As an additional test, the downward continuation of the airborne free-air gravity anomaly, which was omitted at the combination procedure, is considered to demonstrate the effect on the geoid computation.

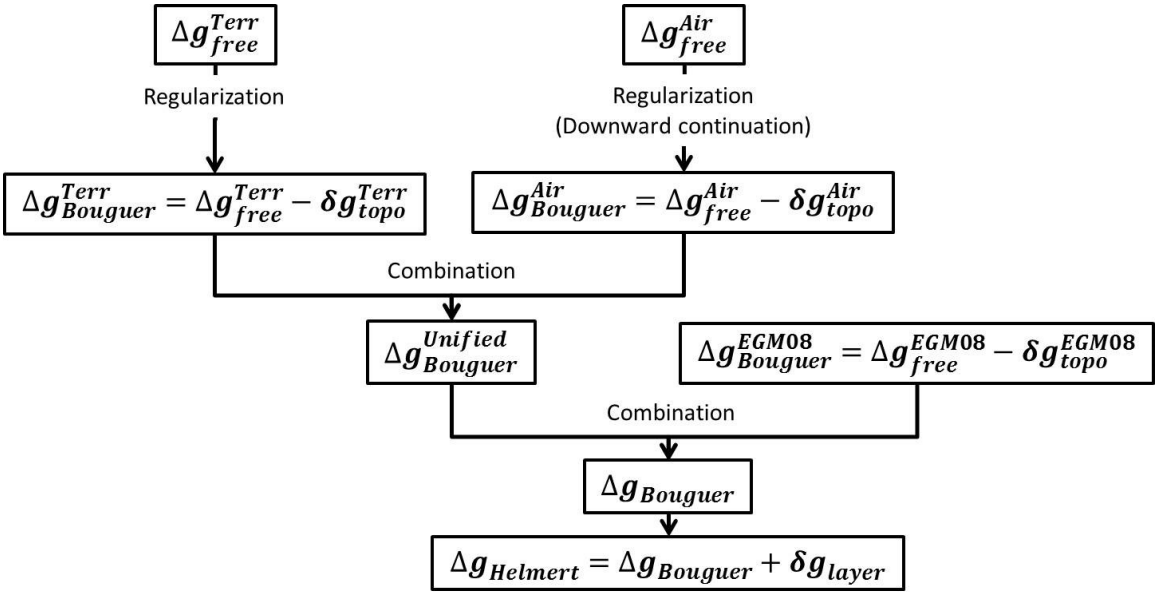

Figure 11. Flowchart of data combination

CHAPTER 4 STOKES'S INTEGRAL MODEL

Stokes's integral in Equ (21) says that the gravity anomaly multiplied by Stokes's kernel (Equ (18)) is continuously integrated over the entire sphere. However, the integral area must be reduced to a relatively small area where data are available, and also evaluated by summation using discretized finite compartments. Truncation errors, due to the limited of area are reduced by the Remove-Compute-Restore (RCR) technique and modification of Stokes's kernel. Indeed, various studies have proven that the accuracy of geoid heights based on locally distributed data depends practically on the size of integral area, the maximum degree of the reference GGMs, and the kernel modification (Wong and Gore, 1969, Forsberg and Featherstone, 1998).

As described in Section 2.6, the RCR technique supplements longer wavelength information to the truncated Stokes's integral by removing the low frequency gravity anomaly from the measurements and restoring the low frequency geoid undulation to the computed residual geoid undulation. The effect of the RCR technique on the geoid model depends on the maximum degree (nmax) of the reference model and the errors embedded in it. There are several possible methods to modify Stokes's kernel. The methods suggested by Molodensky et al. (1962), Wong and Gore (1969), Meissl (1971), and Vanicek and Kleusburg (1987) are widely used. Recently, Featherstone (2013) gave a very nice review about most of the published kernel modifications, which are categorized as deterministic, stochastic, combined, and band-limited.

In this study, the kernel modification by Wong and Gore will be practically applied for South Korea in order to reduce the truncation error. This chapter introduces the kernel modification, and includes the analysis of the effects of the RCR technique, and numerical test results on the choice of spherical capsize of the integral. Also, the systematic effects described in Section 2.3 are numerically estimated.

4.1 Introducing the Kernel modifications

Wong and Gore (1969) modified Stokes's kernel by removing low degree Legendre polynomials from Stokes's function given in Equ (18). The modified kernel is defined by

$$S(\psi)^{Wong\ and\ Gore} = S(\psi) - S_{deg2-M}(\psi) \quad (97)$$

where

$$S_{deg2-M}(\psi) = \sum_{n=2}^{M} \left(\frac{2n+1}{n-1}\right) P_n(cos\psi) \quad (98)$$

Legendre Polynomials are recursively computed by

$$P_0(cos\psi) = 1, \qquad P_1(cos\psi) = cos\psi$$

$$P_n(cos\psi) = -\frac{n-1}{n} P_{n-2}(cos\psi) + \frac{2n-1}{n} cos\psi P_{n-1}(cos\psi) \quad (99)$$

M is arbitrary, but should be less than or equal to n_{max}. The effect of this modification is that the low frequency errors in the gravity anomaly have less influence on the residual geoid undulation (Featherstone, 2013).

4.2 Estimate model error based on simulation data

In this section, we focus on the geoid modeling error for South Korea based on the simulation data. These simulated gravity anomaly data derived from EGM08 are subjected to the same RCR procedure as the actual data to compute the geoid undulations by the Stokes's integral. First, we generate the free-air gravity anomalies based on EGM08 with degree and order 2160 on the whole grid with 30 arcsec interval for South Korea. These refer to the geoid surface approximate to 30 m in height. Second, various maximum degrees (n_{max}) for the RCR technique will be used to find a proper n_{max}. The size of integration area is changed with respect to n_{max}, and the computation point is always located at the center of the area. Third, we will apply the kernel modification developed by Wong and Gore, and finally the computed geoid model is compared to the geoid undulation generated from EGM08 ($n_{max} = 2160$) at GPS/leveling locations as representative of the region. It is expected that the comparison results only include the model error due to the truncation.

Table 21 shows the statistics of the differences between the estimated geoid model by the Stokes's integral and generated geoid undulations from EGM08 at GPS/leveling location. The first column in Table 21 is the n_{max} of EGM08 for the RCR principle, and second

column is the size of integration area related to the n_{max}. Third is the parameter (M) used for the Wong and Gore's kernel modification. Table 21 generally shows that there exist truncation errors caused by the practical application of the Stokes's integral and these are reduced by the RCR principle and kernel modification. The modeling errors vary from 3.7 cm to 18.1 cm in standard deviation depending on n_{max} without the kernel modification. The maximum degrees (n_{max}) of 72, 120 or 180 are too low to represent the lower wavelengths of the gravity field for South Korea, because the error already reaches from 2.8 cm to 7.4 cm in standard deviation when we apply the best combinations of n_{max} and M. Therefore, we should use 240 or higher for n_{max}. The model error with $n_{max} = 240$ decreases to less than 2 cm when we use Wong and Gore's kernel modification with M varying from 90 to 110. The best precision is 1 cm or less in standard deviation when we use 360 degree for n_{max} and Wong and Gore's kernel modification with M between 110 and 130. Figure 12 shows the estimated model error distribution for $n_{max} = 360$ and $M = 120$.

Table 21. The model errors based on the simulated data. The comparison is done at the coordinates of GPS/leveling data [Unit : cm]

n_{max}	Window size	M	mean	St.Dev.	Maximum	Minimum
72	5° × 5°	No mod.	14.7	18.1	47.4	53.5
		36	-1.3	7.4	14.2	16.1
		54	-9.0	15.1	35.9	41.5
120	3° × 3°	No mod.	0.9	11.8	32.4	31.2
		36	0.3	4.1	10.9	-10.6
		54	0.1	4.1	7.6	-10.6
		72	-0.2	7.3	19.6	-19.1
180	2° × 2°	No mod.	0.6	7.8	18.9	-21.5
		54	0.3	3.1	8.2	-8.5
		72	0.2	2.8	6.5	-8.0
		90	0.2	3.7	9.5	-10.6
240	1.5° × 1.5°	No mod.	0.0	6.7	16.7	17.4
		72	0.1	2.5	6.0	-6.4
		90 ~ 110	0.1	1.8 ~ 1.9	5.2 ~ 5.6	-5.1 ~ -4.8
360	1° × 1°	No mod.	0.1	3.7	13.9	-9.3
		72	0.1	1.8	6.0	-4.5
		90	0.0	1.4	4.1	-3.8
		100	0.0	1.2	3.7	-3.6
		110 ~ 130	0.0	0.9 ~ 1.0	2.5 ~ 3.3	-3.4 ~ -3.1
		150	0.0	1.1	3.1	-3.9

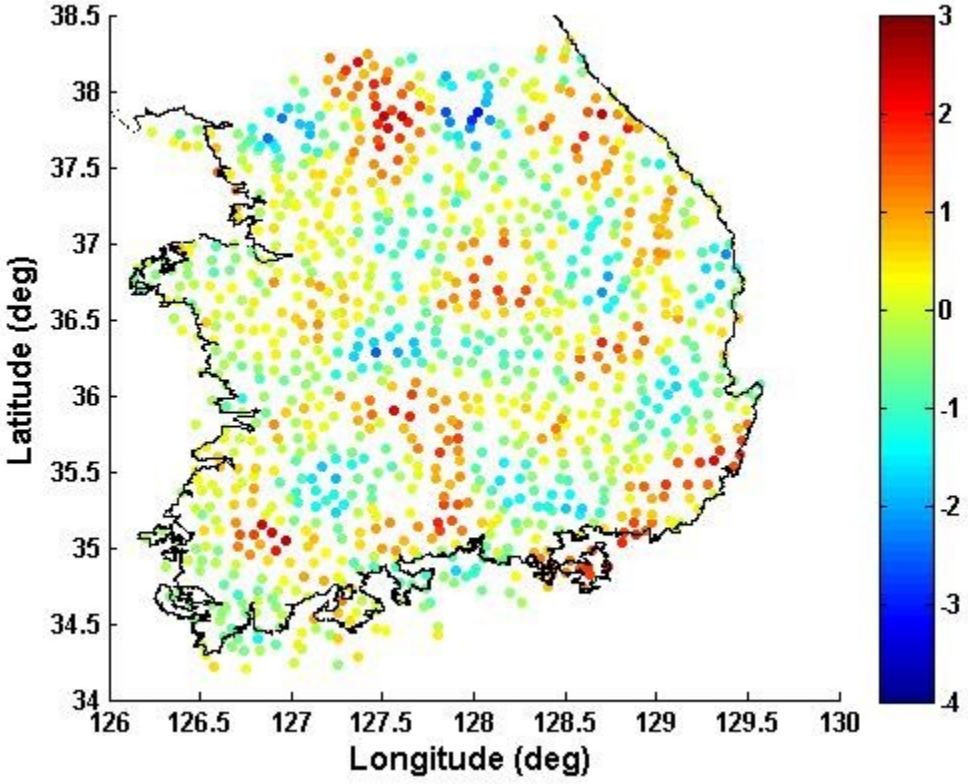

Figure 12. The differences of geoid undulations between those estimated by Stokes's integral and those generated from EGM08. ($n_{max} = 240, M = 120$) [unit : cm]

4.3 Numerical evaluations of systematic effects

The errors incurred during the derivation of the fundamental equation of the physical geodesy were formulated in Section 2.3. The numerical assessments of the effects of model approximation, such as directional derivative, linear approximation and ellipsoidal correction, for South Korea are based on the gravity quantities generated from EGM08 up to degree and order 2160.

The directional derivative effect refers to Equs (28), (29) and the linear approximation of the gravity anomaly uses Equ (31). The spherical approximation is based on Equ (36). Table 22 summarizes the statistics of the systematic effects caused by the linear, directional derivative, and spherical approximation. As seen in Table 22, the linear approximation is very small; hence, it is so negligible, but the spherical approximation varies from -116.6 micogal to 189.3 microgal and the directional derivative has a range from -96.2 microgal to 54.4 microgal. The spherical approximation would be decreased after applying the ellipsoidal correction. The directional derivative error on the geoid undulation is computed by the Stokes's integral given in Equ (21).

Table 22. Statistical results of approximation errors on gravity anomaly [unit : microgal]

	Mean	St.Dev.	RMS	Maximum	Minimum
Linear approximation	-0.016	0.004	0.016	-0.008	-0.024
Spherical Approximation	18.307	36.971	41.255	190.218	-121.003
Directional Derivative	-10.391	18.287	21.033	56.547	-96.691

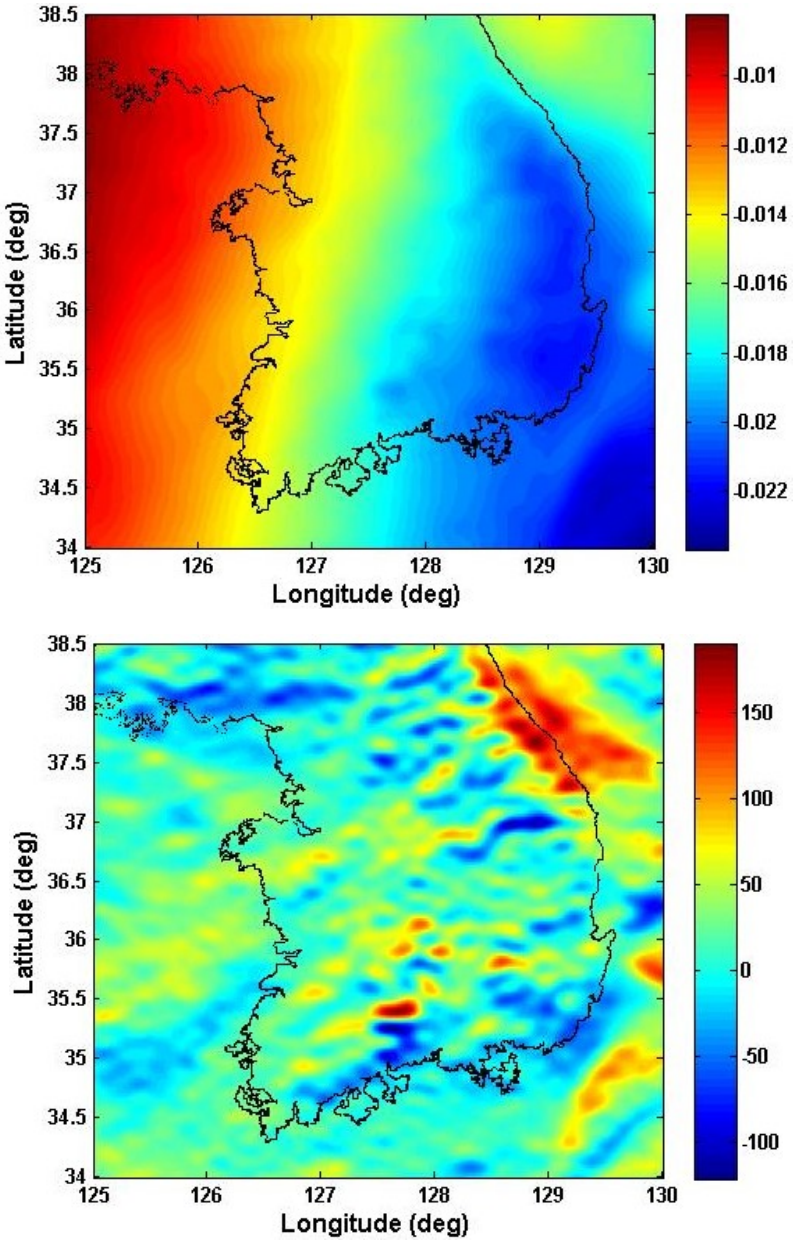

Figure 13. The systamatic effects on the gravity anomaly casued by (Top) Linear approximation (Bottom) Spherical approximation [unit : microgal]

Table 23. Statistical results of approximation errors on geoid undulation [unit : mm]

	Mean	St.Dev	RMS	Maximum	Minimum
Directional Derivative	-2.220	0.690	2.325	-0.900	-4.600

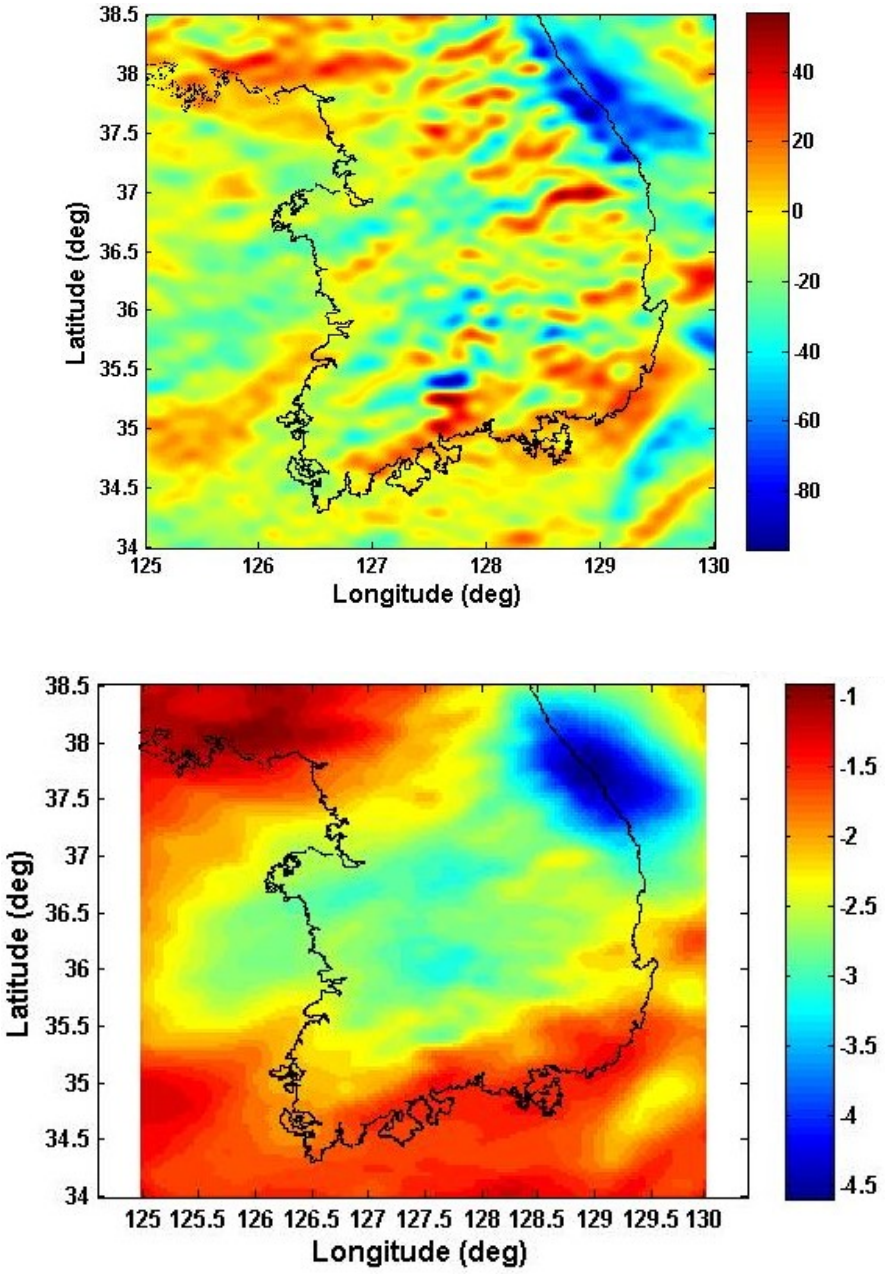

Figure 14. (Top) The directional derivative error on gravity anomaly [unit : microgal] (Bottom) The directional derivative error on geoid undulation [unit : mm]

The ellipsoidal correction is determined by Equs (37) through (40). If we compare Equ (37) and (79), $N_P^{(0)}$ in Equ (37), which is used to compute the ellipsoidal correction, is the residual geoid undulation estimated by the Stokes's integral. The ellipsoidal correction, $N_P^{(1)}$, consists of two terms; the first, Equ (39), is the simple analytical function of $N_P^{(0)}$ and the first three geopotential coefficients of the disturbing potential. And the second, Equs (38) and (40), is an integral of $N_P^{(0)}$ with kernel $K(\psi_{PQ}, \theta_P, \theta_Q)$ over the entire sphere.

For the second term, the attenuation of the kernel permits the truncation of the integral to the area of interest. However, because $N_P^{(0)}$ is already a long-wavelength signal, the area of integration must be extended considerably. Even for the large area used for this purpose, the neglected area on the integral can generate large edge effects (Jekeli et. al., 2009). The large effect of $N_P^{(1)}$ reaches about 70 cm, but the ellipsoidal correction combined with $e^2 \approx 0.0067$ is less than 5 mm.

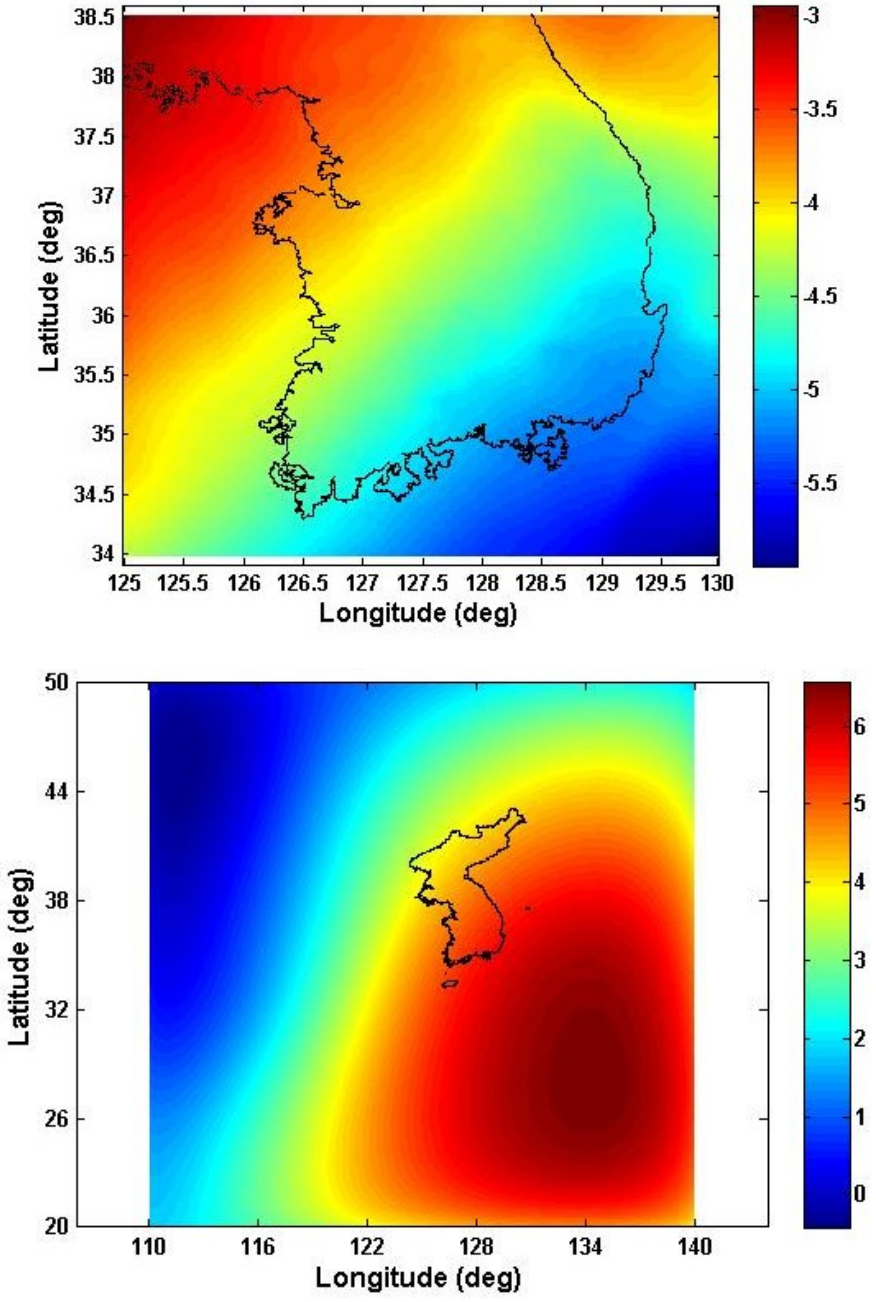

Figure 15. The effects of ellipsoidal correction (Top) $N_P^{(11)}$ (Bottom) $\frac{1}{4\pi}\iint_\sigma N^{(0)}(Q)K(\psi_{PQ},\theta_P,\theta_Q)d\sigma$

CHAPTER 5 VALIDATION OF DEVELOPED GEOID MODELS

5.1 Recently published regional geoid models

Nations have constructed and maintained geodetic and gravimetric networks in order to serve the fundamental mission, which is to provide the geodetic control and gravity-field information for their territories (Torge, 2001). Determining the geoid surface establishes the reference for a vertical datum, and modeling of the geoid undulation contributes to the height system modernization, which makes the determination of orthometric height easier and less costly through the use of GPS. The development of a national geoid model involves a huge amount of data, a reference model such as a GGM, and requires detailed theory and methodology as shown in the previous chapters. This chapter describes how some national geoid models have been developed, focusing on the background, the methodology, and the accuracy. It also provides a comparison to the development of the geoid model for South Korea.

5.1.1 South Korea

In South Korea, many organizations had continuously measured the gravity field for their purposes such as constructing a unified geodetic network and and for geologic exploration since the 1960's. However, there existed no standard or regularized procedure to measure and maintain gravimetric data (Park et al., 2011). The geoid model developments were started in the 1990's, but the estimated precisions have been about 15 cm (Park et al., 2011; Bae et al., 2012). For example, the Korean gravimetric GEOID 98 (KGEOID98), the first Korean national geoid model developed by the National Geography Institute had an accuracy of 16.4 cm in the mean and 42.2 cm in standard deviation when compared to 14 points of GPS/leveling (Yun, 2002). Many studies of the time focused on the use of optimal global geopotential models rather than improving in quality and quantity of gravimetric measurements, in order to improve the precision of the gravimetric geoid model.

With increasing demands for reliable gravimetric data in the late 2000's, the National Geographic Information Institute (NGII) made plans to construct the Unified Control Points (UCP) including geodetic coordinates and gravimetric measurements over the entire territory with 10 km spatial resolution, to measure gravity at the vertical

benchmarks, and to set up a standard procedure for processing and maintaining gravimetric measurements (Park et al., 2011). In addition, many studies supported by the NGII have constructed precise regional geoid models based on the more reliable and greater amount of gravimetric data. The Korean Land Specialization Research Project started in 2008 by the Ministry of Land, Transport and Maritime Affairs obtained new gravimetric measurements in the form of terrestrial and airborne data, as well as additional GPS/leveling, and developed both gravimetric and hybrid geoid models (Bae et al., 2012). The gravimetric geoid model used 14287 terrestrial data, 27343 airborne data and 41260 shipborne, and altimetry- derived DNSC08 data. It was based on Sokes's integral with the RCR technique using EGM08 up to degree and order 360. The topographic effect was also applied, based on the SRTM elevation model, but its computation methodology and effect are not clear. Compared to 1096 GPS/leveling data, the accuracy of the gravimetric geoid model was -14.3 cm in the mean and 5.5 cm in standard deviation. The development procedure and the precision of measurements are given in the study of Bae et al., (2012). Another geoid model, presented by Lee et al., (2012), is a hybrid geoid model in Korea, called KGEOID10. The gravimetric portion of the model was based on 8296 terrestrial gravimetric measurements with EGM08 up to degree 2160 for the RCR technique. Its accuracy reached -163 cm in mean and 12.3 cm in standard deviation (Lee et al., 2012) when compared to 1185 GPS/leveling data. Lee and Kim (2012) published the geoid model, called JNUGEOID2010, which was based on 8316 terrestrial gravity measurement, DNSC08, and EIGEN-GL04C model up to degree 360 for RCR technique. It was developed at 1 arcmin resolution, and its accuracy reached 12.6 cm in mean and 18.0 cm in standard deviation when compared to 735 GPS/levling data (Lee and Kim, 2012). The accuracies of introduced geoid models are the results estimated by comparing to separate GPS/leveling data sets, and these are considerably different. The causes may come from not only the used gravity data, geoid computation methodologies but also the accuracy of the used GPS/leveling data.

5.1.2 Other countries

The National Geodetic Survey (NGS) in the United States has developed and published precise gravimetric geoid models, G96SSS, G99SSS, USGG2003, and recently USGG2009 (Smith and Milbert, 1999; Smith and Roman, 2011; Wang et al., 2012). Before the latest model development, NGS had basically used Helmert's second condensation, Stokes's integral and RCR technique for the geoid model computations, simply called the Helmert-Stokes scheme. The recently published USGG2009 was developed with a totally different methodology, called harmonic downward continuation, which is suitable for using the ultra-high degree reference geopotential model. While the Helmert-Stokes scheme uses residual Helmert's gravity anomaly (approximately Faye anomaly) which is the difference between the Helmert's gravity anomaly and the reference Helmert's gravity anomaly on the topographic surface, the harmonic continuation method uses the residual gravity anomaly on the physical surface, which is the difference between the free-air gravity anomaly and reference free-air gravity anomaly, and also uses the topographic effect separately computed by Residual Terrain

Model (RTM). However, the topographic effect is computed at the level of the potential and is applied like the reference geoid undulation to the residual geoid undulation using Bruns's formula. Continuation of the terrain effect down to the geoid is accomplished by a spherical harmonic development of the effect. NGS concluded that the new method yielded slightly better results than the previous method (Wang et al, 2012). USGG2009 included the latest DNSC08 altimetry-derived anomalies for the ocean, SRTM-DTED1 3arcsec DEM for the topographic reductions, and EGM08 as a reference model. The accuracy of USGG2009 was estimated as 6.3 cm in the standard deviation, compared with 18,398 benchmarks of GPS/leveling (Wang et al, 2012).

Natural Resources Canada has published the gravimetric geoid model series in the last two decades, and recently the Canadian Gravimetric Geoid Model of 2010 (CGG2010), (Huang and Veronneau, 2013). They have also followed the Helmert-Stokes scheme, but improved on the kernel modification of Stokes's integral, the quantity and quality of data, and the global geopotential model. The most recently published CGG2010 was based on the Canadian Gravity Database (CGDB) which included terrestrial, shipborne and airborne gravity data. Canadian Digital Elevation Data (CDED) was used to compute the terrain effects by Helmert's second condensation method. Also, they combined GOCO01S and EGM08 for better accuracy of the long wavelengths in the RCR technique. The accuracy of CGG2010 with 2 arcmin by 2 arcmin resolution was estimated from 2 to 10 cm in standard deviation (Huang and Veronneau, 2012).

Geoscience Australia published gravimetric geoid models, AUSGeoid98 and AUSGeoid09. AUSGeoid09 at 1 arcmin by 1 arcmin grids used terrestrial gravity data, DNSC08 for the ocean area, and the RCR technique with EGM08 model to degree and order 2190, and modified the Stokes's kernel deterministically in order to overcome the limitation of Stokes's integral and improve the accuracy of the model as compared to EGM08. The magnitudes of the residual gravity anomalies with respect to EGM08 were very small; therefore, the contribution of the measurements beyond the EGM08 on the geoid undulation was also quite small. This indicated that EGM08 could be used alone as a gravimetric model over Australia. However, it has been offered that development of a gravimetric-quasi geoid model fitted to this vertical datum is still necessary, primarily because of the gap between the Australian Height Datum and the gravimetric-quasi geoid. The accuracy of the gravimetric component of AUSGeoid09 was estimated as 22.2 cm in standard deviation when AUSGeoid09 was compared to 911 GPS/leveling benchmarks across Australia (Featherstone, 2010).

The International Association of Geodesy (IAG) Geoid and Gravity Commission has continuously developed the representative geoid models for continental Europe, including the gravimetric geoid models, European Gravimetric Geoid 1997 (EGG97) and European Gravimetric Geoid 2007 (EGG07). The recent EGG07 model achieved improvements in the terrestrial and marine gravity under international cooperation. The developers concluded that accurate global geopotential models played an important role in improving the accuracy of the European geoid model (Denker et al, 2005); therefore, the EIGEN-GL04C geopotential model, being a combination of CHAMP, GRACE and terrestrial data, was adopted for the RCR technique. For the short wavelength information,

the high resolution European DEM was created using SRTM3 and GTOPO30, in order to use it for terrain reduction according to the Residual Terrain Model (RTM). The EGG07 covers an area from 25 ºN to 85 ºN in latitude and 50 ºW to 70 ºE in longitude with a 1 arcmin by 1 arcmin grid. The accuracy is 3 - 5 cm at the continental scale and 1 - 2 cm over shorter distances up to a few hundred km (Denker et al, 2008). Table 24 gives a summary of the major gravimetric geoid models with essential characteristics and reported precision. Further details may be found in the listed references.

Table 24. Summary of geoid models

	United State	Canada	Australia	Europe
Reference	Wang et al., 2012	Huang and Veronneau, 2012	Featherstone, 2010	Denker et al, 2008
Model name	USGG2009	CGG2010	AUSGeoid09	EGG07
Model resolution	$1' \times 1'$	$2' \times 2'$	$1' \times 1'$	$1' \times 1'$
Precision	6.3 cm	2 - 10 cm	22.2 cm	3 - 5 cm
Modeling Method	Harmonic continuation method	Stokes's integral	Stokes's integral	Molodensky scheme
RCR model (n_{max})	EGM08 (2160)	Combined GOCO01S and EGM08 (224)	EGM08 (2190)	EIGEN-GL04C (360)
Gravimetric data	Terrestrial Shipborne DNSC08	Terrestrial Shipborne Airborne	Terrestrial, DNSC08	Terrestrial Shipborne Airborne ArcGP project KMS2002
Terrain reduction (Digital Terrain Model)	RTM (SRTM-DTEM1 3")	Helmert's second condensation (CDED)	RTM (GEODATA-DEM9S)	RTM (National DEMs, SRTM3, GTOPO30)

5.2 Numerical computation of geoid undulation

In this section, the geoid model is numerically computed by the terrestrial, the airborne, and the combined data. In Section 5.2.1, the indirect and secondary indirect effect formulated in Section 2.4 are determined by using the SRTM heights at 30 arcsec resolution. And, the numerical results of the determined geoid undulation are summarized in Section 5.2.2.

5.2.1 Indirect and secondary indirect effects

The indirect effects and secondary indirect effect caused by the Helmert's second condensation are determined by Equs (62) and (63) based on averaged SRTM height averaged over 30 arcsec by 30 arcsec spherical grids. Table 25 summarizes the statistics of the indirect and secondary indirect effects, and Figure 16 shows both effects on a map. The largest indirect effect reaches -11.3 cm, and the RMS is about 1 cm, so the indirect effect is significant in the geoid computation. The maximum effect of the secondary indirect effect is about -35 microgal, and it is negligible.

Table 25. Numerical results of indirect and second indirect effects used SRTM elevation averaged to 30arcsec

	Unit	Mean	St.Dev	RMS	Max	Min
Indirect Effect	cm	-0.3	0.9	0.9	0.0	-11.3
Second indirect Effect	microgal	1.0	2.7	2.9	34.9	0.0

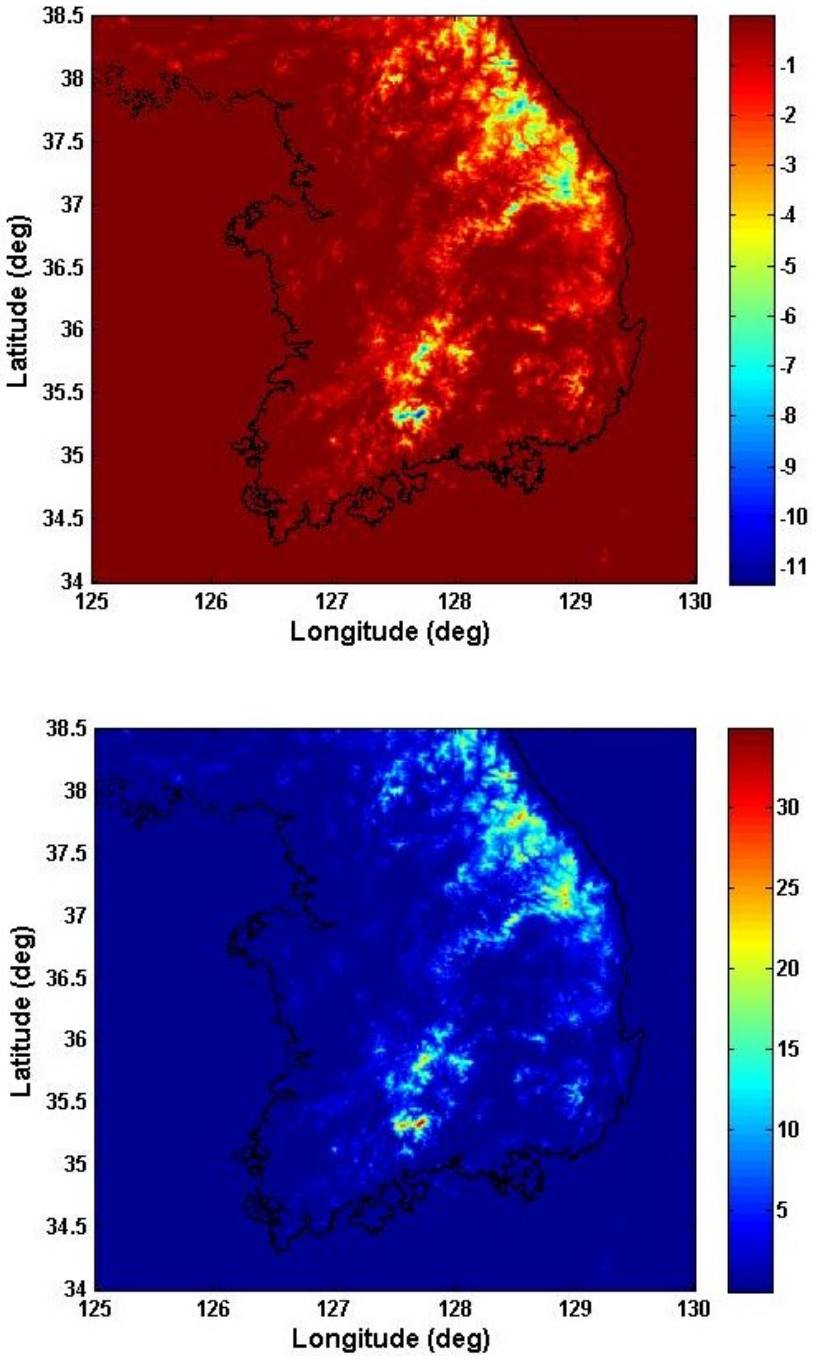

Figure 16. (Top) The indirect effect on gravity anomaly [unit : cm] (Bottom) The secondary indirect effect on the gravity anomaly [unit : microgal], caused by Helmert's second condensation.

5.2.2 Geoid Determination

The geoid models are computed by the Stokes's integral based on the actual measurements. Based on Section 4.2, we use 240 and 360 for maximum degree of the RCR technique and Wong and Gore's kernel modification with $M = 90$ and $M = 120$ truncation parameters, respectively. The geoid models are developed by using the terrestrial data only, the airborne data only, and the unified data, which are combined with EGM08 for ocean areas and land grid cells with no data (Figure 11). The 30 arcsec regularized data are averaged to lower-resolution data, such as 5, 3, 2, and 1 arcmin. The developed geoid models are compared to GPS/leveling measurements at their location by inverse-distance weighted linear interpolation.

First, the developed geoid undulations are based on the free-air gravity anomalies. As shown in Table 26, the airborne-only models have mostly consistent accuracies, compared to GPS/leveling, between 18.8 and 16.0 cm in the mean and from 7 to 5.9 cm in standard deviation. If these are compared to the accuracy of EGM08 for South Korea (Table 6), we find slightly better results for the airborne-only data case on 2 arcmin and 1 arcmin grids data. There is no improvement using airborne data at 3 arcmin or 5 arcmin in resolution. On the other hand, the accuracies of geoid models based on the terrestrial-only or unified data vary considerably depending on the data resolution. Especially, the standard deviations for data with 5, 3, and 2 arcmin resolution are larger than 10 cm. It is probably due to the fact that the point terrestrial data at "lower resolution" do not represent the mean gravity value at these resolutions.

Table 26. The accuracy of the developed geoid models based on the free-air gravity anomaly. [unit : cm]

Data Resolution		$n_{max} = 240$, M = 90		$n_{max} = 360$, M = 120	
		mean	St.Dev.	mean	St.Dev.
5 arcmin	1 Airborne only data	18.8	7.0	18.1	6.9
	2 Terrestrial only data	-12.4	16.5	-5.7	14.2
	3 Unified data	-4.0	13.6	0.7	11.9
3 arcmin	1 Airborne only data	17.5	6.1	17.2	6.0
	2 Terrestrial only data	-7.2	14.3	-1.8	12.4
	3 Unified data	-2.1	12.7	2.0	11.1
2 arcmin	1 Airborne only data	17.2	6.0	17.0	5.9
	2 Terrestrial only data	-2.4	12.3	1.8	10.7
	3 Unified data	1.0	11.1	4.3	9.8
1 arcmin	1 Airborne only data	16.7	5.9	16.7	5.8
	2 Terrestrial only data	6.7	8.7	8.9	7.8
	3 Unified data	8.0	8.1	9.9	7.4
30 arcsec	1 Airborne only data	16.2	6.3	16.0	6.3
	2 Terrestrial only data	12.9	6.7	13.4	6.5
	3 Unified data	12.9	6.7	13.4	6.5

The Stokes's integral and kernel modification are applied to the gravity anomalies considering the terrain effects and downward continuation.

Table 27 includes the statistics of the errors of geoid models with data resolution of 2 arcmin, 1 arcmin, and 30 arcsec, respectively. "No Terr.Effect" is based on the free-air gravity anomaly, the same as Table 26, "Terr.Effect" means the geoid model based on the Helmert gravity anomaly following the procedure in Figure 11. "Terr.Eff+DCd" is based on the gravity anomaly with both the terrain effects and downward continuation applied to the airborne data. The downward continuation is done only for the free-air airborne gravity anomaly because it is more stable compared to the Bouguer or Helmert gravity anomaly. The geoid model includes the indirect effect caused by the considered terrain effects.

Airborne-only data only (2 arcmin resolution) in

Table 27 yield slightly better results in the mean (0.5 cm improvement) with the terrain effects, or in the standard deviation (0.5 cm improvement) with the terrain effects and downward continuation. The geoid model based on the terrestrial-only data has 2 - 3 cm improvement in standard deviation, and considerable difference in the mean.

With 1 arcmin data grid, the geoid models with terrestrial-only or unified data have better accuracy when the terrain effects are applied. These are still slightly worse than the geoid model based on airborne-only data. However, it seems that the terrestrial data contribute to reduce the mean value from 16.6 cm to 14.9 cm. Also, the downward continuation slightly reduces the standard deviation of the error (about 0.5 cm).

In case of 30 arcsec resolution data, it is close to or very slightly worse than the developed geoid undulation based on 1 arcmin. As shown in

Table 27, the accuracies of developed geoid model at 30 arcsec grid are consistent among the different data inputs. It appears that the measurements contribute to the development of the geoid model at the higher resolution even though most of the "data" are EGM08 values. In addition, the terrain effects, particularly on the terrestrial data, improve the accuracy of the geoid model as well as enabling more accurate data combination.

Table 27. . The accuracy of the developed geoid models, which are based on the Helmert gravity anomaly with or without downward continuation. [unit : cm]

Data Resoultuion		2 arcmin					
		No Terr.Effect		Terr.Effect		Terr.Eff+DCd	
		mean	St.Dev	mean	St.Dev	mean	St.Dev
$n_{max} = 240$ M = 90	1 Airborne only	17.2	6.0	16.6	6.1	17.0	5.6
	2 Terrestrial only	-2.4	12.3	17.6	9.5		
	3 Unified data	1.0	11.1	18.4	7.7	18.9	7.4
$n_{max} = 360$ M = 120	1 Airborne only	17.0	5.9	16.5	6.0	16.7	5.6
	2 Terrestrial only	1.8	10.7	17.3	8.6		
	3 Unified data	4.3	9.8	17.9	7.1	18.2	6.8
Data Resoultuion		1 arcmin					
		No Terr.Effect		Terr.Effect		Terr.Eff+DCd	
		mean	St.Dev	mean	St.Dev	mean	St.Dev
$n_{max} = 240$, M = 90	1 Airborne only	16.7	5.9	16.4	6.1	16.6	5.6
	2 Terrestrial only	6.7	8.7	13.8	7.0		
	3 Unified data	8.0	8.1	14.7	6.3	14.9	5.9
$n_{max} = 360$, M = 120	1 Airborne only	16.7	5.8	16.4	6.0	16.6	5.6
	2 Terrestrial only	8.9	7.8	14.4	6.7		
	3 Unified data	9.9	7.4	15.0	6.1	15.2	5.7
Data Resoultuion		30 arcsec					
		No Terr.Effect		Terr.Effect		Terr.Eff+DCd	
		mean	St.Dev	mean	St.Dev	mean	St.Dev
$n_{max} = 240$, M = 90	1 Airborne only	16.2	6.3	16.9	6.4	17.0	5.9
	2 Terrestrial only	12.9	6.7	15.1	6.4		
	3 Unified data	12.9	6.7	15.1	6.4	15.4	5.9
$n_{max} = 360$, M = 120	1 Airborne only	16.0	6.3	16.9	6.3	16.9	5.8
	2 Terrestrial only	13.4	6.5	15.5	6.2		
	3 Unified data	13.4	6.5	15.5	6.2	15.6	5.7

5.3 Validation of the developed geoid model

In this section, we validate the accuracy of the developed geoid models and the effect of the combined gravimetric data on the model. The procedure of determination and validation of geoid undulation in Section 5.2 is summarized by Figure 17. The residual gravity anomaly is determined by subtracting the gravity anomaly generated by EGM08 (nmax = 240 or 360) from the Helmert gravity anomaly as a resultant of the data combination given in Figure 11. The residual gravity anomaly is used as an input to compute the residual geoid undulation by the Stokes's integral with Wong and Gore's kernel modification (M = 90 or 120). The geoid undulation from EGM08 (nmax =240 or 360) is restored to the residual geoid undulation, thus resulting in the developed geoid model. Finally, it is compared to the geoid undulation acquired by GPS/leveling at the locations of GPS/leveling by inverse distance weighted linear interpolation. It is also compared to the geoid undulation generated from EGM08 (nmax : 2160).

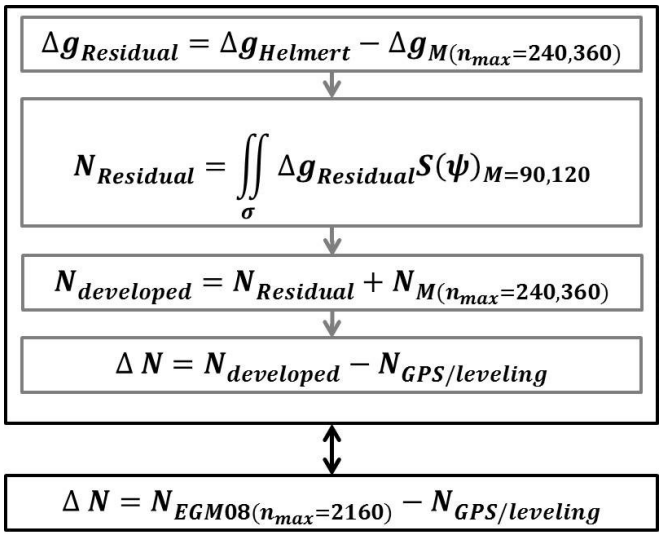

Figure 17. The flowchart of determination and validation of geoid undulation

We choose geoid models, developed by nmax = 360 for the RCR technique and M = 120 for Wong and Gore's kernel modification at 2 arcmin and 1 arcmin resolution given in

Table 27, in order to study them in details. The models using airborne data only and the combined-data case are only considered. Figure 18 shows the differences between the geoid at 2 arcmin resolution and the GPS/leveling geoid undulations. The left part is for the airborne-only case and the right one is based on the combined data. The circles with the solid line in the left figure indicate the improvements and the circle with the dashed lines indicate worse results when compared to the differences between EGM08 ($n_{max} = 2160$) and GPS/leveling shown in Figure 6. The circles with the dashed lines in the right figure show the worse results when we use the combined gravity data instead of the airborne-only data. It appears that the terrestrial data included in the combined data do not contribute to the accuracy of geoid model.

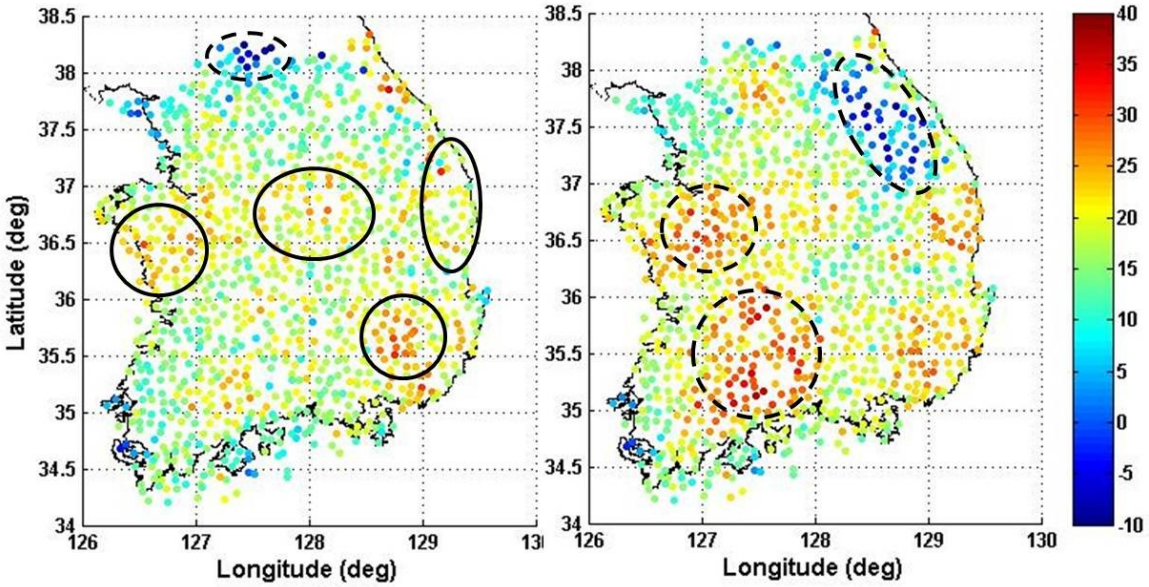

Figure 18. The differences between the developed geoid at 2 arcmin resolution and GPS/leveling geoid undulations [unit : cm]. On the left, the developed geoid model is computed using airborne-only data. The circles with solid line denote improved areas when compared to EGM08 ($n_{max} = 2160$), and the circle with dashed lines indicates worse results. For the right, the developed geoid model is based on the combined data

and the circles with dashed lines indicate worse results when compared to the geoid model based on the airborne-only data.

Similar to the previous analysis, Figure 19 shows the differences between the developed geoid at 1 arcmin resolution and the GPS/leveling geoid undulations. The left part is for the airborne-only case and the right one is based on the combined data. The left figure is very close to the left Figure 18, but the right one is quite different. In the right Figure 19, the two circles with solid lines located in the center-west and the south-east areas show improvements when compared to the geoid model based on airborne-only, as well as geoid undulations generated from EGM08. But, the circle with dashed lines located on the north-east area has worse differences. While the terrestrial data do not increase the accuracy of geoid model at 2 arcmin resolution (the right in Figure 18), these data at 1 arcmin resolution seem to contribute to an increase in accuracy of the geoid model. In summary, the geoid undulations at 2 arcmin resolution (airborne-only) and 1 arcmin resolution (airborne-only and combined data) are determined with precision better than 6 cm in standard deviation when compared to GPS/leveling geoid undulation. The statistics of the developed geoid models and of EGM08 ($n_{max} = 2160$) compared to GPS/leveling seem to show that the effects of additional gravimetric data, which are used to model the geoid undulations, are quite small. Figure 20 shows the error distributions of geoid models based on the airborne-only, combined data at 1 arcmin resolution, and generated from EGM08, compared to GPS/leveling. However, the local improvements by the additional airborne or terrestrial data in some areas are evident in Figures 18 and 19.

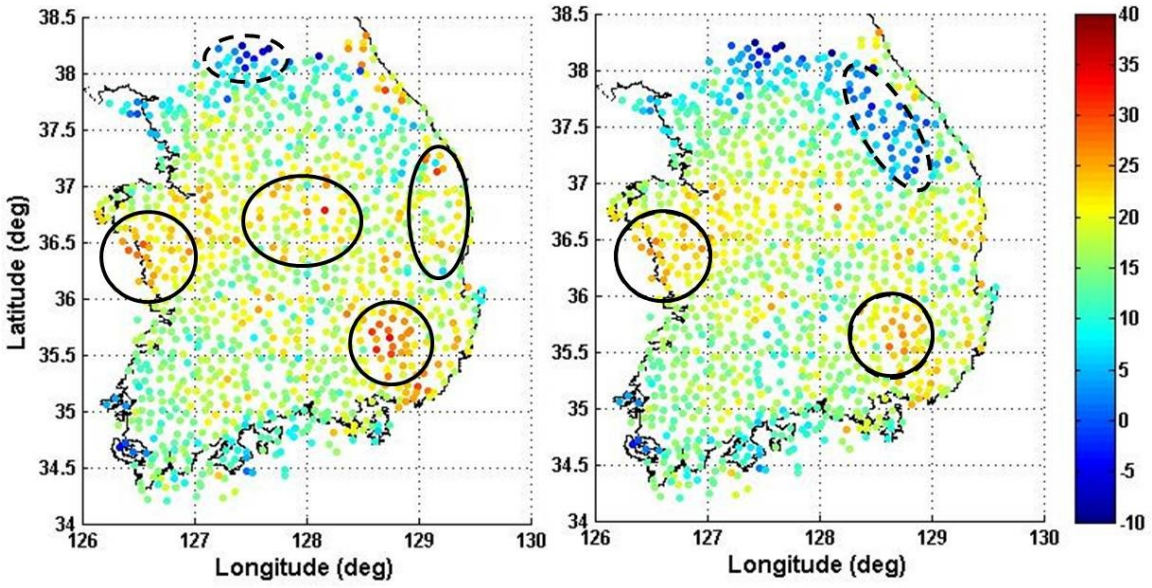

Figure 19. The differences between the developed geoid at 1 arcmin resolution and GPS/leveling geoid undulations [unit : cm]. On the left, the developed geoid model is computed using airborne-only data. The circles with solid lines indicate improved areas when compared to EGM08 ($n_{max} = 2160$), and the circle with dashed line indicates worse results. For the right, the developed geoid model is based on the combined data. The circles with solid line in the center-west and south-east area shows improved results, but the circle with dashed lines in the north-east area indicates worse results when compared to the geoid model based on airborne-only data.

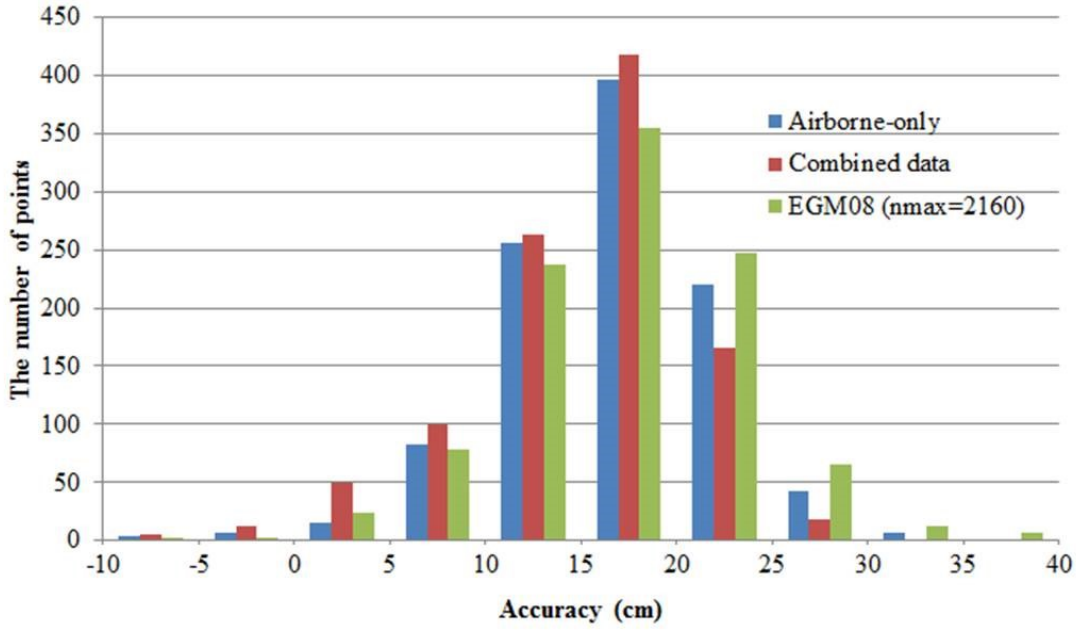

Figure 20. Histogram for the accuracies of geoid undulations compared to GPS/leveling

We conclude that the airborne data slightly contribute to the development of an accurate geoid undulation model. Terrestrial data contribute to the accuracy of geoid undulation differently according to the data resolutions, therefore, there is a need for more densely distributed terrestrial data in the territory in order to improve the accuracy of the geoid undulation. As a future work, we can refine the combination methods focusing on the improvement in the geoid model accuracy. Outlier detection on the data or applying different weighting schemes on the data combination, which is mentioned in Section 3.5, may also be considered.

CHAPTER 6 CONCLUSION AND FUTURE WORK

As an infrastructure for nations, the height system had been traditionally constructed and managed by labor intensive leveling. Since the ellipsoidal height has been accessible due to the developments of GPS, it is available to build and maintain the height system easily and efficiently if we know the accurate geoid undulation. This is called height system modernization, and the accurate geoid undulation is consequently a fundamental component for it. The aim of this dissertation is the determination of an accurate gravimetric geoid model for South Korea. It requires densely and extensively distributed gravimetric measurements. In this study the available terrestrial and airborne gravity data for South Korea are evaluated for their contribution to the geoid modeling effort. Especially, the airborne gravity data were collected in 2008 - 2009 for the development of a precise geoid model. Due to the characteristic of the measuring methods, the two types of gravimetric data have differences in data accuracy, resolution, coverage, and topographic reduction. Therefore, it is also very important to merge the terrestrial and airborne gravity data to a unified data base, which is based on understanding their characteristics.

The consistency test shows that the difference between comparably regularized terrestrial and airborne data at commonly occupied geographic grid cells has a mean value of 9 mgal, and 12 mgal in the standard deviation. Moreover, the terrestrial gravity anomaly measured at the earth's surface is smaller than the airborne gravity value acquired on airborne altitude, approximately 3000 m above the geoid. It is contrary to the expected attenuation of gravity fields according to Newton's law of gravitation, and is due to the fact that the space between levels with terrestrial measurements and airborne measurements is not empty but contains topographic masses.

This dissertation clearly shows that the terrain effect is the most important parameter to consider in order to enhance the consistency of available gravimetric data and produce a unified data base referring to the same gravitational field. The Bouguer reduction affects the terrestrial and airborne gravity data differently depending on the measurement surfaces, and is required to achieve the better agreement of the two gravimetric data. The terrestrial Bouguer gravity anomalies differ from the airborne Bouguer gravity anomaly by -0.7 mgal in the mean and 7.0 mgal in standard deviation. The bias is significantly reduced from -9 mgal, and the standard deviation also has about 5 mgal improvement. The terrain reduction also affects the accuracy of the geoid undulation, especially for the terrestrial data. The geoid undulation based on the Helmert gravity anomaly, which

combines the Bouguer gravity anomaly with the restored condensation layer (Helmert's second condensation method), is more precise than based on the free-air gravity anomaly.

Another considered reduction method is the downward continuation of the airborne gravity data. It is a necessary reduction in order to combine them with other gravimetric measurements, as well as to compute the geoid undulation. However, the downward continuation in this study decreases the consistency between terrestrial and airborne data for any type of gravity anomaly. After downward continuation, the airborne Bouguer gravity anomaly agrees less with the terrestrial Bouguer anomaly. While the downward continuation does increase the difference between two data types, the geoid undulation computed from downward continued airborne data has slightly better accuracy, 5.6 cm versus 6.1 cm in standard deviation.

In addition, there are available Global Geopotential Models (GGMs) such as EGM08, and GOCO03S based on recently acquired GOCE data. Based on the comparisons between the GGMs and the gravimetric measurements, the GGMs have good consistency with the airborne but not the terrestrial data. So, removing a reference gravity anomaly generated from GGMs does not contribute to an increase in the consistency of terrestrial and airborne gravity data.

The numerical computation of the geoid undulation is done by the Stokes's integral with the consideration of Global Geopotential Models (GGMs) and the Remove-Compute-Restore (RCR) technique, combined with a kernel modification. In preparation for the determination of the geoid undulation, the systematic effects due to the approximations and assumptions in the application of the fundamental equation of physical geodesy are numerically estimated on the gravity anomaly and geoid undulation. The linear approximation error is less than 1 microgal and the directional derivative error is less than 0.1 mgal for the gravity anomaly. The spherical approximation error, approximately less than 0.2 mgal on the gravity anomaly, is reduced by the ellipsoidal correction which is less than 5 mm on the geoid undulation. Therefore, we conclude that these effects in the regional area are small and negligible.

The RCR technique and kernel modification by Wong and Gore are applied to reduce the truncation error caused by the limitation of the integration area. EGM08 is chosen as the reference model to represent the long-wavelength gravity field for South Korea, because it has slightly better agreement with the gravity data than GOCO03S. The model error in the Stokes's integral is empirically estimated by simulation data, and it is less than 1 cm if we use degree 360 for RCR and 120 for the kernel modification.

The Stokes's integral is applied to the gravity anomalies, such as the airborne-only data, terrestrial-only data, and combined data, in order to determine the geoid model, and the accuracy is demonstrated by comparing it to independent geoid undulation data determined by GPS/leveling. The results illustrate the influence of each gravimetric data on the determination of geoid undulation. The most accurate geoid model has errors 16.6 cm in the mean and 5.6 cm in standard deviation when we use airborne-only data at 1

arcmin resolution with the terrain effect and downward continuation applied. Another model, which is based on the combined data at 1 arcmin resolution, including the terrain effect and downward continuation, has errors 15.2 cm in the mean and 5.7 cm in standard deviation. The large difference in the mean can be explained by the datum offset, N_0, which is caused by the differences of the reference ellipsoids and datum for the gravimetric and GPS/leveling geoid undulations. It is numerically determined as 14.5 cm for South Korea (Jekeli et. al, 2012).

The airborne-only data geoid models have slightly improved accuracy when the downward continuation and the terrain effect are applied. For this computation, the downward continuation is only applied to the airborne free-air anomaly in order to avoid instability in the downward continuation, and then the terrain effect is applied. The terrestrial-only and combined data geoid models improve comparatively more in accuracy than the airborne-only data model when the terrain effect is applied. However, the results imply that the combined data do not improve the accuracy of the geoid undulation compared to the airborne-only data case.

The geoid models developed in this dissertation can be also compared to the similar geoid model for South Korea computed by Bae et al. (2012). Their model was based on terrestrial, airborne, and shipborne gravimetric data, and has 5.5 cm precision compared to GPS/leveling. The precision of EGM08 is estimated as 13.0 cm globally (Pavlis et al., 2012), and it is estimated as 6.0 cm for South Korea. Based on this statistic, the geoid model developed in this study is improved by only 0.4 cm. But, the spatial distribution of the errors show that the geoid model has improvements in the south-east and center-west areas.

The main contribution of this dissertation is that the bias between terrestrial and airborne gravity anomaly data is explained and reduced by applying the terrain effect through the Bouguer reduction. It is shown that the downward continued airborne gravity data generate more accurate geoid undulations especially in localized analysis even though it does not improve the consistency with respect to the terrestrial data. While the terrain effect on the terrestrial data increases the accuracy of geoid model based on it, denser terrestrial data are required to improve the precision of the geoid undulation. Therefore, the key aspects of future research are

- Downward continuation of airborne gravity data : The terrain-reduced Bouguer gravity anomaly has the best consistency between airborne and terrestrial data, however, there is a difficulty in downward continuation of this anomaly. As a possible solution, downward continuation could be applied separately to the airborne free-air gravity anomaly and the gravitational attraction of the topographic masses. It may contribute to better consistency with respect to the terrestrial data.

- Combination of terrestrial and airborne : Outlier detection of the gravimetric data, especially the terrestrial data, and appropriate weights on the data combination may improve the accuracy of the geoid undulation. In addition, a better interpolation method could be used to fill in areas with no data.

BIBLIOGRAPHY

Bae TS, Lee J, Kwon JH, Hong CK (2012) Update of the precision geoid determination in Korea. Geophysical Prospecting 60:555–571. doi: 10.1111/j.1365-2478.2011.01017.x

Bursa M, Kouba JAN, Kumar M, et al. (1999) GEOIDAL GEOPOTENTIAL AND WORLD HEIGHT SYSTEM. Studiia Geophysica et Geodetica 43:327–337.

Denker H, Barriot J, Barzaghi R, et al. (2009) The Development of the European Gravimetric Geoid Model EGG07. In: Sideris MG (ed) Observing our Changing Earth, International Association of Geodesy Symposia 133. Springer-Verlag Berlin Heidelberg, pp 177–185

Denker H, Torge W (1998) The European Gravimetric Quasigeoid EGG97 - An IAG Supported Continental Enterprise -. Geodesy on the move; gravity, geoid, geodynamics and Antarctica; IAG Scientific Assembly. Rio de Janeiro, Brazil, pp 249–254

Drinkwater MR, Haagmans R, Muzi D, et al. (2007) THE GOCE GRAVITY MISSION : ESA ' S FIRST CORE EARTH EXPLORER. 3rd International GOCE User Workshop. Frascati, Italy, pp 1–8

Farr TG, Rosen PA, Caro E, et al. (2007) The Shuttle Radar Topography Mission. Reviews of Geophysics 45:1–33. doi: 10.1029/2005RG000183

Featherstone WE (2013) Deterministic, stochastic, hybrid and band-limited modifications of Hotine's integral. Journal of Geodesy. doi: 10.1007/s00190-013-0612-9

Featherstone WE, Kirby JF, Hirt C, et al. (2010) The AUSGeoid09 model of the Australian Height Datum. Journal of Geodesy 85:133–150. doi: 10.1007/s00190-010-0422-2

Featherstone WE, Kirby JF, Kearsley a. HW, et al. (2001) The AUSGeoid98 geoid model of Australia: data treatment, computations and comparisons with GPS-levelling data. Journal of Geodesy 75:313–330. doi: 10.1007/s001900100177

Fei ZL, Sideris MG (2000) A new method for computing the ellipsoidal correction for Stokes's formula. Journal of Geodesy 74:223–231. doi: 10.1007/s001900050280

Forsberg R, Featherstone W. (1998) Geoids and cap sizes. In: Forsberg R, Feissl M, Dietrich R (eds) Geodesy on the move. Springer, Berlin Heidelberg New York, pp 194–200

Forsberg R (1994) Terrain effects in geoid computations. Geoid School. pp101–124.

Forsberg, R (2002) Downward continuation of airborne gravity – an Arctic case story. Proceedings of the International Gravity and Geoid Commission Meeting, Thessaloniki

Forsberg, R., Olesen, A. V., Munkhtsetseg, D., & Amarzaya, A. (2007). Downward continuation and geoid determination in Mongolia from airborne and surface gravimetry and SRTM topography. Harita Dergisi

Goiginger H., Rieser D., Mayer-Guerr T., Pail R., Schuh W.-D., Jäggi A., Maier A., GOCO Consortium (2011): The combined satellite-only global gravity field model GOCO02S. European Geosciences Union General Assembly 2011, Wien, 04.04.2011

Heck B (2003) On Helmert's methods of condensation. Journal of Geodesy 77:155–170.

Heiskanen, W.A., and Moritz, H., (1967) Physical Geodesy. San Francisco, WH Freeman.

Hofmann-wellenhof B, Moritz H (2006) Physical Geodesy, second edi. SpringerWienNewYork, Austria

Huang J, Veronneau M (2005) Applications of downward-continuation in gravimetric geoid modeling : case studies in Western Canada. Journal of Geodesy 79:135–145.

Huang J, Véronneau M (2013) Canadian gravimetric geoid model 2010. Journal of Geodesy 87:771–790. doi: 10.1007/s00190-013-0645-0

Hwang C, Hsiao Y-S, Shih H-C, et al. (2007) Geodetic and geophysical results from a Taiwan airborne gravity survey: Data reduction and accuracy assessment. Journal of Geophysical Research 112:B04407. doi: 10.1029/2005JB004220

Jekeli C (1981a) Modifying Stokes' Function to Reduce the Error of Geoid Undulation Computations. Journal of Geophysical Research 86:6985–6990.

Jekeli C (1981b) The downward continuation to the earth's surface of truncated spherical and ellipsoidal harmonic series of the gravity and height anomalies. Columbus, Ohio

Jekeli C, Serpas JG (2003) Review and numerical assessment of the direct topographical reduction in geoid determination. Journal of Geodesy 226–239. doi: 10.1007/s00190-003-0320-7

Jekeli C (2009) Omission error, data requirements, and the fractal dimension of the geoid. In: Sneeuw N, Novak P, Crespi M, Sansò F (eds) VII Hotine-Marussi Symposium on Mathematical Geodesy, International Association of Geodesy Symposia. Springer, Rome, Italy, pp 181–187

Jekeli C, Yang HJ (2009) Methods to Determine a Gravimetric Geoid for South Korea. The Ohio State University, pp1–21.

Jekeli C, Yang HJ, Kwon JH (2009) Evaluation of EGM08 – Globally and Locally in South Korea. Newtons Bulletin 4:38–49.

Jekeli C, Yang HJ, Kwon JH (2012) The offset of the South Korean vertical datum from a global geoid. KSCE Journal of Civil Engineering 16:816–821. doi: 10.1007/s12205-012-1320-3

Lee S, Kim C (2012) Development of regional gravimetric geoid model and comparison with EGM2008 gravity-field model over Korea. 7:387–397. doi: 10.5897/SRE11.1681

Lee DH, Yun HS, Suh YC, et al. (2012) KGEOID10 : A New Hybrid Geoid Model in Korea. EGU General Assembly 2012. Vienna, Austria, p 7383

Lemoine F., Kenyon S., Factor J., et al. (1998) The Development of the Joint NASA GSFC and the National Imagery and Mapping Agency(NIMA). Greenbelt, Maryland 20771

Martinec Z, Matyska C, Grafarend EW, Vanicek P (1993) On Helmert's 2nd condensation method. Journal of Geodesy 18:417–421.

Martinec Z, Grafarend EW (1997) Solution to the Stokes boundary-value problem on an ellipsoid of revolution. Stud Geophys Geod 41: 103–129

Mayer-Gürr, T. (2007), ITG-Grace03s: The latest GRACE gravity field solution computed in Bonn, presented at the Joint International GSTM and SPP Symposium, Potsdam, Germany, 15–17 October. [Available at http://www.igg.uni-bonn.de/apmg/index.php?id=itg-grace03]

Mayer-guerr T, Goiginger H, Rieser D, et al. The satellite - only global gravity field model GOCO02S.

Mayer-Guerr T., Rieser D., Höck E., Brockmann J..M., Schuh W.-D., Krasbutter I., Kusche J., Maier A., Krauss S., Hausleitner W., Baur O., Jäggi A., Meyer U., Prange L., Pail R., Fecher T., Gruber T. (2012): The new combined satellite only model GOCO03s. Abstract submitted to GGHS2012, Venice (Poster).

Meissl P (1971) Preparations for the numerical evaluation of secondorder Molodensky-type formulas,Report 163. Ohio StateUniversity, Columbus, Department of Geodetic Science and Surveying

Molodensky MS, Eremeev VF, Yurkina MI (1962) Methods for Study of the external gravitational field and figure of the earth. Translated from the (1960) original by the Israeli programme for the translation of scientific publications. Jerusalem, Israel

Moritz, H. (1980). Advanced Physical Geodesy (Reprint : 2008). The Ohio State University

Novak P, Heck B (2002) Downward continuation and geoid determination based on band-limited airborne gravity data. Journal of Geodesy 76:269–278.

Novak P, Kern M, Schwarz KP, et al. (2003) On geoid determination from airborne gravity. Journal of Geodesy 76:510–522.

Olesen A (2009) Airborne gravity survey of South Korea 2008/2009. Data acquisition and processing report. DTU Space, Copenhagen.

Pail R, Bruinsma S, Migliaccio F, et al. (2011) First GOCE gravity field models derived by three different approaches. Journal of Geodesy 85:819–843. doi: 10.1007/s00190-011-0467-x

Pail R, Goiginger H, Schuh W-D, et al. (2010) Combined satellite gravity field model GOCO01S derived from GOCE and GRACE. Geophysical Research Letters 37:n/a–n/a. doi: 10.1029/2010GL044906

Park P, Park J-U (2011) 2008-2011 Korean National Report to IAG. XXV General Assembly, Melbourne, Australia, June 27 - Jul 9, 2011

Pavlis NK, Holmes S a., Kenyon SC, Factor JK (2012) The development and evaluation of the Earth Gravitational Model 2008 (EGM2008). Journal of Geophysical Research. doi: 10.1029/2011JB008916

Pavlis NK, Holmes SA, Kenyon SC, Factor JK (2008) An Earth Gravitational Model to Degree 2160 : Presented at the General Assembly of the European Geosciences Union Assembly. Vienna, Austria, pp 0–33

Rapp RH, Pavlis NK (1990a) The Development and Analysis of Geopotential Coefficient Models to Spherical Harmonic Degree 360. Journal of Geophysical Research 95:21,885–21,911.

Rapp RH, Pavlis NK (1990b) The development and analysis of geopotential coefficient models to spherical harmonic degree 360. Journal of geophysical 95:21,885–21,911.

Reigber C, Balmino G, Schwintzer P, et al. (2002) A high-quality global gravity field model from CHAMP GPS tracking data and accelerometry (EIGEN-1S). Geophysical Research Letters 29:94–97.

Rummel R, Yi W, Stummer C (2011) GOCE gravitational gradiometry. Journal of Geodesy 85:777–790. doi: 10.1007/s00190-011-0500-0

Smith DA, Milbert DG (1999) The GEOID96 high-resolution geoid height model for the United States. Journal of Geodesy 73:219–236.

Smith DA, Roman DR (2001) GEOID99 and G99SSS : 1-arc-minute geoid models for the United States. Journal of Geodesy 75:469–490.

Tapley BD (2004) The gravity recovery and climate experiment: Mission overview and early results. Geophysical Research Letters 31:L09607. doi: 10.1029/2004GL019920

Torge, W. (1989). Gravimetry. Berlin; New York : deGruyter

Torge W (2001) Geodesy, 3rd Editio. deGruyter, Berlin

Vaníˇcek P, Kleusberg A (1987) The Canadian geoid—Stokesian approach. Manuscr Geod 12:86–98

Vanicek P, Sun W, Ong P, et al. (1996) Downward Continuation of Helmert's gravity. Journal of Geodesy 71:21–34.

Véronneau M (2001) The Canadian Gravimetric Geoid Model of 2000 (CGG2000). 2000:1–17.

Véronneau M, Huang J, Division GS, Canada NR (2006) The Canadian Gravimetric Geoid Model 2005 (CGG2005). 2005:1–25.

Wang YM, Saleh J, Li X, Roman DR (2012) The US Gravimetric Geoid of 2009 (USGG2009): model development and evaluation. Journal of Geodesy 86:165–180. doi: 10.1007/s00190-011-0506-7

Wichiencharoen C (1982) Fortran programs for computing geoid undulations from potential coefficients and gravity anomalies.Int rep, Department of Geodetic Science and Surveying, TheOhio State University, Columbus

Wong L, Gore R (1969) Accuracy of Geoid Heights from Modified Stokes Kernels. Geophys J R astr Soc 18:81–91.

Yun H-S (2002) Evaluation of ultra-high and high degree geopotential models for improving the KGEOID98. Korean Journal of Gematics 2:7–15.

http://earth-info.nga.mil/GandG/wgs84/gravitymod/egm2008

APPENDIX A

Equs (49), (50) are written by

$$l_{PQ} = \sqrt{l_P^2\left(1+\frac{h}{R}\right) - hh_P\left(1+\frac{h_P}{R}\right) + h^2}$$

$$l_{PQ_0} = \sqrt{l_P^2\left(1+\frac{h_{P_0}}{R}\right) - h_{P_0}h_P\left(1+\frac{h_P}{R}\right) + h_{P_0}^2}$$

First, we consider the terrain effect by the Bouguer reduction. The terms in integral in Equ (45) will be

$$\frac{R+h}{l_{PQ}} - \frac{R+h_P}{l_{PQ_0}}$$

$$\cong \frac{R+h}{l_P\sqrt{\left(1+\frac{h}{R}\right) - \frac{hh_P}{l_P^2}\left(1+\frac{h_P}{R}\right) + \left(\frac{h}{l_P}\right)^2}} - \frac{R+h_P}{l_P\sqrt{l_P^2\left(1+\frac{h_{P_0}}{R}\right) - \frac{h_{P_0}h_P}{l_P^2}\left(1+\frac{h_P}{R}\right) + \left(\frac{h_{P_0}}{l_P}\right)^2}}$$

If we have $h \le h_P \le l_P$ and assume

$$\left|\frac{h}{R} + \frac{h}{l_P^2}\left(h - 2h_P - \frac{h_P^2}{R}\right)\right| < 1, \left|\frac{h_{P_0}}{R} + \frac{h_{P_0}}{l_P^2}\left(h_{P_0} - 2h_P - \frac{h_P^2}{R}\right)\right| < 1$$

If $Q \to P_0$, then $h = h_{P_0}$ and $l_P = h_P$

$$\left|\frac{h_{P_0}}{R} + \frac{h_{P_0}}{h_P^2}\left(h_{P_0} - 2h_P - \frac{h_P^2}{R}\right)\right| = \left|1 - \left(\frac{h_P - h_{P_0}}{h_P}\right)^2\right| < 1$$

Here, P is above the earth's surface, P_0. If $h_P = h_{P_0}$, there need an additional assumption on the slope at P_0. With those assumptions,

$$\frac{R+h}{l_{PQ}}-\frac{R+h_P}{l_{PQ_0}}$$

$$=\frac{R}{l_P}\left(\left(1+\frac{h}{R}\right)\left(1-\frac{1}{2}\left(\frac{h}{R}-\frac{hh_P}{l_P^2}\left(1+\frac{h_P}{R}\right)+\left(\frac{h}{l_P}\right)^2\right)\right)\right.$$

$$\left.-\left(1+\frac{h_{P_0}}{R}\right)\left(1-\frac{1}{2}\left(\frac{h_{P_0}}{R}-\frac{h_{P_0}h_P}{l_P^2}\left(1+\frac{h_P}{R}\right)+\left(\frac{h_{P_0}}{l_P}\right)^2\right)\right)\right)$$

If we neglect $\left({}^{h}/_{R}\right)^{n}$, $n \geq 2$,

$$\frac{R+h}{l_{PQ}}-\frac{R+h_P}{l_{PQ_0}}$$

$$=\frac{R}{l_P}\left(\frac{h-h_{P_0}}{2R}+\frac{h_P\left(h-h_{P_0}\right)}{l_P^2}\left(1+\frac{h_P}{2R}\right)-\frac{1}{2}\frac{h^2-h_{P_0}^2}{l_P^2}\left(1-\frac{h_P}{2R}\right)-\frac{h^3-h_{P_0}^3}{2Rl_P^2}\right)$$

Compared to unity, ${}^{h}/_{R}$ is neglected, then

$$\frac{R+h}{l_{PQ}}-\frac{R+h_P}{l_{PQ_0}}\cong\frac{R}{l_P}\left(\frac{h-h_{P_0}}{2R}+\frac{1}{l_P^2}\left(h_P\left(h-h_{P_0}\right)-\frac{1}{2}\left(h^2-h_{P_0}^2\right)\right)\right)$$

Second, we look at the effect caused by Helmert's second condensation, Equ (55). The last two terms in integral are replaced by Equ (56) under the same approximations,

$$\frac{h-h_P}{2}\left(\frac{R^2-r_P^2}{l_P^3}-\frac{1}{l_P}\right)+\left(\frac{R+h}{l_{PQ}}-\frac{R+h_P}{l_{PQ_0}}\right)$$

$$\cong\frac{h-h_P}{2}\left(\frac{R^2-r_P^2}{l_P^3}-\frac{1}{l_P}\right)$$

$$+\frac{R}{l_P}\left(\frac{h-h_P}{2R}+\frac{1}{l_P^2}\left(h_a(h-h_P)-\frac{1}{2}(h^2-h_P^2)\right)\right)$$

$$=\frac{h-h_P}{2}\frac{R^2-r_P^2}{l_P^3}+\frac{R}{l_P^3}\left(h_a(h-h_P)-\frac{1}{2}(h^2-h_P^2)\right)$$

$$\cong-\frac{Rh_a(h-h_P)}{l_P^3}+\frac{R}{l_P^3}\left(h_a(h-h_P)-\frac{1}{2}(h^2-h_P^2)\right)$$

$$\cong-\frac{R}{2l_P^3}(h^2-h_P^2)$$

$$l_{PQ} \cong \sqrt{l_P^2 - h(2h_a - h)}$$

$$l_{PQ_0} \cong \sqrt{l_P^2 - h_P(2h_a - h)}$$

If $h \le h_a \le l_P$,

$$\frac{R+h}{l_{PQ}} - \frac{R+h_P}{l_{PQ_0}} \cong \frac{R}{l_P\sqrt{1+\frac{h}{l_P^2}(h-2h_a)}} - \frac{R}{l_P\sqrt{1+\frac{h_P}{l_P^2}(h_P-2h_a)}}$$

It can be expanded as a series in Taylor's theorem, assuming

$\left|\frac{h}{l_P^2}(h-2h_a)\right| < 1, \left|\frac{h}{l_P^2}(h-2h_a)\right| < 1$

And ignoring second and higher order derivatives

$$\frac{R+h}{l_{PQ}} - \frac{R+h}{l_{PQ}} \cong \frac{R}{l_P}\left(-\frac{1}{2}\frac{h}{l_P^2}(h-2h_a) + \frac{1}{2}\frac{h_P}{l_P^2}(h_P-2h_a)\right)$$

$$= -\frac{R}{2l_P^3}\left(h^2 - h_P^2 - 2h_a(h-h_P)\right)$$

Second, we look at the effect caused by Helmert's second condensation, Equ (55). The last two terms in integral are replaced by Equ (55) under the same approximations,

$$\frac{h-h_P}{2}\left(\frac{R^2-r_P^2}{l_P^3} - \frac{1}{l_P}\right) + \left(\frac{R+h}{l_{PQ}} - \frac{R+h_P}{l_{PQ_0}}\right)$$

$$\cong \frac{h-h_P}{2}\left(\frac{R^2-r_P^2}{l_P^3} - \frac{1}{l_P}\right) + \frac{R}{l_P}\left(\frac{h-h_P}{2R} + \frac{1}{l_P^2}\left(h_a(h-h_P) - \frac{1}{2}(h^2-h_P^2)\right)\right)$$

$$= \frac{h-h_P}{2}\frac{R^2-r_P^2}{l_P^3} + \frac{R}{l_P^3}\left(h_a(h-h_P) - \frac{1}{2}(h^2-h_P^2)\right)$$

$$\cong -\frac{Rh_a(h-h_P)}{l_P^3} + \frac{R}{l_P^3}\left(h_a(h-h_P) - \frac{1}{2}(h^2-h_P^2)\right)$$

$$\cong -\frac{R}{2l_P^3}(h^2-h_P^2)$$

APPENDIX B

From H&M (Equ 1-122),

$$\frac{R(r^2-R^2)}{l^3}=\sum_{n=0}^{\infty}(2n+1)\left(\frac{R}{r}\right)^{n+1}P_n(cos\psi)$$

Then,

$$\frac{R(r^2-R^2)}{4\pi}\iint_{\sigma}\frac{1}{l^3}d\sigma=\frac{1}{4\pi}\iint_{\sigma}\sum_{n=0}^{\infty}(2n+1)\left(\frac{R}{r}\right)^{n+1}P_n(cos\psi)d\sigma$$

Since the decomposition formula shows

$$P_n=\frac{1}{2n+1}\sum_{m=-n}^{n}\bar{Y}_{nm}(\theta,\lambda)\bar{Y}_{nm}(\theta',\lambda')$$

Then,

$$\frac{R(r^2-R^2)}{4\pi}\iint_{\sigma}\frac{1}{l^3}d\sigma=\frac{1}{4\pi}\iint_{\sigma}\sum_{n=0}^{\infty}(2n+1)\left(\frac{R}{r}\right)^{n+1}\frac{1}{2n+1}\sum_{m=-n}^{n}\bar{Y}_{nm}(\theta,\lambda)\bar{Y}_{nm}(\theta',\lambda')d\sigma$$

$$=\sum_{n=0}^{\infty}(2n+1)\left(\frac{R}{r}\right)^{n+1}\frac{1}{2n+1}\sum_{m=-n}^{n}\bar{Y}_{nm}(\theta,\lambda)\frac{1}{4\pi}\iint_{\sigma}\bar{Y}_{nm}(\theta',\lambda')\,d\sigma$$

And, the solid spherical harmonic has the property

$$\frac{1}{4\pi}\iint_{\sigma}\bar{Y}_{nm}(\theta',\lambda')\,d\sigma=\begin{bmatrix}0:n>0\\1:n=0\end{bmatrix}$$

Finally,

$$\frac{R(r^2-R^2)}{4\pi}\iint_{\sigma}\frac{1}{l^3}d\sigma=\frac{R}{r}$$